UNIVERSITY OF CALIFORNIA
RIVERSIDE

Endocannabinoid System Control of Mucosal Function in Health and Disease

A Dissertation submitted in partial satisfaction
of the requirements for the degree of

Doctor of Philosophy

in

Biomedical Sciences

by

Mark Benjamin Wiley

September 2021

Dissertation Committee:
Dr. Nicholas V. DiPatrizio, Chairperson
Dr. Meera G. Nair
Dr. David D. Lo
Dr. Tara M. Nordgren

The Dissertation of Mark Benjamin Wiley is approved:

_____

_____

_____

_____

Committee Chairperson

University of California, Riverside

Acknowledgement

Dr. Randy Seeley from the University of Michigan, Ann Arbor, MI, USA for donating the Vil-CRE ERT2 mouse line, and Dr. Sylvie Robin from the Curie Institute, Paris, France for providing permission to use the mice. Dr. Meera Nair for providing access and use of the BD Biosciences LSRII Flow Cytometer, Leica Microscope, and for her support throughout this work. Dr. Donovan Argueta, Dr. Pedro Perez, Dr. Hashini Batugedara, Dr. Jiang Li, Sang Yong Kim, Chengming Li, Bryant Avalos, Courtney Wood, Camila Alvarez, and Sarah Bobardt for technical support. Cannabinoid and Cannabis Research and Journal of Frontiers in Physiology for publication of much of the work here.

This work was supported by the National Institute of Diabetes and Digestive and Kidney Diseases (Grant no. 5R01DK119498-02) and the Tobacco Related Disease Research Program (Grant no. T29KT0232).

Dedication

This work would not have been possible without the endless support of countless people. Dr. Nicholas DiPatrizio immediately took me into his lab despite my lack of experience and he never stopped motivating me to be a better scientist. Dr. Meera Nair introduced me to my love for immunology and has been an instrumental mentor throughout my PhD. I feel incredibly lucky to have had two mentors with such infectious passion for their work and I hope to one day call them my colleagues. Thank you to my dissertation committee: Dr. David Lo and Dr. Tara Nordgren who not only pushed me when I needed it, but also encouraged me when I was struggling. UCR is a special place and I am extremely proud to call myself an alumnus of the School of Medicine.

I also want to thank Biomedical Sciences for choosing me to join this prestigious program which gave me the opportunity to meet my beautiful wife. Thank you to the love of my life, Dr. Maham Rais, who is a constant source of inspiration. Your intelligence challenges me daily and your support may be the only reason I made it through some of the toughest times of my graduate school career. I also want to thank our cat, Ivy, who always makes the toughest days end with a smile. Thank you to my mom for raising me when no one else could or would and for teaching me to prioritize my education. Thank you to my brothers for teaching me that competition in life is constant which only makes you a better man. Finally, thank you to my grandfather, “Grampy”, who has been the greatest influence in my life. Dedication, determination, and sacrifice are only a few of the life lessons you taught me that got me through my PhD.

ABSTRACT OF THE DISSERTATION

Endocannabinoid System Control of Mucosal Function in Health and Disease

by

Mark Benjamin Wiley

Doctor of Philosophy, Graduate Program in Biomedical Sciences
University of California, Riverside, September 2021
Dr. Nicholas V. DiPatrizio, Chairperson

The endocannabinoid (eCB) system is a complex lipid signaling system consistent of the endogenously produced ligands, 2-arachidonoyl-*sn*-glycerol (2-AG) and anandamide (AEA), which signal along the cannabinoid receptors [cannabinoid receptor subtype-1 (CB_1R), -2 (CB_2R) and others] and the enzymes which produce and degrade 2-AG and AEA. The eCB system is expressed throughout the human body controlling a wide variety of homeostatic functions. It was previously reported that blockade of host peripheral CB_1R signaling exacerbated metrics of infection with the soil-transmitted nematode *Nippostrongylus brasiliensis* (*N. brasiliensis*).

Therefore, I hypothesized that host CB_1R signaling is protective in host-helminth interactions using *N. brasiliensis* as a model for hookworm infection in rodents. This study identified that peripheral blockade of CB_1R, but not CB_2R, lead to significant increases in lung tissue damage, lung hemorrhaging, and lung eosinophilia in response to *N. brasiliensis* infection with no changes in parasite burden. Because *N. brasiliensis* can

produce eCBs at quantifiable levels, I developed novel enzyme assays to quantitate enzyme activity for the biosynthetic and degradative eCB enzymatic machinery, including a novel assay to determine the rate of AEA metabolism which does not require the use of radioactive materials. These methods identified that the enzyme alpha/beta hydrolase domain containing-6 contributes to ~55% of all monoacylglycerol metabolism in the lungs of rodents. Furthermore, when these methods were applied to a mouse model of diet induced obesity (DIO) in the large intestine, I found that the eCB system of the colon is severely dysregulated in response to DIO and that mice lacking intestinal epithelial CB_1R signaling have exacerbated metrics of diet-induced gut-barrier dysfunction in the large intestine. Furthermore, the RNA expression/regulation in the colon mucosa of the DIO mice lacking intestinal epithelial CB_1R signaling is dysregulated with a decrease in tight-junction protein RNA expression and an increase in the inflammatory profile. These studies suggest a potential role for the eCB system in several disease models in mucosal tissues providing novel methods for quantitation of eCB metabolism and evidence that CB_1R signaling has a strong role in inflammatory processes.

Table of Contents

Chapter 5

List of Figures

List of Tables

Abbreviations

2-AG: 2-arachidonoyl-*sn*-glycerol

2-DG: 2-docosohexaenoylglycerol

2-LG: 2-linoleoylglycerol

2-OG: 2-oleoylglycerol

2-PG: 2-palmitoylglycerol

ABHD12: Alpha/beta Hydrolase Domain Containing-12

ABHD6: Alpha/beta Hydrolase Domain Containing-6

AEA: Anandamide

BAL: Bronchoalveolar Lavage

BSA: Bovine Serum Albumin

Ca^{2+}: Calcium

CB_1R: Cannabinoid Receptor Subtype-1

CB_2R: Cannabinoid Receptor Subtype-2

cDNA: Complimentary Deoxyribonucleic Acid

$Cnr2^{-/-}$: Cannabinoid Receptor Subtype-2-null Mice

DAG: Diacylglycerol

DEGs: Differentially Expressed Genes

DGL: Diacylglycerol Lipase

DHEA: Docosohexaenoylethanolamide

DIO: Diet-induced Obesity

DPI: Days Post Infection

DSS: Dextran Sodium Sulfate

eCB- Endocannabinoid

ESI: Electrospray Ionization

FAAH: Fatty Acid Amide Hydrolase

FAE: Fatty Acid Ethanolamide

FFA: Free Fatty Acid

FITC: Fluoerscein isothiocyanate

H&E: Hematoxylin and Eosin

HCl: Hydrochloric Acid

IBD: Inflammatory Bowel Disease

$iCB_1R^{-/-}$: Intestinal Epithelial Cannabinoid Receptor Subtype-1 Deficient Mice

LLOQ: Lower Limit of Quantitation

MAG: Monoacylglycerol

MGL: Monoacylglycerol Lipase

MLI: Mean Linear Intercept

MRM: Multiple Reactions Monitoring

N. brasiliensis: *Nippostrongylus brasiliensis*

NAAA: N-acylethanolamine acid amidase

NAPE: N-acylphosphatidylethanolamine

NAPE-PLD: N-acylphosphatidylethanolamine-specific Phospholipase D

NAT: N-acyltransferase

OCT: Optimal Cutting Temperature

OEA: Oleoylethanolamide

PA: Palmitic Acid

PBS: Phosphate Buffered Saline

PEA: Pamitoylethanolamide

PEG: Polyethylene Glycol

PFA: Paraformaldehyde

qPCR: Quantitative Polymerase Chain Reaction

RNA: Ribonucleic Acid

SD: Standard Diet

SIR: Selected Ion Reading

Th2: T-helper Type 2

THC: Δ^9-Tetrahydrocannabinol

THL: Tetrahydrolipstatin

TNBS: Trinitrobenzenesulfonic Acid

UPLC-MS/MS: Ultra Performance Liquid Chromatography Coupled to Tandem Mass Spectrometry

Veh: Vehicle

WD: Western Diet

WT: Wild Type

Chapter 1 – Introduction

The endocannabinoid (eCB) system consists of the endogenously produced lipid signaling ligands 2-arachidonoyl-*sn*-glycerol (2-AG) and anandamide (AEA), their receptors [cannabinoid receptor subtype-1 (CB_1R), -2 (CB_2R), and others], and the enzymatic machinery necessary to produce and degrade these lipids (Devane et al., 1992; Devane et al., 1987; DiPatrizio, 2021; Kaminski et al., 1992; Mechoulam et al., 1995). These eCBs are produced on demand from lipid precursors found in the plasma membrane of cells (DiPatrizio, 2021). Despite sharing activity at both CB_1R and CB_2R, 2-AG and AEA are produced and degraded via distinct pathways. The eCB 2-AG, and several other monoacylglycerol (MAG) species, is produced via diacylglycerol lipase (DGL) and is degraded by monoacylglycerol lipase (MGL) (Alexander & Kendall, 2007; DiPatrizio, 2021). Conversely, AEA-and many other fatty acid ethanolamides (FAEs)-is produced in a Ca^{2+} dependent manner involving both N-acyltransferase (NAT) and N-acyl phosphatidylethanolamide phospholipase-specific D (NAPE-PLD) and is further degraded via fatty acid amide hydrolase (FAAH) (Cadas et al., 1997; Cadas et al., 1996; Cravatt et al., 1996; Di Marzo et al., 1994; Wei et al., 2006). The eCB system is found throughout the human body and has been shown to be implicated in several different disease models. Activation of CB_1R has been shown to drive obesity and food seeking behavior through both central and peripheral mechanisms (Argueta & DiPatrizio, 2017; Argueta et al., 2019; Cardinal et al., 2012; Higuchi et al., 2012). However, CB_2R expression is largely found on immune tissue and activation is primarily associated with immunosuppression (Carayon et al., 1998; Galiègue et al., 1995; Pandey et al., 2009;

Turcotte et al., 2016). As methods of detection and disease models continue to develop, the potential role for the eCB system as a therapeutic target in human disease is ever expansive. Here, we discuss the role for the eCB system in several mucosal contexts including parasitic infections, eCB metabolism in mucosal tissue, and eCBs in diet-induced gut-barrier dysfunction and inflammatory bowel disease (IBD).

Parasitic Endocannabinoids

More than 1 billion humans are infected with helminths worldwide, with highly dense infection rates in regions of extreme poverty where healthcare and hygiene are underdeveloped (Hotez et al., 2008; Lynn et al., 2021; Weatherhead et al., 2017). Medical intervention is often required for clearance of infection with these parasites, which can lead to serious chronic comorbidities such as anemia and growth retardation (Batugedara, Li, et al., 2018; Bouchery et al., 2018; Hotez et al., 2008; Pine et al., 2018; Weatherhead et al., 2017). Parasitology research has led to the development of several anthelmintic drugs which effectively treat helminth infections through targeting the growth development of the worm (Holden-Dye & Walker, 2014). However, several of these compounds are highly susceptible to resistance, therefore more sustainable and accessible therapeutic options are necessary to treat individuals (Holden-Dye & Walker, 2014). Understanding host responses to parasitic infections provides useful insight in the development of novel therapeutics. Upon infection, antigen presenting cells (APC) will interact with and process parasitic antigens, the APC will then present this antigen to a naïve T-cell, polarizing the immune cell and stimulating a T-helper type 2 (Th2) immune response (Anthony et al., 2007; Holgate, 2012; Pine et al., 2018), This Th2 response

includes secretion of specific effector molecules (IgE, IL-4, IL-5, IL-13) which leads to increased recruitment and activation of eosinophils and alternatively activated macrophages (Anthony et al., 2007; Nutman, 2015).

This Th2 response provides an effective means for intestinal parasite clearance as it promotes what has been coined as, "weep and sweep" action in the gut (Anthony et al., 2007; Harris & Loke, 2017). Secretion of IL-5 from Th2 T-cells promotes eosinophil recruitment and activation to enhance clearance, while IL-4 and IL-13 promote both mucous secretion from intestinal goblet cells and smooth muscle activation in the gut (Anthony et al., 2007; Harris & Loke, 2017). The layer of mucous provides a barrier to inhibit parasitic attachment to the intestinal wall while eosinophilia promotes worm killing and smooth muscle contraction helps pass the worms out of the alimentary canal. Taken together, this creates an uninhabitable environment for the parasite.

Despite the advancements made in immunology and development of the "weep and sweep" theory, significant mechanisms of the Th2 immune response and host-parasite interactions remain largely unknown. The soil-transmitted nematode, *Nippostrongylus brasiliensis* (*N. brasiliensis*), infects rodents through similar mechanisms as soil-transmitted hookworms in humans, thereby providing a model for studying the Th2 response and host-parasite interactions (Bouchery et al., 2018; Haley, 1961). Rodents infected with *N. brasiliensis* recruit several eosinophils to the site of infection to promote worm clearance, similar to what is seen in helminth infection in humans (Knott et al., 2009). In addition, mice infected with *N. brasiliensis* display significant weight loss by 2 days post-infection (DPI) coupled to a reduction in food

intake, which is recovered by 5 DPI (Batugedara, Argueta, et al., 2018). At 5–6 DPI, *N. brasiliensis* migrates up the trachea and down the esophagus into the small intestine (jejunum), where they establish adulthood in the intestinal phase of infection (7–8 DPI) (Hawdon & Hotez, 1996). In the intestine, female *N. brasiliensis* releases fertilized eggs into the fecal matter for expulsion into the soil where the eggs hatch and their life cycle begins anew (Hawdon & Hotez, 1996).

Models such as *N. brasiliensis* have led to the elucidation of some of the host-parasite interactions and worm clearance (i.e. "weep and sweep"), however, recent evidence indicates these interactions are more complex than previously suspected (Anthony et al., 2007; Batugedara, Argueta, et al., 2018). It was recently reported that infection with *N. brasiliensis* leads to increased levels of the lipid signaling eCBs in the infected tissue (i.e. lung and jejunum epithelium) (Batugedara, Argueta, et al., 2018).. Pharmacological blockade of eCB signaling at peripheral CB_1R during the intestinal phase of *N. brasiliensis* infection (4-7 DPI) led to an increase in worm fecundity, decrease in IL-5 production in the small intestine and spleen, and a reduction in IL-4 and IL-10 production in the spleen (Batugedara, Argueta, et al., 2018). Consistent with these findings, longitudinal studies in humans showed associations between cannabis use and decreased helminth burden; however, whether the protective effect was from CB_1R signaling or a toxic effect of cannabis on the helminth is unclear (Roulette et al., 2016). The eCB receptors have been found on virtually all immune cells and their activation is generally associated with immunosuppression (Chiurchiu et al., 2015; Nagarkatti et al., 2009; Pandey et al., 2009). Furthermore, eCBs can readily be metabolized into

eicosanoids to mediate inflammatory processes providing a strong potential role for eCBs in parasitic infections (Alhouayek & Muccioli, 2014; Kozak et al., 2000; Kudalkar et al., 2016).

Strikingly, it was also found that *N. brasiliensis* is capable of producing the eCBs 2-AG and AEA at varying concentrations dependent upon their stage in life cycle (Batugedara, Argueta, et al., 2018). Whether or not these eCBs are being secreted by the worms and at a high enough concentration to act on host receptors remains unclear. Furthermore, functional cannabinoid receptors and/or enzymatic machinery necessary to degrade and produce these eCBs have not yet been identified in *N. brasiliensis* or any other helminth yet. Future studies identifying if these eCBs are being secreted into the microenvironment to mediate eicosanoid formation and/or eCB receptor activity may direct therapeutic development to manipulate lipid signaling in host-parasite interactions to promote clearance and host health.

Endocannabinoid Metabolism

Although the classical mechanism of eCB production and degradation has been identified, there are several alternative enzymes capable of metabolizing eCBs found throughout the human body which vary in activity and concentration based on tissue and cell type (Blankman et al., 2007; Bottemanne et al., 2019; DiPatrizio, 2021; Marrs et al., 2010; Piomelli et al., 2020; Tsuboi et al., 2018). The majority of production and degradation of several MAG species including 2-AG, 2-docosohexaenoylglycerol (2-DG), 2-pamitoylglycerol (2-PG), 2-oleoylglycerol (2-OG), and 2-linoleoylglycerol (2-

LG) are thought to be regulated by DGL and MGL respectively (Alexander & Kendall, 2007; DiPatrizio, 2021; Ghafouri et al., 2004). Studies have identified that alpha/beta serine hydrolase domain containing-6 and -12 are also capable of degrading 2-AG and MAGs (Fiskerstrand et al., 2010; Marrs et al., 2010; Savinainen et al., 2012). ABHD6 activity has been well characterized in rodent brain where it contributes 5-10% of total MAG metabolism in brain homogenates and ~50% of metabolism in neuronal cultures (Marrs et al., 2010; Savinainen et al., 2012). Furthermore, macrophages produce significant 2-AG in the presence of LPS and WWL 70-a specific inhibitor of ABHD6 activity-which suggests a substantial role for ABHD6 activity in these cells (Bottemanne et al., 2019). Macrophages are commonly found in several major organs throughout the human body (i.e. liver, lungs) providing a unique therapeutic target for manipulating lipid metabolism in specific cells and regions of the organism (Batugedara, Li, et al., 2018; Pine et al., 2018) Other studies suggest that mutations in ABHD12 may contribute to neurodegenerative diseases due to alterations in eCB metabolism (Fiskerstrand et al., 2010). Studies have identified unique enzymes found in yeast capable of metabolizing MAGs (Yju3p) which may be present in other organisms (i.e. *N. brasiliensis*) or in specific locations or cell types found in mammals (Heier et al., 2010).

Despite sharing activity at the same receptors (CB_1R and CB_2R), AEA-and many other FAEs-do not share metabolic processes. Production of FAEs such as AEA, docosohexaenoylethanolamide (DHEA), oleoylethanolamide (OEA), and palmitoylethanolamide (PEA) is governed by a multi-step process involving two unique enzymes (Cadas et al., 1997; Cadas et al., 1996; Di Marzo et al., 1994; Hussain et al.,

2017). N-acylphosphatidylethanolamine (NAPE), the precursor to several FAEs, is produced by the activity in NAT in a Ca^{2+} and cAMP-dependent manner (Hussain et al., 2017; Tsuboi et al., 2018). Fatty acids (i.e. arachidonate) are transferred from the sn-1 position of a phospholipid to the amino group of the phosphatidylethanolamine via NAT to produce distinct NAPEs, which are then hydrolyzed by NAPE-PLD to produce FAEs, including AEA (Cadas et al., 1997; Cadas et al., 1996; Di Marzo et al., 1994; Hussain et al., 2017; Tsuboi et al., 2018). The majority of FAE metabolism is thought to be regulated by FAAH, however there is increasing evidence the enzyme N-acylethanolamine acid amidase (NAAA) is also a major contributor to FAEs degradation (Piomelli et al., 2020; Scalvini et al., 2020). NAAA expression has been identified primarily in endosomal-lysosomal compartments of adaptive and innate immune cells (Piomelli et al., 2020; Tsuboi et al., 2018; Tsuboi et al., 2007).

Expression and activity of unique enzymes in specific cell types and tissues permits targeted therapeutic development to enhance or inhibit eCB/lipid metabolism in regions of interest. Direct pharmacological manipulation of CB_1R activity with, for example, globally-acting antagonists/inverse agonists (i.e., rimonabant) reduces body weight and improves a host of metabolic parameters in human obesity; however, these drugs reach the brain and can lead to psychiatric side effects that preclude their use in the clinic for the treatment of metabolic disease (Christensen et al., 2007). In contrast to directly targeting cannabinoid receptors, pharmacological manipulation of enzymes responsible for the biosynthesis or degradation of eCBs may provide a safe therapeutic strategy for treatment of a variety of disorders. Accordingly, reliable methods for

identifying tissue-specific changes in eCB turnover in several disease models is critical to directing targeted therapeutic development. Development of DIO has been shown to dysregulate the eCB system through both central and peripheral mechanisms, driving feeding behavior (Argueta & DiPatrizio, 2017; Argueta et al., 2019; Cardinal et al., 2012; Di Marzo et al., 2001; Higuchi et al., 2012). Several biochemical and molecular assays are commonly used to analyze eCB system activity, including qPCR-based analysis of gene expression for eCB system components (i.e. receptors and enzymes) (Argueta et al., 2019; Avalos et al., 2020). However, quantitation of gene expression does not provide a full characterization of the state of the eCB system in any given tissue. For example, DIO mice display elevated levels of 2-AG and other MAGs in the jejunum mucosa when compared to lean controls leading to an increase in eCB activity at local CB_1Rs which promotes overeating (Argueta et al., 2019). Surprisingly, gene expression of DGLβ in the small intestine mucosa was increased in DIO, however, *ex vivo* analysis of activity of DGL in these mice revealed an increase in the rate of DGL activity in the jejunum mucosa leading to an increase in 2-AG production (Argueta et al., 2019). Therefore, characterization of the eCB system in several disease models must be fully explored to determine the state of the lipid signaling system in the tissue of interest to further direct therapeutic development.

Endocannabinoids in Obesity and Inflammatory Bowel Disease

More than 70% of US adults are considered to be overweight or obese which contributes to more than 200 million dollars in costs to the US healthcare system (Hammond & Levine, 2010; Ogden et al., 2012). Obesity causes dysregulation of several

systems throughout the human body leading to comorbidities. Inflammatory bowel disease (IBD) is heavily associated with obesity with more than 2 million individuals diagnosed across North America (Ng et al., 2017). An over-active immune response compromises the barrier function of the intestinal tissue in IBD with idiopathic etiology (Bouma & Strober, 2003; Vancamelbeke & Vermeire, 2017). The gut-barrier is essential for protecting the organism from potentially harmful pathogens ingested via the alimentary canal and consists of 3 layers: 1) the mucous barrier consistent of IgA antibodies and mucins, 2) single cell layer of epithelial cells lining the entire small and large intestine, and 3) transmembrane tight junction proteins which provide protection from organisms and ions that can pass between epithelial cells (Vancamelbeke & Vermeire, 2017) (see Figure 1.1). Tight-junction protein assembly consists of several components including Zonula Occludin (ZO-1), Occludin, and Claudin family proteins (Krause et al., 2008; Vancamelbeke & Vermeire, 2017). Several claudins have been identified to contribute to barrier function including claudin-3, which helps to regulate cell-cell contact points between epithelial cells (Milatz et al., 2010). Claudin-15 regulates Na^+ and H_2O transport between epithelial cells which may contribute to the formation of a "leaky-gut" in DIO (Rosenthal et al., 2020) (see Figure 1.1). However, the function a few claudin family proteins (i.e. claudin-12) have not yet been elucidated.

It has been observed that IBD diagnosis rates have increased exclusively in well-developed regions of the world and the high-fat, high-sugar diets consumed in many well developed western civilizations may be contributing to this outcome (Actis et al., 2019; Martinez-Medina et al., 2014). Western diet-induced obesity has been shown to have

profound effects on eCB regulation throughout the organism (Argueta & DiPatrizio, 2017; DiPatrizio, 2021). Expression of the eCB system has been identified in the large intestine where its function is largely unknown (Lee et al., 2016; Wright et al., 2005). Activation of CB_1R on small intestinal enteroendocrine cells regulates release of the satiety hormone cholecystokinin (CCK), suggesting an essential role for CB_1R signaling on intestinal epithelial cell function (Argueta et al., 2019). Due to the enhanced inflammatory response in IBD models, several studies have implicated the role for CB_2R signaling in directly modulating the immune response (Acharya et al., 2017; Harvey et al., 2013; Harvey et al., 2014). The exact role for CB_1R signaling in gut-barrier function remains largely unknown due to conflicting results. Caco-2 cells display an exacerbated increase in permeability when eCBs are co-administered apically with inflammatory cytokines (Alhamoruni et al., 2012). Caco-2 cells exposed to the same inflammatory conditions display a decrease in permeability when an MGL inhibitor is applied basolaterally (Karwad et al., 2017). However, *ex vivo* experiments have shown that colonic tissue exposed to inflammatory cytokines have improved outcomes in colitis development when AEA is added, regardless of location (Harvey et al., 2013). Furthermore, CB_1R agonists and FAAH inhibitors improve outcomes of *in vivo* mouse models of colitis which are acting systemically (Massa et al., 2004). Conflicting results appear to be dependent upon receptor localization (basolateral vs. apical), the type of agonist used (synthetic vs. endogenous vs. phytocannabinoid), and the model used to induce disrupted gut-barrier function (Alhamoruni et al., 2010; Alhamoruni et al., 2012;

Karwad et al., 2017). Therefore, more research is necessary to identify the exact mechanism by which CB_1R signaling is contributing to gut-barrier function.

Currently accepted models studying IBD development often include the use of harsh chemicals (i.e. dextran sodium sulfate, DSS) which cause epithelial cell apoptosis along the intestinal tract stimulating a strong inflammatory response at the site of damage (Eichele & Kharbanda, 2017). Disruption of the gut-barrier via DIO provides a model for dysregulating paracellular permeability without compromising tissue architecture. Previous research found that DIO stimulates an increase in paracellular permeability in the large intestine through a down regulation of tight-junction protein expression (ZO-1, Occludin) and an increase in inflammatory makers (IL-6, TNFα, T-cell infiltrate) in the tissue (Lam et al., 2012; Lee et al., 2017). This provides an ideal model for identifying discrete changes in gut-barrier function which may be initiating changes in paracellular permeability in IBD. The specific diet that is used to recapitulate diet-induced gut-barrier dysfunction, however, should be carefully considered. Western diet is often used to induced DIO in rodents which is high in both fat and sugar, while other models employ high-fat only diets which can have differential effects throughout the organism. Diet has been identified as a key contributor to the microbiota populations that will thrive in the gut which can directly manipulate the inflammatory state of the tissue (Cani, 2016; Cani et al., 2016; Pujo et al., 2021). Future studies utilizing diet to compromise gut-barrier function should carefully consider the mechanism by which each diet may be contributing to both microbiota populations and ultimately gut-barrier function.

Conclusions

The eCB system is a multi-faceted complex lipid signaling system implicated in several models of disease. Elucidating the role for eCB signaling in parasitic infections and the Th2 immune response may drive therapeutic development surrounding host-parasite interactions. Furthermore, future studies should consider targeting enzymatic machinery as opposed to directly manipulating activity at the eCB receptors as this has been shown to have negative psychiatric side-effects. Lastly, the eCB system appears to be playing a vital role in moderating gut-barrier function, however the model for barrier function disruption plays a key role in determining the treatment outcomes. Therefore, identification of markers in circulation for the mechanism of gut-barrier dysfunction occurring in each patient is critical for determining if targeting the eCB system will provide beneficial outcomes for the individual.

References

Acharya, N., Penukonda, S., Shcheglova, T., Hagymasi, A. T., Basu, S., & Srivastava, P. K. (2017). Endocannabinoid system acts as a regulator of immune homeostasis in the gut. *Proc Natl Acad Sci U S A*, *114*(19), 5005-5010. https://doi.org/10.1073/pnas.1612177114

Actis, G. C., Pellicano, R., Fagoonee, S., & Ribaldone, D. G. (2019). History of Inflammatory Bowel Diseases. *J Clin Med*, *8*(11). https://doi.org/10.3390/jcm8111970

Alexander, S. P., & Kendall, D. A. (2007). The complications of promiscuity: endocannabinoid action and metabolism. *Br J Pharmacol*, *152*(5), 602-623. https://doi.org/10.1038/sj.bjp.0707456

Alhamoruni, A., Lee, A. C., Wright, K. L., Larvin, M., & O'Sullivan, S. E. (2010). Pharmacological effects of cannabinoids on the Caco-2 cell culture model of intestinal permeability. *J Pharmacol Exp Ther*, *335*(1), 92-102. https://doi.org/10.1124/jpet.110.168237

Alhamoruni, A., Wright, K. L., Larvin, M., & O'Sullivan, S. E. (2012). Cannabinoids mediate opposing effects on inflammation-induced intestinal permeability. *British Journal of Pharmacology*, *165*(8), 2598-2610. https://doi.org/10.1111/j.1476-5381.2011.01589.x

Alhouayek, M., & Muccioli, G. G. (2014). COX-2-derived endocannabinoid metabolites as novel inflammatory mediators. *Trends in Pharmacological Sciences*, *35*(6), 284-292. https://doi.org/10.1016/j.tips.2014.03.001

Anthony, R. M., Rutitzky, L. I., Urban, J. F., Stadecker, M. J., & Gause, W. C. (2007). Protective immune mechanisms in helminth infection. *Nat Rev Immunol*, *7*(12), 975-987. https://doi.org/10.1038/nri2199

Argueta, D. A., & DiPatrizio, N. V. (2017). Peripheral endocannabinoid signaling controls hyperphagia in western diet-induced obesity. *Physiol Behav*, *171*, 32-39. https://doi.org/10.1016/j.physbeh.2016.12.044

Argueta, D. A., Perez, P. A., Makriyannis, A., & DiPatrizio, N. V. (2019). Cannabinoid CB1 receptors inhibit gut-brain satiation signaling in diet-induced obesity. *Front Physiol*, *10*, 704. https://doi.org/10.3389/fphys.2019.00704

Avalos, B., Argueta, D. A., Perez, P. A., Wiley, M., Wood, C., & DiPatrizio, N. V. (2020). Cannabinoid CB1 receptors in the intestinal epithelium are required for

acute western-diet preferences in mice. *Nutrients*, *12*(9). https://doi.org/10.3390/nu12092874

Batugedara, H. M., Argueta, D., Jang, J. C., Lu, D., Macchietto, M., Kaur, J., Ge, S., Dillman, A. R., DiPatrizio, N. V., & Nair, M. G. (2018). Host and helminth-derived endocannabinoids are generated during infection with effects on host immunity. *Infect Immun*. https://doi.org/10.1128/iai.00441-18

Batugedara, H. M., Li, J., Chen, G., Lu, D., Patel, J. J., Jang, J. C., Radecki, K. C., Burr, A. C., Lo, D. D., Dillman, A. R., & Nair, M. G. (2018). Hematopoietic cell-derived RELMα regulates hookworm immunity through effects on macrophages. *J Leukoc Biol*, *104*(4), 855-869. https://doi.org/10.1002/jlb.4a0917-369rr

Blankman, J. L., Simon, G. M., & Cravatt, B. F. (2007). A comprehensive profile of brain enzymes that hydrolyze the endocannabinoid 2-arachidonoylglycerol. *Chem Biol*, *14*(12), 1347-1356. https://doi.org/10.1016/j.chembiol.2007.11.006

Bottemanne, P., Paquot, A., Ameraoui, H., Alhouayek, M., & Muccioli, G. G. (2019). The alpha/beta-hydrolase domain 6 inhibitor WWL70 decreases endotoxin-induced lung inflammation in mice, potential contribution of 2-arachidonoylglycerol, and lysoglycerophospholipids. *FASEB J*, *33*(6), 7635-7646. https://doi.org/10.1096/fj.201802259R

Bouchery, T., Filbey, K., Shepherd, A., Chandler, J., Patel, D., Schmidt, A., Camberis, M., Peignier, A., Smith, A. A. T., Johnston, K., Painter, G., Pearson, M., Giacomin, P., Loukas, A., Bottazzi, M. E., Hotez, P., & LeGros, G. (2018). A novel blood-feeding detoxification pathway in Nippostrongylus brasiliensis L3 reveals a potential checkpoint for arresting hookworm development. *PLoS Pathog*, *14*(3), e1006931. https://doi.org/10.1371/journal.ppat.1006931

Bouma, G., & Strober, W. (2003). The immunological and genetic basis of inflammatory bowel disease. *Nat Rev Immunol*, *3*(7), 521-533. https://doi.org/10.1038/nri1132

Cadas, H., di Tomaso, E., & Piomelli, D. (1997). Occurrence and biosynthesis of endogenous cannabinoid precursor, N-arachidonoyl phosphatidylethanolamine, in rat brain. *J Neurosci*, *17*(4), 1226-1242. https://www.ncbi.nlm.nih.gov/pubmed/9006968

Cadas, H., Gaillet, S., Beltramo, M., Venance, L., & Piomelli, D. (1996). Biosynthesis of an endogenous cannabinoid precursor in neurons and its control by calcium and cAMP. *J Neurosci*, *16*(12), 3934-3942. https://www.ncbi.nlm.nih.gov/pubmed/8656287

Cani, P. D. (2016). Interactions between gut microbes and host cells control gut barrier and metabolism. *Int J Obes Suppl*, *6*(Suppl 1), S28-S31. https://doi.org/10.1038/ijosup.2016.6

Cani, P. D., Plovier, H., Van Hul, M., Geurts, L., Delzenne, N. M., Druart, C., & Everard, A. (2016). Endocannabinoids - at the crossroads between the gut microbiota and host metabolism. *Nature Reviews Endocrinology*, *12*(3), 133-143. https://doi.org/10.1038/nrendo.2015.211

Carayon, P., Marchand, J., Dussossoy, D., Derocq, J. M., Jbilo, O., Bord, A., Bouaboula, M., Galiegue, S., Mondiere, P., Penarier, G., Le Fur, G., Defrance, T., & Casellas, P. (1998). Modulation and functional involvement of CB2 peripheral cannabinoid receptors during B-cell differentiation. *Blood*, *92*(10), 3605-3615. <Go to ISI>://WOS:000076962500015

Cardinal, P., Bellocchio, L., Clark, S., Cannich, A., Klugmann, M., Lutz, B., Marsicano, G., & Cota, D. (2012). Hypothalamic CB1 Cannabinoid Receptors Regulate Energy Balance in Mice. *Endocrinology*, *153*(9), 4136-4143. https://doi.org/10.1210/en.2012-1405

Chiurchiu, V., Battistini, L., & Maccarrone, M. (2015). Endocannabinoid signalling in innate and adaptive immunity. *Immunology*, *144*(3), 352-364. https://doi.org/10.1111/imm.12441

Christensen, R., Kristensen, P. K., Bartels, E. M., Bliddal, H., & Astrup, A. (2007). Efficacy and safety of the weight-loss drug rimonabant: a meta-analysis of randomised trials. *Lancet*, *370*(9600), 1706-1713. https://doi.org/10.1016/S0140-6736(07)61721-8

Cravatt, B. F., Giang, D. K., Mayfield, S. P., Boger, D. L., Lerner, R. A., & Gilula, N. B. (1996). Molecular characterization of an enzyme that degrades neuromodulatory fatty-acid amides. *Nature*, *384*(6604), 83-87. https://doi.org/10.1038/384083a0

Devane, W. A., Hanus, L., Breuer, A., Pertwee, R. G., Stevenson, L. A., Griffin, G., Gibson, D., Mandelbaum, A., Etinger, A., & Mechoulam, R. (1992). Isolation and structure of a brain constituent that binds to the cannabinoid receptor. *Science*, *258*(5090), 1946-1949. https://doi.org/10.1126/science.1470919

Devane, W. A., Howlett, A. C., Johnson, M. R., Melvin, L. S., & Milne, G. M. (1987). Structural studies leading to the discovery of a physiologically relevant cannabinoid receptor-site in rat-brain. *Abstracts of Papers of the American Chemical Society*, *194*, 17-MEDI. <Go to ISI>://WOS:A1987J291202505

Di Marzo, V., Fontana, A., Cadas, H., Schinelli, S., Cimino, G., Schwartz, J. C., & Piomelli, D. (1994). Formation and inactivation of endogenous cannabinoid anandamide in central neurons. *Nature*, *372*(6507), 686-691. https://doi.org/10.1038/372686a0

Di Marzo, V., Goparaju, S. K., Wang, L., Liu, J., Batkai, S., Jarai, Z., Fezza, F., Miura, G. I., Palmiter, R. D., Sugiura, T., & Kunos, G. (2001). Leptin-regulated endocannabinoids are involved in maintaining food intake. *Nature*, *410*(6830), 822-825. https://doi.org/10.1038/35071088

DiPatrizio, N. V. (2021). Endocannabinoids and the Gut-Brain Control of Food Intake and Obesity. *Nutrients*, *13*(4). https://doi.org/10.3390/nu13041214

Eichele, D. D., & Kharbanda, K. K. (2017). Dextran sodium sulfate colitis murine model: An indispensable tool for advancing our understanding of inflammatory bowel diseases pathogenesis. *World J Gastroenterol*, *23*(33), 6016-6029. https://doi.org/10.3748/wjg.v23.i33.6016

Fiskerstrand, T., H'mida-Ben Brahim, D., Johansson, S., M'zahem, A., Haukanes, B. I., Drouot, N., Zimmermann, J., Cole, A. J., Vedeler, C., Bredrup, C., Assoum, M., Tazir, M., Klockgether, T., Hamri, A., Steen, V. M., Boman, H., Bindoff, L. A., Koenig, M., & Knappskog, P. M. (2010). Mutations in ABHD12 cause the neurodegenerative disease PHARC: An inborn error of endocannabinoid metabolism. *Am J Hum Genet*, *87*(3), 410-417. https://doi.org/10.1016/j.ajhg.2010.08.002

Galiègue, S., Mary, S., Marchand, J., Dussossoy, D., Carrière, D., Carayon, P., Bouaboula, M., Shire, D., Le Fur, G., & Casellas, P. (1995). Expression of central and peripheral cannabinoid receptors in human immune tissues and leukocyte subpopulations. *Eur J Biochem*, *232*(1), 54-61. https://www.ncbi.nlm.nih.gov/pubmed/7556170

Ghafouri, N., Tiger, G., Razdan, R. K., Mahadevan, A., Pertwee, R. G., Martin, B. R., & Fowler, C. J. (2004). Inhibition of monoacylglycerol lipase and fatty acid amide hydrolase by analogues of 2-arachidonoylglycerol. *Br J Pharmacol*, *143*(6), 774-784. https://doi.org/10.1038/sj.bjp.0705948

Haley, A. J. (1961). Biology of the rat-nematode *Nippostrongylus brasiliensis*. Systematics, hosts, and geographic distribution. *Journal of Parasitology*, *47*(5), 727-731. https://doi.org/10.2307/3275460

Hammond, R. A., & Levine, R. (2010). The economic impact of obesity in the United States. *Diabetes Metab Syndr Obes*, *3*, 285-295. https://doi.org/10.2147/dmsott.S7384

Harris, N. L., & Loke, P. (2017). Recent Advances in Type-2-Cell-Mediated Immunity: Insights from Helminth Infection. *Immunity*, *47*(6), 1024-1036. https://doi.org/10.1016/j.immuni.2017.11.015

Harvey, B. S., Nicotra, L. L., Vu, M., & Smid, S. D. (2013). Cannabinoid CB2 receptor activation attenuates cytokine-evoked mucosal damage in a human colonic explant model without changing epithelial permeability. *Cytokine*, *63*(2), 209-217. https://doi.org/10.1016/j.cyto.2013.04.032

Harvey, B. S., Sia, T. C., Wattchow, D. A., & Smid, S. D. (2014). Interleukin 17A evoked mucosal damage is attenuated by cannabidiol and anandamide in a human colonic explant model. *Cytokine*, *65*(2), 236-244. https://doi.org/10.1016/j.cyto.2013.10.006

Hawdon, J. M., & Hotez, P. J. (1996). Hookworm: developmental biology of the infectious process. *Curr Opin Genet Dev*, *6*(5), 618-623. https://www.ncbi.nlm.nih.gov/pubmed/8939719

Heier, C., Taschler, U., Rengachari, S., Oberer, M., Wolinski, H., Natter, K., Kohlwein, S. D., Leber, R., & Zimmermann, R. (2010). Identification of Yju3p as functional orthologue of mammalian monoglyceride lipase in the yeast Saccharomycescerevisiae. *Biochim Biophys Acta*, *1801*(9), 1063-1071. https://doi.org/10.1016/j.bbalip.2010.06.001

Higuchi, S., Irie, K., Yamaguchi, R., Katsuki, M., Araki, M., Ohji, M., Hayakawa, K., Mishima, S., Akitake, Y., Matsuyama, K., Mishima, K., Iwasaki, K., & Fujiwara, M. (2012). Hypothalamic 2-arachidonoylglycerol regulates multistage process of high-fat diet preferences. *PLoS One*, *7*(6), e38609. https://doi.org/10.1371/journal.pone.0038609

Holden-Dye, L., & Walker, R. J. (2014). Anthelmintic drugs and nematicides: studies in Caenorhabditis elegans. *WormBook*, 1-29. https://doi.org/10.1895/wormbook.1.143.2

Holgate, S. T. (2012). Innate and adaptive immune responses in asthma. *Nat Med*, *18*(5), 673-683. https://doi.org/10.1038/nm.2731

Hotez, P. J., Brindley, P. J., Bethony, J. M., King, C. H., Pearce, E. J., & Jacobson, J. (2008). Helminth infections: the great neglected tropical diseases. *J Clin Invest*, *118*(4), 1311-1321. https://doi.org/10.1172/jci34261

Hussain, Z., Uyama, T., Tsuboi, K., & Ueda, N. (2017). Mammalian enzymes responsible for the biosynthesis of N-acylethanolamines. *Biochim Biophys Acta Mol Cell Biol Lipids*, *1862*(12), 1546-1561. https://doi.org/10.1016/j.bbalip.2017.08.006

Kaminski, N. E., Abood, M. E., Kessler, F. K., Martin, B. R., & Schatz, A. R. (1992). Identification of a functionally relevant cannabinoid receptor on mouse spleen-cells that is involved in cannabinoid-mediated immune modulation. *Molecular Pharmacology*, *42*(5), 736-742. <Go to ISI>://WOS:A1992JY34200002

Karwad, M. A., Couch, D. G., Theophilidou, E., Sarmad, S., Barrett, D. A., Larvin, M., Wright, K. L., Lund, J. N., & O'Sullivan, S. E. (2017). The role of CB1 in intestinal permeability and inflammation. *Faseb Journal*, *31*(8), 3267-3277. https://doi.org/10.1096/fj.201601346R

Knott, M. L., Matthaei, K. I., Foster, P. S., & Dent, L. A. (2009). The roles of eotaxin and the STAT6 signalling pathway in eosinophil recruitment and host resistance to the nematodes Nippostrongylus brasiliensis and Heligmosomoides bakeri. *Mol Immunol*, *46*(13), 2714-2722. https://doi.org/10.1016/j.molimm.2009.05.016

Kozak, K. R., Rowlinson, S. W., & Marnett, L. J. (2000). Oxygenation of the endocannabinoid, 2-arachidonylglycerol, to glyceryl prostaglandins by cyclooxygenase-2. *Journal of Biological Chemistry*, *275*(43), 33744-33749. https://doi.org/10.1074/jbc.M007088200

Krause, G., Winkler, L., Mueller, S. L., Haseloff, R. F., Piontek, J., & Blasig, I. E. (2008). Structure and function of claudins. *Biochim Biophys Acta*, *1778*(3), 631-645. https://doi.org/10.1016/j.bbamem.2007.10.018

Kudalkar, S. N., Kingsley, P. J., & Marnett, L. J. (2016). Assay of Endocannabinoid Oxidation by Cyclooxygenase-2. *Endocannabinoid Signaling: Methods and Protocols, 1412*, 205-215. https://doi.org/10.1007/978-1-4939-3539-0_21

Lam, Y. Y., Ha, C. W., Campbell, C. R., Mitchell, A. J., Dinudom, A., Oscarsson, J., Cook, D. I., Hunt, N. H., Caterson, I. D., Holmes, A. J., & Storlien, L. H. (2012). Increased gut permeability and microbiota change associate with mesenteric fat inflammation and metabolic dysfunction in diet-induced obese mice. *PLoS One*, *7*(3), e34233. https://doi.org/10.1371/journal.pone.0034233

Lee, J. C., Lee, H. Y., Kim, T. K., Kim, M. S., Park, Y. M., Kim, J., Park, K., Kweon, M. N., Kim, S. H., Bae, J. W., Hur, K. Y., & Lee, M. S. (2017). Obesogenic diet-induced gut barrier dysfunction and pathobiont expansion aggravate experimental colitis. *PLoS One*, *12*(11), e0187515. https://doi.org/10.1371/journal.pone.0187515

Lee, Y., Jo, J., Chung, H. Y., Pothoulakis, C., & Im, E. (2016). Endocannabinoids in the gastrointestinal tract. *Am J Physiol Gastrointest Liver Physiol*, *311*(4), G655-G666. https://doi.org/10.1152/ajpgi.00294.2015

Lynn, M. K., Morrissey, J. A., & Conserve, D. F. (2021). Soil-Transmitted Helminths in the USA: a Review of Five Common Parasites and Future Directions for Avenues of Enhanced Epidemiologic Inquiry. *Curr Trop Med Rep*, 1-11. https://doi.org/10.1007/s40475-020-00221-2

Marrs, W. R., Blankman, J. L., Horne, E. A., Thomazeau, A., Lin, Y. H., Coy, J., Bodor, A. L., Muccioli, G. G., Hu, S. S., Woodruff, G., Fung, S., Lafourcade, M., Alexander, J. P., Long, J. Z., Li, W., Xu, C., Möller, T., Mackie, K., Manzoni, O. J., Cravatt, B. F., & Stella, N. (2010). The serine hydrolase ABHD6 controls the accumulation and efficacy of 2-AG at cannabinoid receptors. *Nat Neurosci*, *13*(8), 951-957. https://doi.org/10.1038/nn.2601

Martinez-Medina, M., Denizot, J., Dreux, N., Robin, F., Billard, E., Bonnet, R., Darfeuille-Michaud, A., & Barnich, N. (2014). Western diet induces dysbiosis with increased E coli in CEABAC10 mice, alters host barrier function favouring AIEC colonisation. *Gut*, *63*(1), 116-124. https://doi.org/10.1136/gutjnl-2012-304119

Massa, F., Marsicano, G., Hermann, H., Cannich, A., Monory, K., Cravatt, B. F., Ferri, G. L., Sibaev, A., Storr, M., & Lutz, B. (2004). The endogenous cannabinoid system protects against colonic inflammation. *J Clin Invest*, *113*(8), 1202-1209. https://doi.org/10.1172/jci19465

Mechoulam, R., Benshabat, S., Hanus, L., Ligumsky, M., Kaminski, N. E., Schatz, A. R., Gopher, A., Almog, S., Martin, B. R., Compton, D. R., Pertwee, R. G., Griffin, G., Bayewitch, M., Barg, J., & Vogel, Z. (1995). Identification of an endogenous 2-monoglyceride, present in canine gut, that binds to cannabinoid receptors. *Biochemical Pharmacology*, *50*(1), 83-90. https://doi.org/10.1016/0006-2952(95)00109-d

Milatz, S., Krug, S. M., Rosenthal, R., Gunzel, D., Muller, D., Schulzke, J. D., Amasheh, S., & Fromm, M. (2010). Claudin-3 acts as a sealing component of the tight junction for ions of either charge and uncharged solutes. *Biochim Biophys Acta*, *1798*(11), 2048-2057. https://doi.org/10.1016/j.bbamem.2010.07.014

Nagarkatti, P., Pandey, R., Rieder, S. A., Hegde, V. L., & Nagarkatti, M. (2009). Cannabinoids as novel anti-inflammatory drugs. *Future Med Chem*, *1*(7), 1333-1349. https://doi.org/10.4155/fmc.09.93

Ng, S. C., Shi, H. Y., Hamidi, N., Underwood, F. E., Tang, W., Benchimol, E. I., Panaccione, R., Ghosh, S., Wu, J. C. Y., Chan, F. K. L., Sung, J. J. Y., & Kaplan, G. G. (2017). Worldwide incidence and prevalence of inflammatory bowel disease in the 21st century: a systematic review of population-based studies. *Lancet*, *390*(10114), 2769-2778. https://doi.org/10.1016/S0140-6736(17)32448-0

Nutman, T. B. (2015). Looking beyond the induction of Th2 responses to explain immunomodulation by helminths. *Parasite Immunol*, *37*(6), 304-313. https://doi.org/10.1111/pim.12194

Ogden, C. L., Carroll, M. D., Kit, B. K., & Flegal, K. M. (2012). Prevalence of obesity in the United States, 2009-2010. *NCHS Data Brief*(82), 1-8. https://www.ncbi.nlm.nih.gov/pubmed/22617494

Pandey, R., Mousawy, K., Nagarkatti, M., & Nagarkatti, P. (2009). Endocannabinoids and immune regulation. *Pharmacological Research*, *60*(2), 85-92. https://doi.org/10.1016/j.phrs.2009.03.019

Pine, G. M., Batugedara, H. M., & Nair, M. G. (2018). Here, there and everywhere: Resistin-like molecules in infection, inflammation, and metabolic disorders. *Cytokine*, *110*, 442-451. https://doi.org/10.1016/j.cyto.2018.05.014

Piomelli, D., Scalvini, L., Fotio, Y., Lodola, A., Spadoni, G., Tarzia, G., & Mor, M. (2020). N-Acylethanolamine Acid Amidase (NAAA): Structure, Function, and Inhibition. *J Med Chem*, *63*(14), 7475-7490. https://doi.org/10.1021/acs.jmedchem.0c00191

Pujo, J., Petitfils, C., Le Faouder, P., Eeckhaut, V., Payros, G., Maurel, S., Perez-Berezo, T., Van Hul, M., Barreau, F., Blanpied, C., Chavanas, S., Van Immerseel, F., Bertrand-Michel, J., Oswald, E., Knauf, C., Dietrich, G., Cani, P. D., & Cenac, N. (2021). Bacteria-derived long chain fatty acid exhibits anti-inflammatory properties in colitis. *Gut*, *70*(6), 1088-1097. https://doi.org/10.1136/gutjnl-2020-321173

Rosenthal, R., Gunzel, D., Piontek, J., Krug, S. M., Ayala-Torres, C., Hempel, C., Theune, D., & Fromm, M. (2020). Claudin-15 forms a water channel through the tight junction with distinct function compared to claudin-2. *Acta Physiol (Oxf)*, *228*(1), e13334. https://doi.org/10.1111/apha.13334

Roulette, C. J., Kazanji, M., Breurec, S., & Hagen, E. H. (2016). High prevalence of cannabis use among Aka foragers of the Congo Basin and its possible relationship to helminthiasis. *Am J Hum Biol*, *28*(1), 5-15. https://doi.org/10.1002/ajhb.22740

Savinainen, J. R., Saario, S. M., & Laitinen, J. T. (2012). The serine hydrolases MAGL, ABHD6 and ABHD12 as guardians of 2-arachidonoylglycerol signalling through cannabinoid receptors. *Acta Physiol (Oxf)*, *204*(2), 267-276. https://doi.org/10.1111/j.1748-1716.2011.02280.x

Scalvini, L., Ghidini, A., Lodola, A., Callegari, D., Rivara, S., Piomelli, D., & Mor, M. (2020). N-Acylethanolamine Acid Amidase (NAAA): Mechanism of

Palmitoylethanolamide Hydrolysis Revealed by Mechanistic Simulations. *ACS Catalysis*, *10*(20), 11797-11813.

Tsuboi, K., Uyama, T., Okamoto, Y., & Ueda, N. (2018). Endocannabinoids and related N-acylethanolamines: biological activities and metabolism. *Inflamm Regen*, *38*, 28. https://doi.org/10.1186/s41232-018-0086-5

Tsuboi, K., Zhao, L. Y., Okamoto, Y., Araki, N., Ueno, M., Sakamoto, H., & Ueda, N. (2007). Predominant expression of lysosomal N-acylethanolamine-hydrolyzing acid amidase in macrophages revealed by immunochemical studies. *Biochim Biophys Acta*, *1771*(5), 623-632. https://doi.org/10.1016/j.bbalip.2007.03.005

Turcotte, C., Blanchet, M. R., Laviolette, M., & Flamand, N. (2016). The CB2 receptor and its role as a regulator of inflammation. *Cell Mol Life Sci*, *73*(23), 4449-4470. https://doi.org/10.1007/s00018-016-2300-4

Vancamelbeke, M., & Vermeire, S. (2017). The intestinal barrier: a fundamental role in health and disease. *Expert Rev Gastroenterol Hepatol*, *11*(9), 821-834. https://doi.org/10.1080/17474124.2017.1343143

Weatherhead, J. E., Hotez, P. J., & Mejia, R. (2017). The Global State of Helminth Control and Elimination in Children. *Pediatr Clin North Am*, *64*(4), 867-877. https://doi.org/10.1016/j.pcl.2017.03.005

Wei, B. Q., Mikkelsen, T. S., McKinney, M. K., Lander, E. S., & Cravatt, B. F. (2006). A second fatty acid amide hydrolase with variable distribution among placental mammals. *J Biol Chem*, *281*(48), 36569-36578. https://doi.org/10.1074/jbc.M606646200

Wright, K., Rooney, N., Feeney, M., Tate, J., Robertson, D., Welham, M., & Ward, S. (2005). Differential expression of cannabinoid receptors in the human colon: cannabinoids promote epithelial wound healing. *Gastroenterology*, *129*(2), 437-453. https://doi.org/10.1016/j.gastro.2005.05.026

Tables and Figures

Figure 1.1

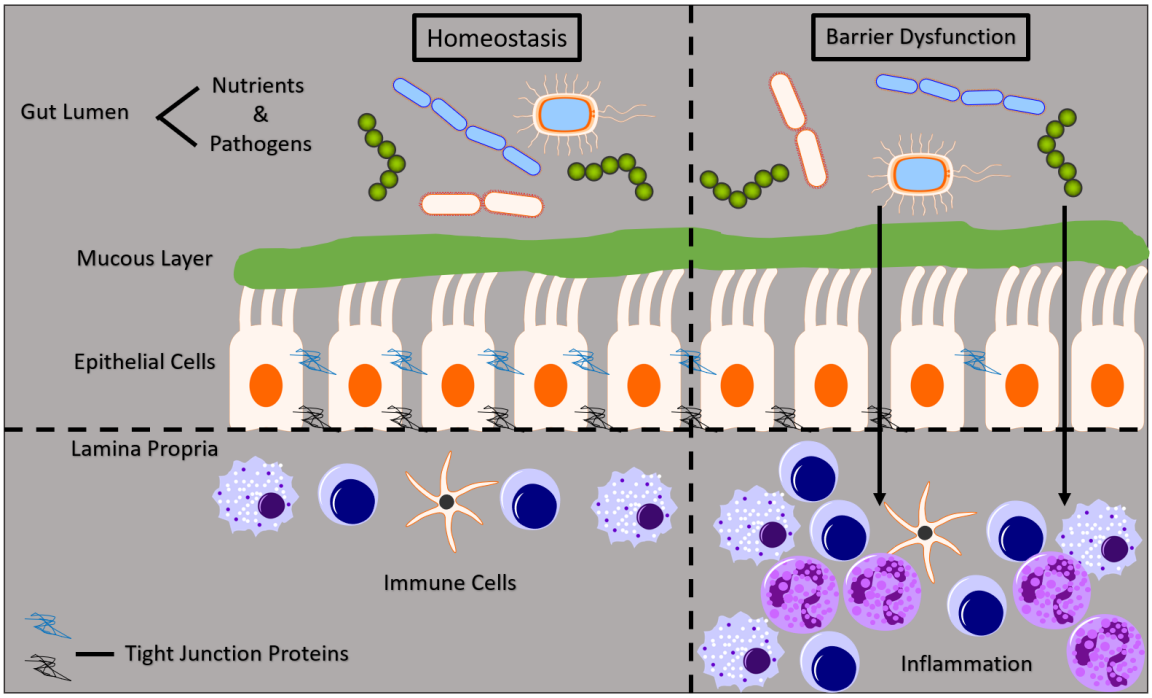

Figure 1.1: The gut-barrier consists of three layers: the mucous layer, epithelial cell layer, and tight-junction proteins anchoring the epithelial cells together (left). These layers keep pathogens from exiting the alimentary canal and into tissue/circulation where they can stimulate inflammation and damage. In DIO, tight-junction protein expression becomes dysregulated which may permit pathogens to enter the tissue and stimulate an inflammatory response in the gut (right).

Chapter 2 – Cannabinoid Receptor Subtype-1 Regulates Allergic Airway Eosinophilia During Lung Helminth Infection

Abstract

Over 1 billion humans carry infectious helminth parasites that can lead to chronic comorbidities such as anemia and growth retardation in children. Helminths induce a T-helper type 2 (Th2) immune response in the host and can cause severe tissue damage and fibrosis if chronic. We recently reported that mice infected with the soil-transmitted helminth, *Nippostrongylus brasiliensis*, displayed elevated levels of endocannabinoids (eCBs) in the lung and intestine. eCBs are lipid-signaling molecules that control inflammation; however, their function in infection is not well defined. A combination of pharmacological approaches and genetic mouse models was used to investigate roles for the eCB system in inflammatory responses and lung injury in mice during parasitic infection with *N. brasiliensis*. Hemorrhaging of lung tissue in mice infected with *N. brasiliensis* was exacerbated by inhibiting peripheral cannabinoid receptor subtype-1 (CB_1Rs) with the peripherally restricted CB_1R antagonist, AM6545. In addition, these mice exhibited an increase in nonfunctional alveolar space and prolonged airway eosinophilia compared to vehicle-treated infected mice. In contrast to mice treated with AM6545, infected cannabinoid receptor subtype-2-null mice ($Cnr2^{-/-}$) did not display any changes in these parameters compared to wildtype mice. Roles for the eCB system in Th2 immune responses are not well understood; however, increases in its activity in response

to infection suggest an immunomodulatory role. Moreover, these findings suggest a role for eCB signaling at CB_1Rs but not cannabinoid receptor subtypes-2 in the resolution of Th2 inflammatory responses, which become host destructive over time.

Introduction

It is estimated that more than 1 billion humans are infected with helminths worldwide, with high prevalence in impoverished regions (Weatherhead et al., 2017). Infection with these parasites can lead to serious chronic comorbidities such as growth retardation and anemia (Bouchery et al., 2018; Hotez, 2008; Weatherhead et al., 2017). In addition, infection leads to a T-helper type 2 (Th2) host immune response to enhance clearance; however, many parasitic infections are chronic in nature and require medical intervention (Batugedara, Li, et al., 2018; Pine et al., 2018). Indeed, chronic tissue inflammation may lead to severe fibrosis and limit the functional capacity of the tissue. This Th2 response includes recruitment of several effector immune cells, including eosinophils, which contribute to the pathogenesis of allergies and asthma, and identifying factors that regulate this response is essential for improving therapeutics for parasitic infections (Hirahara et al., 2019; Holgate, 2012).

One model of parasitic infection used by our group and others is the soil-transmitted nematode, *Nippostrongylus brasiliensis*, which infects rodents through similar mechanisms as soil-transmitted hookworms in humans (Bouchery et al., 2018; Jang et al., 2015). Subcutaneous infection permits *N. brasiliensis* to enter circulation and

migrate to the lungs by 2 days post-infection (DPI) where *N. brasiliensis* ingests host red blood cells to fuel their development, which can lead to anemia (Bouchery et al., 2018).

Rodents infected with *N. brasiliensis* recruit several eosinophils to the site of infection to promote worm clearance, similar to what is seen in helminth infection in humans (Knott et al., 2009). In addition, mice infected with *N. brasiliensis* display significant weight loss by 2 DPI coupled to a reduction in food intake, which is recovered by 5 DPI (Batugedara, Argueta, et al., 2018). At 5–6 DPI, *N. brasiliensis* migrates up the trachea and down the esophagus into the small intestine (jejunum), where they establish adulthood in the intestinal phase of infection (7–8 DPI) (Hawdon & Hotez, 1996). In the intestine, female *N. brasiliensis* releases fertilized eggs into the fecal matter for expulsion into the soil where the eggs hatch and their life cycle begins anew (Hawdon & Hotez, 1996).

We reported that *N. brasiliensis* infection was associated with increased levels of the endocannabinoids (eCBs) in infected organs (i.e., lung and jejunum epithelium), and pharmacological inhibition of eCB signaling at peripheral cannabinoid receptor subtype-1 (CB_1Rs) during the intestinal phase exacerbated metrics of infection, which suggests that CB_1R signaling may be host protective (Batugedara, Argueta, et al., 2018). Consistent with these findings, longitudinal studies in humans showed associations between cannabis use and decreased helminth burden; however, whether the protective effect was from CB_1R signaling or a toxic effect of cannabis on the helminth is unclear (Roulette et al., 2016). In this study, we explored the role of endogenous cannabinoids (eCBs) in soil-transmitted helminth infections.

The eCBs, 2-arachidonoyl-sn-glycerol (2-AG) and anandamide, are bioactive lipids that bind and activate CB_1R and cannabinoid receptor subtype-2 (CB_2R) on cells throughout the body where they regulate numerous physiological functions, including inflammation (Argueta & DiPatrizio, 2017; Avalos et al., 2020; DiPatrizio, 2016; DiPatrizio & Piomelli, 2012). Furthermore, these receptors are expressed on several immune cell subpopulations, including eosinophils (Galiègue et al., 1995). Indeed, chemotaxis stimulated by interleukin-5 is enhanced in eosinophils that were cotreated with 2-AG in a CB_2R-dependent manner (Galiègue et al., 1995; Larose et al., 2014). Pharmacological activation of CB_2Rs on eosinophils, however, failed to elicit the same response, suggesting a potential role for eicosanoids, which have been shown to contribute to eosinophil migration (Powell & Rokach, 2013). Moreover, genetic deletion of CB_1Rs and CB_2Rs had no effect on ovalbumin-stimulated lung eosinophilia in a mouse model of asthma, which suggests that eCB signaling at these receptors may not be required in associated allergic responses (Kaplan et al., 2010). Nonetheless, activation of cannabinoid receptors on a variety of immune cells has been linked to immunosuppression; however, these effects are cell specific and context dependent (Nagarkatti et al., 2009; Pandey et al., 2009). Despite these limited studies, specific roles for the eCB system in parasitic infections remain largely unknown. We now investigated roles for the eCB system in inflammatory responses and lung injury during parasitic infection.

Materials and Methods

Mice and Chemicals

C57BL/6 wild-type (WT) and $Cnr2^{-/-}$ male mice were purchased from the Jackson Laboratory or bred inhouse. All mice in experiments were age-matched (6- to 10-week-old) males given ad libitum access to a standard rodent chow. Mice were placed into single housing units (TSE Systems, Chesterfield, MO) 3 days before recording feeding behavior to allow for acclimation. Daily feeding was monitored using PhenoMaster software (TSE Systems). Mice in the CB_1R blockade experiments received intraperitoneal injections of vehicle control (7.5% dimethyl sulfoxide, 7.5% Tween 80, and 85% saline) or AM6545 (10 mg/kg/2 mL vehicle; Cayman Chemical, Ann Arbor, MI) 1 day before infection and everyday thereafter up to the day of harvest. All protocols for animal use and euthanasia were approved by the University of California Riverside Institutional Animal Care and Use Committee (protocols A-20200023 and A-20180023) and were in accordance with National Institutes of Health guidelines, the Animal Welfare Act, and Public Health Service Policy on Humane Care and Use of Laboratory Animals.

Infection

N. brasiliensis nematodes were obtained from the laboratory of Graham Le Gros (Malaghan Institute, New Zealand), and the life cycle was maintained in Sprague-Dawley rats (Harlan Laboratories) as previously described (Batugedara, Argueta, et al., 2018; Jang et al., 2015). Rat fecal matter containing *N. brasiliensis* eggs was cultured for 1–2 weeks and hatched, and infectious L3 larvae were recovered using Baermann apparatus.

Mice were anesthetized with isoflurane and received a subcutaneous injection of 500–750 infective L3 *N. brasiliensis* larvae suspended in 1X phosphate buffered saline (PBS). During the intestinal phase of infection (7–8 DPI) mice were euthanized using CO_2 asphyxiation, and the small intestine was removed and cut longitudinally before incubating in 1X PBS at 37^{O}C for 2 h to permit parasite migration out of the tissue. The number of worms was then manually quantified under a light microscope. Mice were placed into temporary single housing cages for 5–10 min (sufficient time for defecation to occur), and fecal matter was collected into pre-weighed tubes filled with 1X PBS. This mixture was homogenized, through pipetting, in a 1X PBS solution saturated with salt (NaCl), which permitted the eggs in the solution to float to the top. This mixture was added to the McMaster counting chamber for quantification under a light microscope as previously described (Batugedara, Argueta, et al., 2018; Batugedara, Li, et al., 2018; Jang et al., 2015). The experimenter was blinded to conditions associated with counting worms and egg burden.

Tissue Collection, Sample Processing, and Flow Cytometry

Cells recovered, at the time of harvest, from a bronchoalveolar lavage (BAL) were collected from both the left and right lungs through three sequential washes with 0.8 mL of 1X PBS. Two hundred microliters of the BAL fluid was quantified for hemorrhaging through plate reading using a Varioskan Lux (Thermo Scientific) at 540 nm as previously described (Meng & Alayash, 2017). The BAL fluid was treated with ammonium-chloride-potassium (ACK) lysis buffer, and cells were isolated by centrifugation. Blocking occurred using 10 lg/mL rat immunoglobulin G and 5 lg/mL

anti-CD16/32 (2.4G2) and stained using antibodies (25 min, 4C, 1:400 dilution in 50 µL fluorescence-activated cell sorting buffer) for SiglecF (E50-2440) and CD11c (N418) (all from BD Bioscience). Cells were washed then analyzed on an LSR II instrument (BD Biosciences), and data analysis was performed using FlowJo v10 (Tree Star, Inc.). Cell populations were identified as macrophages ($CD11c^{+}SiglecF^{+}$) and eosinophils ($CD11c^{-}SiglecF^{+}$).

Histology

Lungs were recovered for histological sectioning as previously described (Batugedara, Li, et al., 2018). Following recovery of the BAL fluid, lungs were inflated with fixative (0.8 mL): one part 4% paraformaldehyde (PFA)/30% sucrose in 1X PBS and two parts optimal cutting temperature embedding medium (Fisher Scientific). Recovery of the BAL fluid before inflation with fixative removed all blood cells from the lung air spaces; therefore, little to no red blood cells outside the vasculature were observed in the images. Lungs were stored for 24 h in 4% PFA (15 mL) followed by a 48 h incubation in 30% sucrose (20 mL). Lungs were then blocked and sectioned at 8 µm and stained with hematoxylin and eosin. Sections were visualized under a DM5500B microscope (Leica).

Histological Quantifications

One to three images per animal were taken at 4X in the lower left lobe of the left lung and used for all methods of image analysis. Infection with *N. brasiliensis* affects the whole lung and not specific regions (Marsland et al., 2008); therefore, the most easily

identifiable region of the lungs (lower left lobe of the left lung) was chosen as the representative area to evaluate while ensuring consistency across all images. The investigator was blinded to conditions throughout all methods of analysis. Mean linear intercept (MLI) was performed as previously described (Chen et al., 2020; Sutherland et al., 2018) Using QuPath open source software v0.2.1, a grid with x- and y-spacing maintained at 15 mm was laid across the image, and y-intercepts were manually counted across 10 lines. The MLI was calculated as follows:

$MLI = \sum Line\ Lengths\ (mm) + \sum intercepts$. Nonfunctional alveolar space was quantitated using the same images used for MLI, and measurements (mm) of the nonfunctional space were performed using QuPath open source software's ''wand tool'' and ''polygon'' functions. Inclusion criteria: any open space not connected to an airway was included, and measurements > 70.00 mm^2 were included to ensure that nonpathological measurements were utilized. This method of analysis permitted for quantitation of average area of nonfunctional alveolar space and total area of nonfunctional alveolar space.

Statistical Analysis

Data were analyzed by GraphPad Prism 8 software using unpaired Student's t-tests (two-tailed) and regular or repeated measures two-way analysis of variances with Newman–Keuls or Sidak's multiple comparisons post hoc test, respectively, when appropriate. Results are expressed as mean ± standard error of the mean, and significance was determined at $p < 0.05$.

Results

CB_1R Blockade Exacerbates Lung Hemorrhaging in *N. brasiliensis* Infection

Compared to vehicle-treated mice infected with *N. brasiliensis*, blockade of peripheral CB_1Rs with the peripherally-restricted CB_1R antagonist, AM6545 (10 mg/kg), throughout *N. brasiliensis* infection exacerbated hemorrhaging (Figure 2.1A, from 0.515 – 0.099 AU to 0.338 – 0.064 AU; n = 21/19, respectively, $p < 0.05$). Compared to infected WT mice, no changes in hemorrhaging were observed in infected $Cnr2^{-/-}$ mice (Figure 2.1B, from 0.427 – 0.111 AU to0.359 – 0.124 AU; n = 9, $p > 0.05$). No changes in infection-induced weight loss were observed in infected mice treated with AM6545, compared to vehicle treatment (Figure 2.1C), or in global $Cnr2^{-/-}$ mice, compared to WT (Figure 2.1D). The transient weight loss was coupled to hypophagia at 2 DPI and returned to baseline by 4 DPI regardless of treatment or genotype (Figure 2.1E, F).

CB_1R Blockade Exacerbates Lung Tissue Damage

Representative images (4x) of lung tissue samples used for image analysis in all groups are provided in Figure 2.2A-H. Representative images at a higher magnification (20x) are provided in Figure 2.3A-H. Compared to vehicle treatment, MLI was increased in *N. brasiliensis* infected mice treated with AM6545 (Figure 2.2I, from 0.451 – 0.021 mm/int to 0.678 – 0.103 mm/int; n = 14/13, respectively, $p = 0.0123$). In contrast to AM6545-treated mice, no change in MLI was found between infected WT and $Cnr2^{-/-}$ mice (Figure 2.2J, from 0.439 – 0.014mm/int to 0.440 – 0.007 mm/int; n = 8, $p = 0.937$).

A secondary method of quantitation confirmed that, compared to vehicle-treated mice infected with *N. brasiliensis*, infected mice treated with AM6545 displayed an increase in total and average nonfunctional alveolar space (Figure 2.4A, total: from 7309 – 482mm^2 to 11,762 – 1,036mm^2, $p < 0.001$; Figure 2.4B, average: from Avg: 190.2 – 3.9mm^2 to 318.7 – 26.1mm^2, $p < 0.001$). In contrast to AM6545-treated mice, no change in total and average nonfunctional alveolar space was found between infected WT and Cnr2$^{-/-}$ mice (Figure 2.4C, total: from 5250 – 623mm^2 to 6254 – 675mm^2, $p = 0.329$; Figure 2.4D, average: from 334.5 – 35.9mm^2 to 374.3 – 33.8mm^2, $p = 0.771$).

Inhibition of Peripheral CB$_1$Rs Leads to Increased Airway Eosinophilia

Alveolar macrophages were gated as SiglecF$^+$CD11c$^+$, while eosinophils were SiglecF$^+$CD11c$^-$ as displayed in the representative flow plots from each condition (Figure 2.5A–D) (Stevens et al., 2007). Alveolar macrophages were the main cell population in the naive BAL, and frequency was reduced following *N. brasiliensis* infection due to an increase in infiltrating eosinophils (Figure 2.5G, J). Compared to vehicle treatment in *N. brasiliensis* infected mice, treatment with AM6545 throughout infection significantly increased the frequency (Figure 2.5E, from 10.7 – 1.6% to 16.1 – 1.9%; $n = 21$, $p < 0.01$) and number (Figure 2.5F, from 1.8e3 – 3.3e2 cells to 3.6e3 – 6.4e2 cells; $n = 20$ and 21, $p < 0.01$) of eosinophils recovered in BAL samples. Compared to infected WT mice, no changes were found in infected Cnr2$^{-/-}$ for percent (Fig. 2.5H, from 12.59 – 3.424% to 11.62 – 3.734%; $n = 10$; $p = 0.964$) or number (Figure 2.5I, from 4.6e3 – 1.7e3 cells to 4.4e3 – 1.6e3 cells; n = 9/10, respectively; $p = 0.995$) of eosinophils recovered in BAL.

Parasite Burden is Unaffected by Inhibition of CB_1Rs or in $Cnr2^{-/-}$ Mice

Compared to vehicle treatment in mice infected with *N. brasiliensis*, treatment with AM6545 throughout *N. brasiliensis* infection had no effect on egg burden by 6 DPI (Figure 2.6A, from 9.89 – 2.87 eggs/g [103] to 11.78 – 3.0 eggs/g [103], p = 0.831) and 7 DPI (from 72.12 – 16.22 eggs/g [103] to 54.72 – 14.83 eggs/g [103], p = 0.369). Similarly, compared to infected WT mice, no changes in egg burden were found in infected $Cnr2^{-/-}$ mice by 6 DPI (Figure 2.6B, from 10.876 – 5.043 eggs/g [103] to 22.035 – 20.122 eggs/g [103], p = 0.896) and 7 DPI (from 167.849 – 69.775 eggs/g [103] to 149.928 – 20.122 eggs/g [103], p = 0.897). Moreover, compared to vehicle treatment in mice infected with *N. brasiliensis*, no changes were observed in parasite burden in mice treated with AM6545 (Figure 2.6C, from 58 – 15 to 58 – 13 worms, p = 0.996). In addition, no changes in parasite burden were observed between infected WT and $Cnr2^{-/-}$ mice (Figure 2.6D, from 46 – 23 to 63 – 24 worms, p = 0.626).

Discussion

Following subcutaneous infection, *N. brasiliensis* migrate into circulation and lodge themselves in the lung alveoli by 2 DPI, which bursts capillaries and causes extensive hemorrhaging and damage (Batugedara, Li, et al., 2018; Reece et al., 2006). To identify how CB_1Rs and CB_2Rs influence recovery from this lung damage, BAL samples collected in the intestinal phase of infection (7–8 DPI) were measured at 540 nm, which is a correlate for hemoglobin from hemorrhaging (Meng & Alayash, 2017). These data

suggested that mice receiving daily injections of AM6545 had increased hemorrhaging in the lungs compared to all other groups. Compared to naïve mice, *N. brasiliensis* infection consistently caused weight loss as previously described (Batugedara, Argueta, et al., 2018), however, manipulation of the eCB system did not alter this weight loss or the transient hypophagia which accompanies the weight loss. Collectively, the results suggest that acute lung injury is exacerbated when peripheral CB_1Rs are inhibited throughout *N. brasiliensis* infection.

Infection with tissue-migrating *N. brasiliensis* results in extensive lung damage and disruption in the alveolar architecture as the parasite migrates through lung tissue. *N. brasiliensis* infection also has long-term pathologic consequences, including emphysema and fibrosis (Marsland et al., 2008). To identify if increased hemorrhaging in AM6545-treated mice was coupled to more severe lung tissue damage, multiple methods of image analysis were performed to evaluate lung alveolar architecture. Qualitatively, images of lung tissue samples used for image analysis in all groups (Figure 2.2A–H) indicated less functional alveolar tissue throughout the lungs of *N. brasiliensis* infected mice, which appear to be further reduced in mice treated with AM6545. To provide quantitative evidence of reduced alveolar tissue, MLI analysis was performed on all groups tested, as previously described (Chen et al., 2020; Sutherland et al., 2018) and was further confirmed by a second, novel, method of analysis to measure the area of non-functional alveolar tissue in a given image. These data align with the extensive hemorrhaging observed in the AM6545-treated mice (Figure 2.1A, B). Taken together, these data indicate that there was a decrease in functional alveolar tissue in mice treated with

AM6545, caused either by increased infection-induced injury or a defect in alveolar tissue healing. Recent evidence suggests that overactivation of CB_1R in the lungs contributes to idiopathic pulmonary fibrosis, which appears to be alveolar macrophage mediated (Cinar et al., 2017). However, parasitic infections stimulate a Th2 immune response, which results in eosinophil recruitment and polarization of macrophages into alternatively activated macrophages, which are protective (Anthony et al., 2007; Batugedara, Li, et al., 2018; Chen et al., 2012). Thus, the role for CB_1R signaling in the lungs may depend on the inflammatory context, which inflammatory cell type is most prevalent, and the activation state of these cells.

To identify if there was an inflammatory cell associated with the increase in lung tissue damage and hemorrhaging in response to *N. brasiliensis* infection, flow cytometry was performed on the cells collected in the BAL samples. *N. brasiliensis* infection stimulates a polarized Th2 immune response in the host which includes recruitment of eosinophils to the lungs, and therefore, eosinophils were strongly considered when the flow cytometry experiments were performed (Anthony et al., 2007; Chen et al., 2012; Knott et al., 2009). BAL eosinophils and alveolar macrophages were gated based on surface expression for SiglecF and CD11c (Stevens et al., 2007). The finding that CB_1R blockade prolongs lung eosinophilia in *N. brasiliensis* infection suggests that deficiencies in CB_1R signaling in the lung promote host destructive Th2 inflammatory processes in *N. brasiliensis* infection, while constitutive activity at CB_1Rs in the lung may provide protection during infection. A direct test of this hypothesis, however, remains for future studies.

Adulthood is established by *N. brasiliensis* in the small intestine where fertilized eggs are released into the fecal matter as early as 6 DPI (Hawdon & Hotez, 1996). To identify the fecundity of *N. brasiliensis* when host CB_1R or CB_2R is inhibited, fecal egg burden was quantified at 6 and 7 DPI. Surprisingly, no changes in parasite burden or worm fecundity was observed across any conditions, despite the significant alterations in inflammation. In contrast to this current study where peripheral CB_1Rs were also blocked early during the lung phase of infection, our previously reported study indicated that blockade of peripheral CB_1R signaling in the intestinal phase of infection (4–7 DPI) exacerbated egg burden at 8 DPI only with no changes in worm burden (Batugedara, Argueta, et al., 2018). Similarly, no changes in worm burden were observed in the current study in mice receiving daily administration of AM6545 throughout *N. brasiliensis* infection; however, the increase in parasite fecundity was ablated. This result suggests a possible role for CB_1R signaling in the lung phase of infection (1–4 DPI) in these processes, which may lead to changes in parasite fertility. Furthermore, we recently reported that *N. brasiliensis* is capable of producing eCBs, which peak in concentration during the lung phase of infection (Batugedara, Argueta, et al., 2018). These parasite-derived eCBs may be acting on host CB_1Rs to mediate the immune response in the microenvironment; future studies designed to directly test this hypothesis and the mechanism(s) involved are warranted.

These studies suggest an immunomodulatory role for CB_1Rs in host-destructive inflammatory responses to parasitic infections (Table 2.1). Prolonged eosinophilia may contribute to exacerbated host tissue damage in mice treated with the CB_1R inhibitor,

AM6545; however, the specific mechanism(s) in this response remains to be identified. Despite the well-defined roles for the eCB system in nutrient seeking and sensing, no changes in feeding behavior were observed when CB_1R or CB_2R signaling was disrupted throughout infection. Moreover, the increase in infection-induced inflammatory processes in mice treated with AM6545 was not associated with altered parasite clearance, which suggests that blockade of CB_1R signaling during the lung phase of infection may not impact parasite burden. Nonetheless, it is possible that metabolism of eCBs may contribute to eicosanoid formation, which can act as a chemoattractant to immune cells and contribute to prolonged eosinophilia in the lungs of AM6545-treated mice. Future research should consider eicosanoid formation and signaling in conjunction with CB_1R signaling in immune cells to control immune cell trafficking. Collectively, these studies provide further insight into the role for CB_1R signaling in the Th2 response and parasitic infections.

References

Anthony, R. M., Rutitzky, L. I., Urban, J. F., Stadecker, M. J., & Gause, W. C. (2007). Protective immune mechanisms in helminth infection. *Nat Rev Immunol*, *7*(12), 975-987. https://doi.org/10.1038/nri2199

Argueta, D. A., & DiPatrizio, N. V. (2017). Peripheral endocannabinoid signaling controls hyperphagia in western diet-induced obesity. *Physiol Behav*, *171*, 32-39. https://doi.org/10.1016/j.physbeh.2016.12.044

Avalos, B., Argueta, D. A., Perez, P. A., Wiley, M., Wood, C., & DiPatrizio, N. V. (2020). Cannabinoid CB1 receptors in the intestinal epithelium are required for acute western-diet preferences in mice. *Nutrients*, *12*(9). https://doi.org/10.3390/nu12092874

Batugedara, H. M., Argueta, D., Jang, J. C., Lu, D., Macchietto, M., Kaur, J., Ge, S., Dillman, A. R., DiPatrizio, N. V., & Nair, M. G. (2018). Host and helminth-derived endocannabinoids are generated during infection with effects on host immunity. *Infect Immun*. https://doi.org/10.1128/iai.00441-18

Batugedara, H. M., Li, J., Chen, G., Lu, D., Patel, J. J., Jang, J. C., Radecki, K. C., Burr, A. C., Lo, D. D., Dillman, A. R., & Nair, M. G. (2018). Hematopoietic cell-derived RELMα regulates hookworm immunity through effects on macrophages. *J Leukoc Biol*, *104*(4), 855-869. https://doi.org/10.1002/jlb.4a0917-369rr

Bouchery, T., Filbey, K., Shepherd, A., Chandler, J., Patel, D., Schmidt, A., Camberis, M., Peignier, A., Smith, A. A. T., Johnston, K., Painter, G., Pearson, M., Giacomin, P., Loukas, A., Bottazzi, M. E., Hotez, P., & LeGros, G. (2018). A novel blood-feeding detoxification pathway in Nippostrongylus brasiliensis L3 reveals a potential checkpoint for arresting hookworm development. *PLoS Pathog*, *14*(3), e1006931. https://doi.org/10.1371/journal.ppat.1006931

Chen, C. M., Hwang, J., Chou, H. C., & Chen, C. (2020). Anti-Tn Monoclonal Antibody Attenuates Hyperoxia-Induced Lung Injury by Inhibiting Oxidative Stress and Inflammation in Neonatal Mice. *Front Pharmacol*, *11*, 568502. https://doi.org/10.3389/fphar.2020.568502

Chen, F., Liu, Z., Wu, W., Rozo, C., Bowdridge, S., Millman, A., Van Rooijen, N., Urban, J. F., Wynn, T. A., & Gause, W. C. (2012). An essential role for TH2-type responses in limiting acute tissue damage during experimental helminth infection. *Nat Med*, *18*(2), 260-266. https://doi.org/10.1038/nm.2628

Cinar, R., Gochuico, B. R., Iyer, M. R., Jourdan, T., Yokoyama, T., Park, J. K., Coffey, N. J., Pri-Chen, H., Szanda, G., Liu, Z., Mackie, K., Gahl, W. A., & Kunos, G. (2017). Cannabinoid CB1 receptor overactivity contributes to the pathogenesis of idiopathic pulmonary fibrosis. *JCI Insight*, *2*(8). https://doi.org/10.1172/jci.insight.92281

DiPatrizio, N. V. (2016). Endocannabinoids in the Gut. *Cannabis Cannabinoid Res*, *1*(1), 67-77. https://doi.org/10.1089/can.2016.0001

DiPatrizio, N. V., & Piomelli, D. (2012). The thrifty lipids: endocannabinoids and the neural control of energy conservation. *Trends Neurosci*, *35*(7), 403-411. https://doi.org/10.1016/j.tins.2012.04.006

Galiègue, S., Mary, S., Marchand, J., Dussossoy, D., Carrière, D., Carayon, P., Bouaboula, M., Shire, D., Le Fur, G., & Casellas, P. (1995). Expression of central and peripheral cannabinoid receptors in human immune tissues and leukocyte subpopulations. *Eur J Biochem*, *232*(1), 54-61. https://www.ncbi.nlm.nih.gov/pubmed/7556170

Hawdon, J. M., & Hotez, P. J. (1996). Hookworm: developmental biology of the infectious process. *Curr Opin Genet Dev*, *6*(5), 618-623. https://www.ncbi.nlm.nih.gov/pubmed/8939719

Hirahara, K., Shinoda, K., Morimoto, Y., Kiuchi, M., Aoki, A., Kumagai, J., Kokubo, K., & Nakayama, T. (2019). Immune Cell-Epithelial/Mesenchymal Interaction Contributing to Allergic Airway Inflammation Associated Pathology. *Front Immunol*, *10*, 570. https://doi.org/10.3389/fimmu.2019.00570

Holgate, S. T. (2012). Innate and adaptive immune responses in asthma. *Nat Med*, *18*(5), 673-683. https://doi.org/10.1038/nm.2731

Hotez, P. J. (2008). Neglected infections of poverty in the United States of America. *PLoS Negl Trop Dis*, *2*(6), e256. https://doi.org/10.1371/journal.pntd.0000256

Jang, J. C., Chen, G., Wang, S. H., Barnes, M. A., Chung, J. I., Camberis, M., Le Gros, G., Cooper, P. J., Steel, C., Nutman, T. B., Lazar, M. A., & Nair, M. G. (2015). Macrophage-derived human resistin is induced in multiple helminth infections and promotes inflammatory monocytes and increased parasite burden. *PLoS Pathog*, *11*(1), e1004579. https://doi.org/10.1371/journal.ppat.1004579

Kaplan, B. L., Lawver, J. E., Karmaus, P. W., Ngaotepprutaram, T., Birmingham, N. P., Harkema, J. R., & Kaminski, N. E. (2010). The effects of targeted deletion of cannabinoid receptors CB1 and CB2 on intranasal sensitization and challenge

with adjuvant-free ovalbumin. *Toxicol Pathol*, *38*(3), 382-392. https://doi.org/10.1177/0192623310362706

Knott, M. L., Matthaei, K. I., Foster, P. S., & Dent, L. A. (2009). The roles of eotaxin and the STAT6 signalling pathway in eosinophil recruitment and host resistance to the nematodes Nippostrongylus brasiliensis and Heligmosomoides bakeri. *Mol Immunol*, *46*(13), 2714-2722. https://doi.org/10.1016/j.molimm.2009.05.016

Larose, M. C., Turcotte, C., Chouinard, F., Ferland, C., Martin, C., Provost, V., Laviolette, M., & Flamand, N. (2014). Mechanisms of human eosinophil migration induced by the combination of IL-5 and the endocannabinoid 2-arachidonoyl-glycerol. *J Allergy Clin Immunol*, *133*(5), 1480-1482, 1482.e1481-1483. https://doi.org/10.1016/j.jaci.2013.12.1081

Marsland, B. J., Kurrer, M., Reissmann, R., Harris, N. L., & Kopf, M. (2008). Nippostrongylus brasiliensis infection leads to the development of emphysema associated with the induction of alternatively activated macrophages. *Eur J Immunol*, *38*(2), 479-488. https://doi.org/10.1002/eji.200737827

Meng, F., & Alayash, A. I. (2017). Determination of extinction coefficients of human hemoglobin in various redox states. *Anal Biochem*, *521*, 11-19. https://doi.org/10.1016/j.ab.2017.01.002

Nagarkatti, P., Pandey, R., Rieder, S. A., Hegde, V. L., & Nagarkatti, M. (2009). Cannabinoids as novel anti-inflammatory drugs. *Future Med Chem*, *1*(7), 1333-1349. https://doi.org/10.4155/fmc.09.93

Pandey, R., Mousawy, K., Nagarkatti, M., & Nagarkatti, P. (2009). Endocannabinoids and immune regulation. *Pharmacological Research*, *60*(2), 85-92. https://doi.org/10.1016/j.phrs.2009.03.019

Pine, G. M., Batugedara, H. M., & Nair, M. G. (2018). Here, there and everywhere: Resistin-like molecules in infection, inflammation, and metabolic disorders. *Cytokine*, *110*, 442-451. https://doi.org/10.1016/j.cyto.2018.05.014

Powell, W. S., & Rokach, J. (2013). The eosinophil chemoattractant 5-oxo-ETE and the OXE receptor. *Prog Lipid Res*, *52*(4), 651-665. https://doi.org/10.1016/j.plipres.2013.09.001

Reece, J. J., Siracusa, M. C., & Scott, A. L. (2006). Innate immune responses to lung-stage helminth infection induce alternatively activated alveolar macrophages. *Infect Immun*, *74*(9), 4970-4981. https://doi.org/10.1128/iai.00687-06

Roulette, C. J., Kazanji, M., Breurec, S., & Hagen, E. H. (2016). High prevalence of cannabis use among Aka foragers of the Congo Basin and its possible relationship to helminthiasis. *Am J Hum Biol*, *28*(1), 5-15. https://doi.org/10.1002/ajhb.22740

Stevens, W. W., Kim, T. S., Pujanauski, L. M., Hao, X., & Braciale, T. J. (2007). Detection and quantitation of eosinophils in the murine respiratory tract by flow cytometry. *J Immunol Methods*, *327*(1-2), 63-74. https://doi.org/10.1016/j.jim.2007.07.011

Sutherland, T. E., Rückerl, D., Logan, N., Duncan, S., Wynn, T. A., & Allen, J. E. (2018). Ym1 induces RELMα and rescues IL-4Rα deficiency in lung repair during nematode infection. *PLoS Pathog*, *14*(11), e1007423. https://doi.org/10.1371/journal.ppat.1007423

Weatherhead, J. E., Hotez, P. J., & Mejia, R. (2017). The Global State of Helminth Control and Elimination in Children. *Pediatr Clin North Am*, *64*(4), 867-877. https://doi.org/10.1016/j.pcl.2017.03.005

Figures and Legends

Figure 2.1

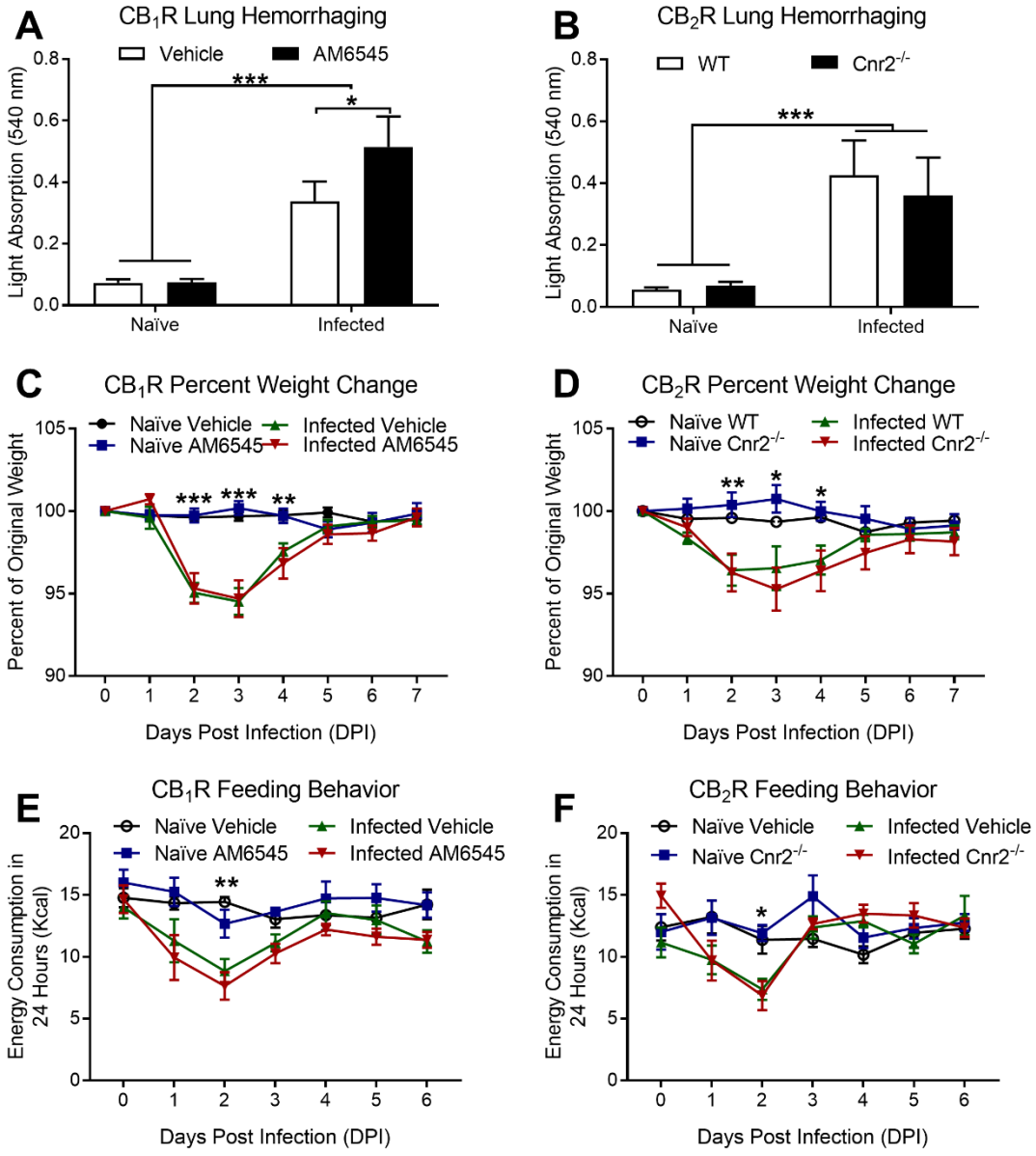

Figure 2.1 Blockade of peripheral CB_1Rs with AM6545 exacerbated *Nippostrongylus brasiliensis* infection induced lung hemorrhaging at 7 DPI compared to mice receiving vehicle treatment [(A): n = 19, veh; n = 21, AM6545]. No changes in lung hemorrhaging occurred between infected CB_2R-null ($Cnr2^{-/-}$) and WT control mice [(B): n = 9, WT; n = 9, $Cnr2^{-/-}$]. Mice infected with *N. brasiliensis* exhibited weight loss, which was unaffected by AM6545 or in CB_2R-null mice [(D): n = 9, WT; n = 9, $Cnr2^{-/-}$] by 2 DPI. Body weights returned to baseline levels by 5 DPI. Similarly, energy consumption was reduced at 2 DPI, which returned to baseline by 4 DPI [(E, F): n = 14, veh; n = 14, AM6545; n = 9, WT; n = 9, $Cnr2^{-/-}$]. Regular two-way ANOVA with Newman–Keul's multiple comparison post hoc test (A, B); repeated measures two-way ANOVA with Sidak's multiple comparison post hoc test (C–F); *$p < 0.05$, **$p < 0.01$, ***$p < 0.001$. Results are expressed as mean – SEM. ANOVA, analysis of variance; CB_1R, cannabinoid receptor subtype-1; CB_2R, cannabinoid receptor subtype-2; DPI, days post infection; SEM, standard error of the mean; WT, wild-type.

Figure 2.2

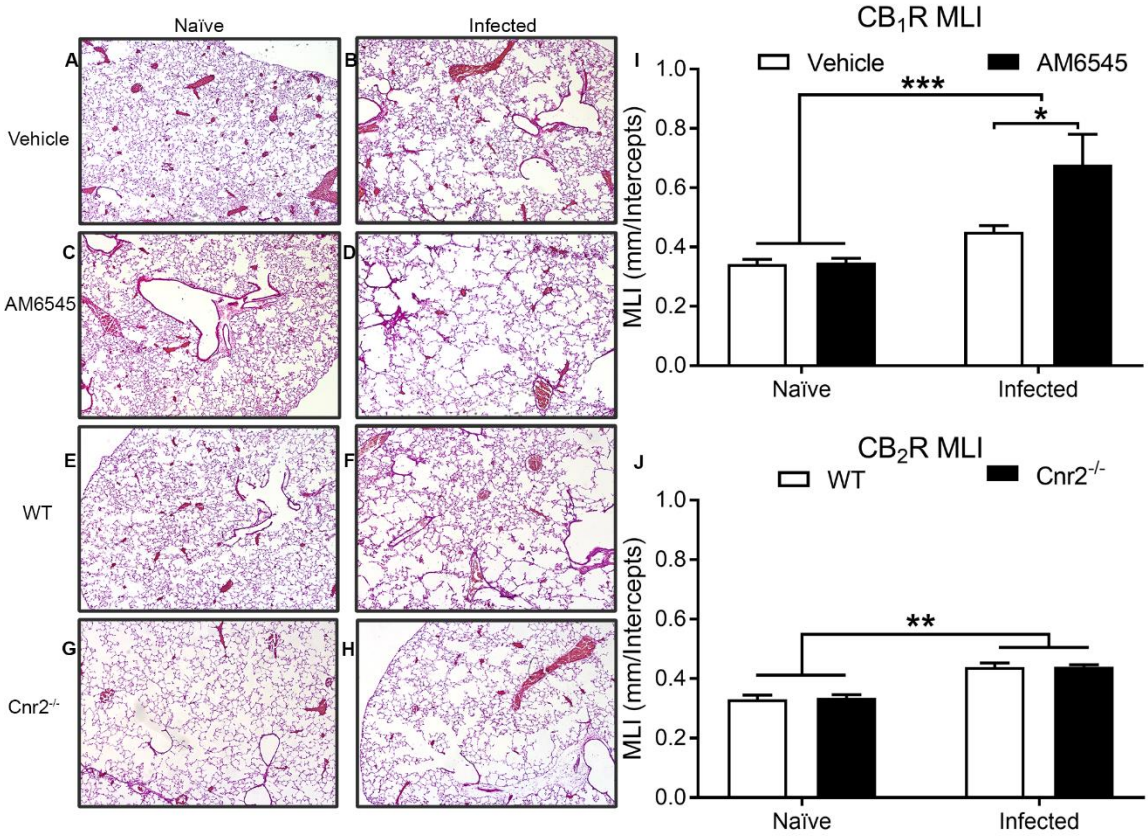

Figure 2.2: Representative images of lung tissue damage in naive and infected mice receiving vehicle or AM6545 treatment (A–D) and in naive and infected WT and CB_2R-null mice (E–H). Quantification of lung tissue damage was performed using MLI analysis, which indicates that peripheral blockade of CB_1Rs increased lung tissue damage in *N. brasiliensis* infection [(I): n = 13, veh; n = 14, AM6545], while absence of CB_2Rs globally had no effect [(J) n = 8, WT; n = 8, $Cnr2^{-/-}$). Regular two-way ANOVA with Newman–Keul's multiple comparison post hoc test (I, J); *p < 0.05, **p < 0.01, ***p < 0.001. Results are expressed as mean – SEM. MLI, mean linear intercept.

Figure 2.3

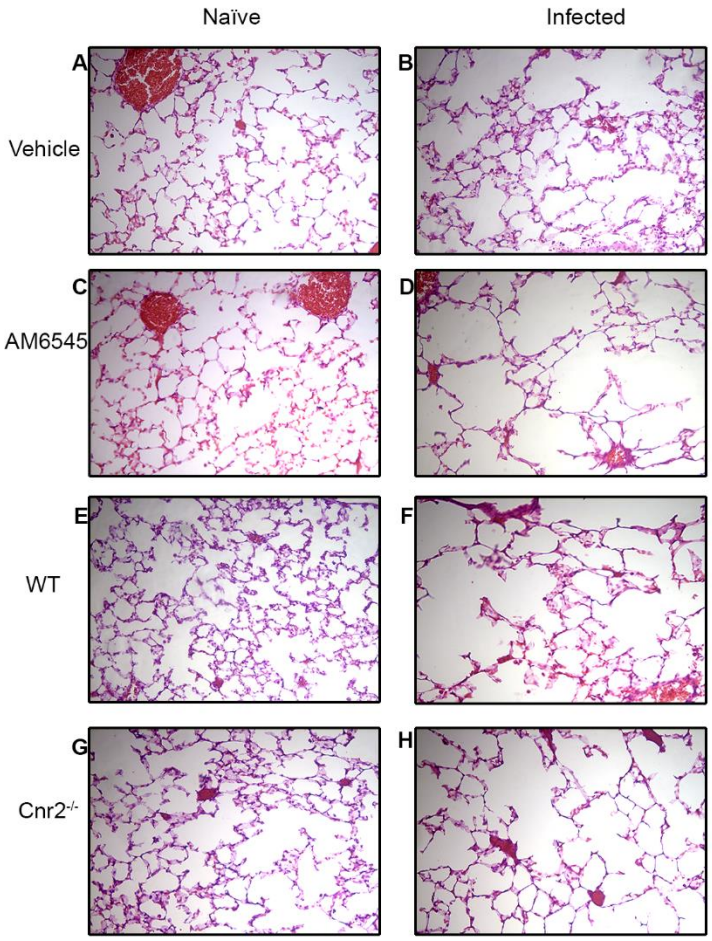

Figure 2.3: Representative images (20x) of lung tissue in naïve and infected mice receiving vehicle or AM6545 treatment (A-D) and in naïve and infected wild-type (WT) and CB_2R-null mice (E-H).

Figure 2.4

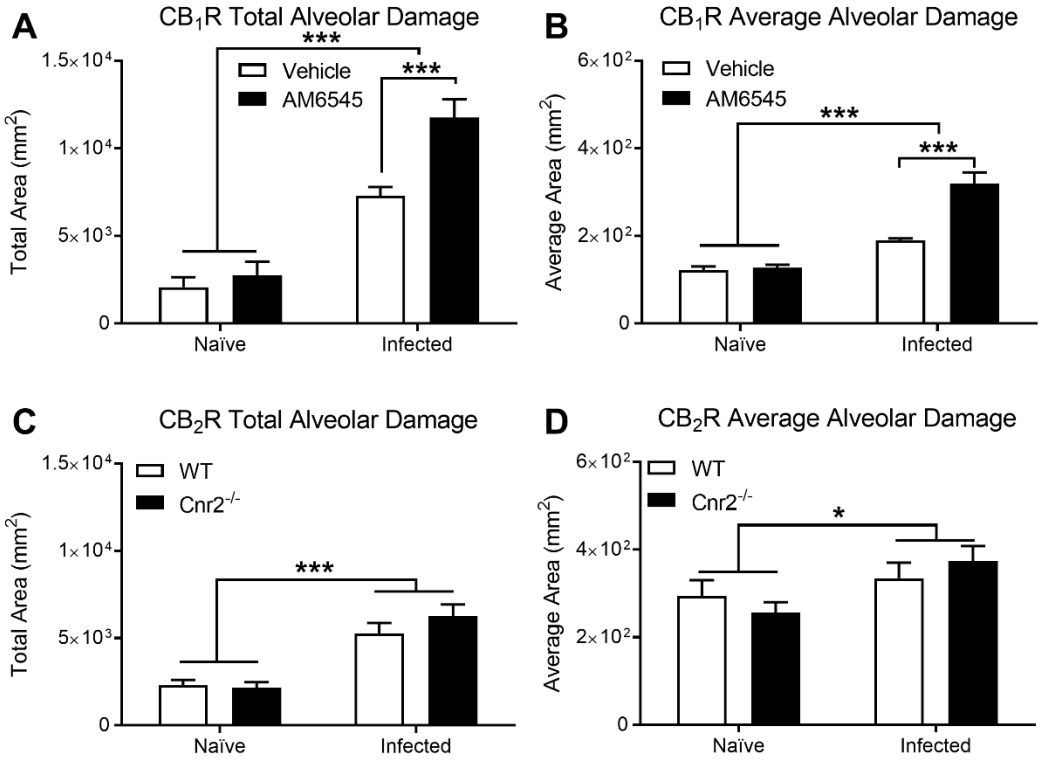

Figure 2.4: Mice infected with *N. brasiliensis* that received AM6545 treatment displayed an increase in both average and total area of nonfunctional tissue compared to vehicle-treated mice infected with *N. brasiliensis* [(A, B): n = 13, veh; n = 14, AM6545]. CB_2R-null mice displayed no change in these parameters compared to infected WT mice [(C, D); n = 8]. Regular two-way ANOVA with Newman–Keul's multiple comparison post hoc test (A–D); *$p < 0.05$, ***$p < 0.001$. Results are expressed as mean – SEM.

Figure 2.5

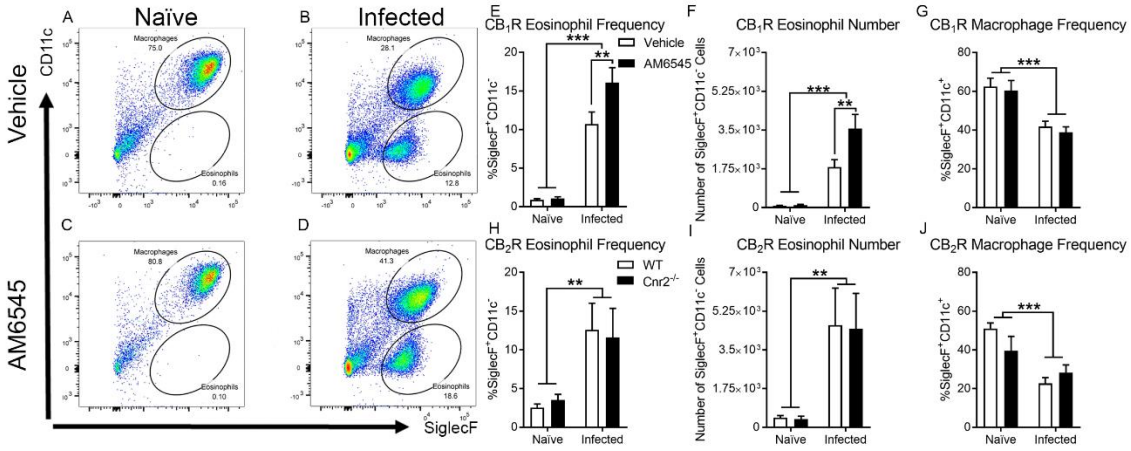

Figure 2.5: Representative flow plots from cells collected in a bronchoalveolar lavage wash where airway macrophages ($SiglecF^{+}Cd11c^{+}$) were separated from eosinophils ($SiglecF^{+}Cd11c^{-}$) (A–D). Mice infected with *N. brasiliensis* that received AM6545 treatment had increased raw number and percent of eosinophils (SiglecF +$Cd11c^{-}$) compared to infected vehicle-treated mice infected with *N. brasiliensis* [(E, F): n = 20, veh; n = 21, AM6545]. Infection with *N. brasiliensis* induced lung eosinophilia in both CB_2R-null and WT mice; however, no differences were observed across genotype [(H, I): n = 9, WT; n = 10, $Cnr2^{-/-}$]. Alveolar macrophages were the main cell population in naive mice, and frequency was reduced in *N. brasiliensis* infected samples [(G, J): n = 20, veh; n = 21, AM6545; n = 9, WT; n = 10, $Cnr2^{-/-}$]. Regular two-way ANOVA with Newman–Keul's multiple comparison post hoc test (E–H); **p < 0.01, ***p < 0.001. Results are expressed as mean – SEM.

Figure 2.6

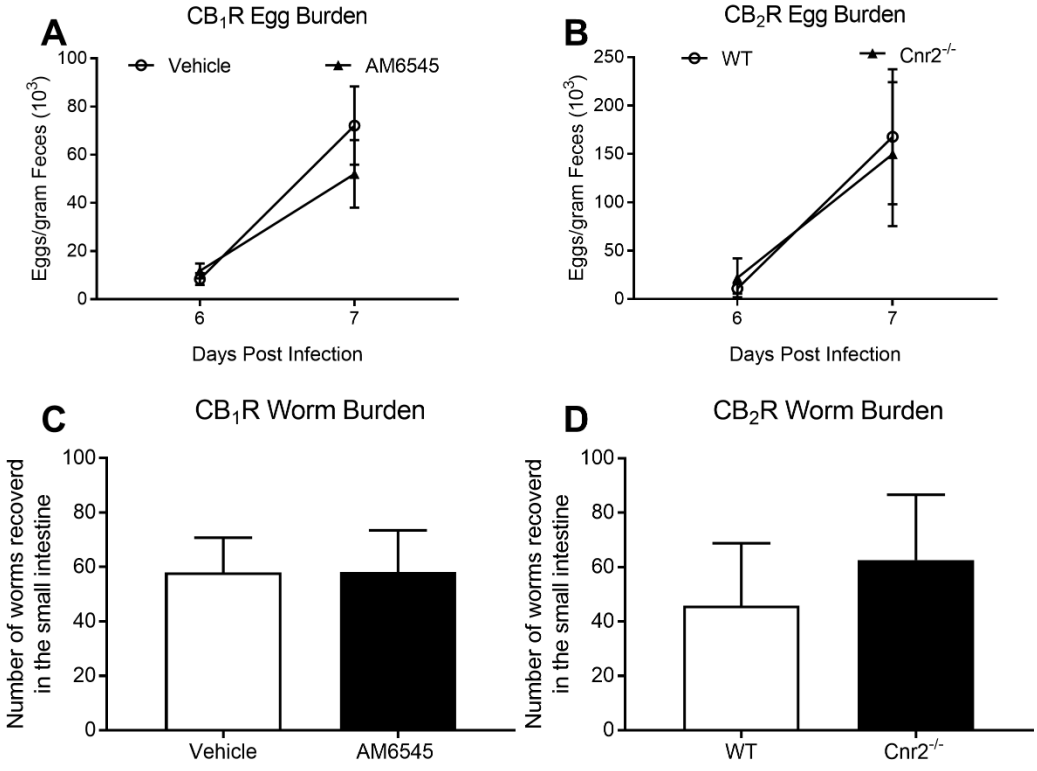

Figure 2.6: Egg burden of infected mice at 6 and 7 DPI indicated no change in parasite fecundity irrespective of treatment or genotype [(A, B): n = 18, veh; n = 21, AM6545; n = 13, WT; n = 14, $Cnr2^{-/-}$]. No change in worms recovered from the small intestine was observed across treatment or genotype [(C, D): n = 18, veh; n = 21, AM6545; n = 13, WT; n = 14, $Cnr2^{-/-}$]. Repeated measures two-way ANOVA with Sidak's multiple comparison post hoc test (A, B); unpaired two-tailed student's t-test (C, D). Results are expressed as mean – SEM.

Table 2.1

	Peripheral CB_1R blockade	Global $Cnr2^{-/-}$
Hemorrhaging	↑	—
Lung eosinophilia	↑	—
Lung tissue damage	↑	—
Parasite burden	—	—

Table 2.1: No changes were observed in any of the measured parameters in CB_2R-null mice infected with *Nippostrongylus brasiliensis* compared to WT infected mice. Despite the evidence for an enhanced immune response to infection when peripheral CB_1R signaling is inhibited, there is no change in parasite burden or parasite fecundity suggesting an immunomodulatory role for CB1R signaling in response to *N. brasiliensis* infection. Collectively, these data suggest a host-protective role for CB_1Rs in parasitic helminth infection.

Chapter 3 – UPLC-MS/MS Method for Analysis of Endocannabinoid and Related Lipid Metabolism in Mouse Mucosal Tissue

Abstract

The endocannabinoid system is expressed in cells throughout the body and controls a variety of physiological and pathophysiological functions. We describe robust and reproducible UPLC-MS/MS-based methods for analyzing metabolism of the endocannabinoids, 2-arachidonoyl-*sn*-glycerol and arachidonoyl ethanolamide, and related monoacylglycerols (MAGs) and fatty acid ethanolamides (FAEs), respectively, in mouse mucosal tissues (i.e., intestine and lung). These methods are optimized for analysis of activity of the MAG biosynthetic enzyme, diacylglycerol lipase (DGL), and MAG degradative enzymes, monoacylglycerol lipase (MGL) and alpha/beta hydrolase domain containing-6 (ABHD6). Moreover, we describe a novel UPLC-MS/MS-based method for analyzing activity of the FAE degradative enzyme, fatty acid amide hydrolase (FAAH), that does not require use of radioactive substrates. In addition, we describe *in vivo* pharmacological methods to inhibit MAG biosynthesis selectively in the mouse small-intestinal epithelium. These methods will be useful for profiling endocannabinoid metabolism in rodent mucosal tissues in health and disease.

Introduction

The endocannabinoid (eCB) system is expressed in cells throughout the body and consists of lipid signaling molecules including the primary eCBs, 2-arachidonoyl-s*n*-glycerol (2-AG) and arachidonoyl ethanolamide (anandamide, AEA), their biosynthetic and degradative enzymes, and the cannabinoid receptors [cannabinoid receptor subtype-1 (CB_1R) and subtype-2 (CB_2R), and possibly others] (Devane et al., 1992; Devane et al., 1987; Kaminski et al., 1992; Mechoulam et al., 1995; Pertwee, 2015; Piomelli, 2003); see Figure 3.1). ECBs are produced upon cellular activation and synthesized from lipid precursors found in the plasma membrane of cells (DiPatrizio, 2021). 2-AG and AEA activate the same cannabinoid receptors; however, their biosynthesis and degradation are controlled by distinct enzymatic pathways. Diacylglycerol lipase (DGL) hydrolyzes distinct diacylglycerol precursors and generates 2-AG and other related monoacylglycerol (MAGs) species including 2-docosohexaenoylglycerol (2-DG), 2-pamitoylglycerol (2-PG), 2-oleoylglycerol (2-OG), and 2-linoleoylglycerol (2-LG) (Alexander & Kendall, 2007; DiPatrizio, 2021; Ghafouri et al., 2004). These MAGs are degraded via monoacylglycerol lipase (MGL) into free fatty acids and glycerol (DiPatrizio, 2021). Furthermore, alpha/beta hydrolase domain containing-6 (ABHD6) and -12 (ABHD12) are capable of degrading MAGs, including 2-AG, and contribute to total MAG degradation in the brain (Blankman et al., 2007; DiPatrizio, 2021; Marrs et al., 2010).

In contrast to MAGs, fatty acid ethanolamides (FAEs) are synthesized from N-acylphosphatidylethanolamine (NAPE), which is produced by activity of N-

acyltransferase (NAT) in a Ca^{2+} and cAMP-dependent manner (Cadas et al., 1997; Cadas et al., 1996; Di Marzo et al., 1994; Hussain et al., 2017; Tsuboi et al., 2018). NAT transfers a fatty acid (i.e., arachidonate) from the sn-1 position of a phospholipid to the amino group of the phosphatidylethanolamine to produce distinct NAPEs (Cadas et al., 1997; Cadas et al., 1996; Di Marzo et al., 1994; Hussain et al., 2017; Tsuboi et al., 2018). NAPE is then hydrolyzed via N-acyl phosphatidylethanolamine-specific phospholipase D (NAPE-PLD) to produce FAEs that include AEA, oleoylethanolamide (OEA), and docosohexaenoylethanolamide (DHEA) (DiPatrizio, 2021). These FAEs are subsequently degraded by fatty acid amide hydrolase (FAAH) into free fatty acids and ethanolamine (Cravatt et al., 1996; Wei et al., 2006). Furthermore, N-acylethanolamine acid amidase (NAAA) also hydrolyzes some FAEs, including palmitoylethanolamide (PEA), and has been identified primarily in endosomal-lysosomal compartments of adaptive and innate immune cells (Piomelli et al., 2020; Tsuboi et al., 2018; Tsuboi et al., 2007).

Direct pharmacological manipulation of CB_1R activity with, for example, globally-acting antagonists/inverse agonists (i.e., rimonabant) reduces body weight and improves a host of metabolic parameters in human obesity; however, these drugs reach the brain and can lead to psychiatric side effects that preclude their use in the clinic for the treatment of metabolic disease (Christensen et al., 2007). In contrast to directly targeting cannabinoid receptors, pharmacological manipulation of enzymes responsible for the biosynthesis or degradation of eCBs may provide a safe therapeutic strategy for treatment of a variety of disorders. Accordingly, reliable methods for identifying tissue-specific changes in eCB turnover is critical for informing development of therapeutics

that target metabolism of eCBs. Several existing methods for detecting changes in enzyme activity rely on fluorogenic or chromogenic enzyme substrates and products which, while highly effective, are not optimal for monitoring activity of a variety of enzymatic reactions (de Rond et al., 2019; Sun et al., 2018). The introduction of a label, including non-natural fluorogenic residues near the carboxyl- or amino-terminal side of the substrate, can significantly alter its conversion to product by the enzyme of interest (Su et al., 2006). Therefore, the use of label-free assays provides significant improvements in accurately determining enzymatic activity. Furthermore, nearly all enzymatic reactions involve a change in substrate mass, therefore mass spectrometry (MS) is ideal for quantitation of enzyme activity. Coupling a chromatographic step (i.e., liquid chromatography) to MS provides physical and temporal separation of analytes and significantly increases sensitivity. These advantages have motivated work to develop LC-MS/MS based methods for analyzing enzyme activity (Ohira et al., 2018).

Here, we describe methods using ultra-performance liquid chromatography/tandem mass spectrometry (UPLC-MS/MS) to assess activity of enzymes responsible for biosynthesis and degradation of eCBs and related lipids in distinct mouse mucosal tissues. These methods are optimized for quantitation of the rate of metabolism of eCBs by DGL, MGL, ABHD6, and FAAH. Moreover, novel methods are described for measuring FAAH activity that does not require use of radioactive compounds as substrates (Dainese et al., 2020; Fu et al., 2007).

Materials and Methods

Chemicals and Compounds

The following compounds were used as substrates: dinonadecadienoin (19:2 DAG, Nu-Chek Prep, Waterville, MN, United States) for the DGL assay, non-adecadienoin (19:2 MAG; Nu-Chek Prep) for the MGL and ABHD6 assays, and [$^2H_4$]-palmitoyl-ethanolamide ([$^2H_4$]-PEA, Cayman Chemical, Ann Arbor, MI, United States) for FAAH assays. The following compounds were used as internal standards for both lipid extracts and enzyme assays: [$^2H_5$]-2-AG (Cayman Chemical, Ann Arbor, MI, United States) for lipid extracts and the DGL assay, heptadecanoic acid (17:1 FFA; Nu-Chek Prep) for the MGL/ABHD6 and FAAH activity assays, [$^2H_4$]-OEA (Cayman Chemical, Ann Arbor, MI, United States) and [$^2H_4$]-AEA (Cayman Chemical, Ann Arbor, MI, United States) for lipid extracts. The following chemicals were used as inhibitors for enzyme assays: tetrahydrolipstatin (THL) (Cayman Chemical, Ann Arbor, MI, United States) for DGL inhibition, JZL 184 (Cayman Chemical, Ann Arbor, MI, United States) for MGL inhibition, WWL 70 (Cayman Chemical, Ann Arbor, MI, United States) for ABHD6 inhibition, and URB597 (Cayman Chemical, Ann Arbor, MI, United States) for FAAH inhibition. Commercially available substrates or internal standards, (i.e., odd-numbered fatty acid chains, deuterated molecules) were used across assays due to their low cost and to ensure that detection of products of reactions were selective for their unique substrates versus endogenously produced molecules that can interfere with detection and quantitation of activity.

Tissue Harvest and Preparation for Enzyme Assays

Adult C57BL/6J male mice (Jackson Laboratories) were maintained with ad libitum access to food and water, and were anesthetized using isoflurane prior to tissue harvest. Proximal small-intestinal (jejunum) and lung were removed and rinsed in ice-chilled 1x PBS (pH = 7.0). Jejunum was opened longitudinally, and gently washed. Glass slides were used to scrape the intestinal epithelium layer, placed on dry ice, and then snap frozen in liquid N_2. Lung tissue was removed, rinsed in ice-chilled 1X PBS (pH = 7.0), and snap frozen using liquid N_2. Samples were stored at -80^{O}C until processing. All procedures met the United States National Institute of Health guidelines for care and use of laboratory animals and were approved by the Institutional Animal Care and Use Committee (IACUC Protocol 20200022) of the University of California, Riverside.

Oral Gavage and Tissue Harvest

Adult C57BL/6J male mice were food-deprived for 24 h prior to harvest with ad libitum access to water. To prevent coprophagia, animals were maintained on elevated wire-bottom cages for a 72-hour acclimation period and during the 24-hour food deprivation. One hour prior to harvest, mice received an oral gavage (100 mL of 10 mg/mL) of the DGL inhibitor, THL, in polyethylene glycol (PEG) or PEG alone as control. Jejunum intestinal epithelium and lungs were harvested as described above (see section “Tissue Harvest and Preparation for Enzyme Assays”).

Protein Preparation

Approximately 100 mg of intestinal epithelium or 50 mg of lung tissue was weighed and placed into 2 mL of chilled 50 mM Tris–HCl, 320 mM sucrose buffer (pH = 7.5). Samples were blade homogenized at 15,000 + rpm for 10–20 s. The blade was twice cleaned with chilled water and acetone washes between samples. Homogenized samples were used for assay-specific protein isolations described below.

DGL, MGL, and ABHD6 Protein Isolation

Homogenized samples were centrifuged at 800 x g for 15 min at 4^{O}C. The supernatant was collected in a 2.0 mL centrifuge tube and sonicated twice for 10 s. Samples underwent two sequential freeze thaw cycles using liquid N_2. Samples were again centrifuged at 800 x g, 15 min, 4^{O}C and the supernatant was collected. Total protein was then quantified via BCA assay and normalized between all samples. Protein isolations for each assay and each tissue were performed separately.

Enzyme Assays

MAG Biosynthetic Enzyme Activity Assay

Substrate solutions were prepared by drying stock 19:2 DAG (20 nmol/reaction) under N_2 steam (99.998% pure) and reconstituted in a solution of 50 mM Tris–HCl with 0.2% Triton x-100 (pH = 7.0). This solution was bath sonicated for 60 min at room temperature while protein samples were prepared. Normalized protein samples (100 mL) from jejunum epithelium homogenates or lung homogenates were incubated at room

temperature with the MGL inhibitor, JZL 184 (6 mM) for 10 min to ensure the product of interest was not metabolized (Long et al., 2009). In addition, the ABHD6 inhibitor, WWL 70 (10 mM), was added to lung protein isolates for the 10-minute room temperature incubation to ensure the product of interest was not metabolized (Tchantchou & Zhang, 2013). Dose-inhibition experiments included addition of the DGL inhibitor, THL [albeit not selective for DGL, see (Hoover et al., 2008); (DiPatrizio et al., 2015)]. Next, 100 mL of DGL substrate solution was added to normalized protein samples (100 mL; 200 mL final volume) and incubated in water bath at 37^{O}C for 30 min. The reaction was stopped by the addition of 1.0 mL of chilled methanol containing 25 pmol of the internal standard [$^{2}H_5$]-2-AG. The products of the reaction were extracted via lipid extraction methods (see section "Lipid Extraction for Enzyme Assays") and quantified via UPLC-MS/MS (see section "Quantitation of MAG Biosynthetic Enzyme Activity Assay Products").

MAG Degradative Enzyme Activity Assays

Substrate solutions were prepared by drying stock 19:2 MAG (50 nmol/reaction) under N_2 steam and adding fatty acid free BSA (0.25%) and stock 50 mM Tris–HCl (pH = 8.0). The MGL substrate solution was then sonicated for 60 min while protein samples were prepared. Dose-inhibition experiments included a 10-min pre-incubation of protein samples at room temperature with varying concentrations of either the selective MGL inhibitor, JZL 184, and/or the selective ABHD6 inhibitor, WWL 70, prior to addition of the substrate solution. MGL substrate solution was added to normalized protein (400 mL; 500 mL final volume) samples and incubated in a water bath at 37^{O}C for 10 min (jejunum

protein) or 30 min (lung protein). The reaction was stopped using 1.0 mL of chilled methanol containing the internal standard 17:1 FFA (5 nmol/reaction) and placed on ice. The products of the reaction were extracted via lipid extraction methods (see section "Lipid Extraction for Enzyme Assays") and quantified via UPLC-MS/MS (see section "Quantitation of MAG Degradative Enzyme Activity Assay Products").

FAE Degradative Enzyme Activity Assay

Substrate solutions were prepared by drying stock [$^2H_4$]-PEA (5 nmol/reaction) under N_2 steam and adding fatty acid free BSA (0.25%) and stock 50 mM Tris–HCl (pH = 8.0). The substrate solution was then bath sonicated for 60 min while protein samples were prepared. Dose-inhibition experiments included a 10-minute incubation at room temperature with varying concentrations of the FAAH inhibitor URB597 (Piomelli et al., 2006) prior to incubation with the substrate. Next, 100 mL of FAAH substrate solution was added to normalized protein samples (400 mL; 500 mL final volume) and incubated at 37^{O}C for 30 min. The reaction was stopped using 1.0 mL of methanol containing the internal standard 17:1 FFA (5 nmol/reaction) and immediately placed on ice. The products of the reaction were extracted via lipid extraction methods (see section "Lipid Extraction for Enzyme Assays") and quantified via UPLC-MS/MS (see section "Quantitation of FAE Degradative Enzyme Activity").

Lipid Extractions

Lipid Extraction for Enzyme Assays

Lipids were extracted using liquid-liquid extraction with chloroform (2.0 mL) followed by 0.8 mL 0.2-micron ultra-purified water. Samples were centrifuged (1500 x g, 5 min, 4^{O}C) and the lower organic phase was collected. The samples were further purified, as previously described (Batugedara, Argueta, et al., 2018), via open-bed silica gel column chromatography which was washed with a 9:1 chloroform:methanol mixture to elute MAGs, FAEs, and FFAs for collection. Eluates were dried under N_2 steam (99.998% pure) and resuspended in 0.2 mL of methanol:chloroform (1:1). Products were detected and quantified via UPLC-MS/MS techniques (see section "UPLCMS/MS Detection of Analytes").

Tissue Lipid Extraction for FAE and MAG Quantitation

Frozen tissue samples were weighed and homogenized in 1.0 mL of methanol containing the internal standards [$^2H_5$]-2-AG (500 pmol), [$^2H_4$]-AEA (1 pmol), and [$^2H_4$]-OEA (10 pmol). Lipids were extracted using chloroform (2.0 mL) prior to being washed with 1.0 mL 0.2-micron ultra-purified water. Following centrifugation (1,500 x g, 15 min, 4^{O}C), the lower organic phase was collected and dried under N_2 steam (99.998% pure). A second chloroform wash (1.0 mL) was then performed followed by another centrifugation (1,500 x g, 15 min, 4^{O}C) and collection of the lower phase. Samples were reconstituted in 2.0 mL of chloroform and purified via open-bed silica gel column chromatography. Columns were washed with a 9:1 chloroform:methanol mixture to elute MAGs and FAEs

for collection. Collected eluates were dried under N_2 steam (99.998% pure) and resuspended in 0.2 mL of methanol:chloroform (1:1) prior to analysis via UPLC-MS/MS (see section "Quantitation of MAGs and FAEs").

UPLC-MS/MS Detection of Analytes

Data was acquired using an Acquity I-Class UPLC with direct line connection to a Xevo TQ-S Micro Mass Spectrometer (Waters Corporation, Milford, MA, United States) with electrospray ionization (ESI) sample delivery. Lipids were separated using an Acquity UPLC BEH C_{18} column (2.1 x 50 mm i.d., 1.7 mm, Waters) and inline Acquity guard column (UPLC BEH C_{18} VanGuard PreColumn; 2.1 x 5 mm i.d.; 1.7 mm, Waters), and eluted by an analyte specific gradient of water and methanol (both containing 0.25% acetic acid, 5mM ammonium acetate). Samples were kept at 10^{O}C in the sample manager and the column was maintained at 40^{O}C. Argon (99.998%) was used as collision gas.

Quantitation of MAG Biosynthetic Enzyme Activity Assay Products

Analytes were eluted at a flow rate of 0.4 mL/min and gradient: 80% methanol 0.0–0.5 min, 80–100% methanol 0.5–2.5 min, 100% methanol 2.5–3.0 min, 100–80% methanol 3.0–3.1 min, and 80% methanol 3.1–4.5 min. MS/MS detection was in positive ion mode with capillary voltage maintained at 1.10 kV. Cone voltages and collision energies for respective analytes: 19:2 MAG = 18 v, 10 v; [$^2H_5$]-2-AG = 25 v, 44 v. Lipids were quantified using a stable isotope serial dilution method detecting H^+ or Na^+ adducts of the molecular ions [M + H/Na] + in multiple reactions monitoring (MRM) mode

(variable amounts of product 19:2 MAG versus fixed amount of internal standard [$^2H_5$]-2-AG). Acyl migration from sn-2 to sn-1 positions in monoacylglycerols is known to occur (Roxana et al., 2001; Stella et al., 1997); thus the sum of these isoforms ([$^2H_5$]-1-AG and [$^2H_5$]-2-AG) is presented. Extracted ion chromatograms for MRM transitions were used to quantify analytes: 19:2 MAG (m/z = 386.4 > 277.2) product of DGL assay and [$^2H_5$]-2-AG (m/z = 384.3 > 93.4) as internal standard.

Quantitation of MAG Degradative Enzyme Activity Assay Products

Data was acquired using equipment described above (see section "UPLC-MS/MS Detection of Analytes") and eluted by a gradient of water and methanol (containing 0.25% acetic acid, 5 mM ammonium acetate) at a flow rate of 0.4 mL/min and gradient: 90% methanol 0.0–0.1 min, 90–100% methanol 0.1–2.0 min, 100% methanol 2.0–2.1 min, 100–90% methanol 2.1–2.2 min, and 90% methanol 2.2–2.5 min. MS detection was in negative ion mode with capillary voltage maintained at 3.00 kV. Cone voltages for nonadecadienoic acid (19:2 FFA) = 48 v and 17:1 FFA = 64 v. Lipids were quantified using a dilution series detecting deprotonated molecular ions in selected ion reading (SIR) mode (variable amounts of product 19:2 FFA versus fixed amount of internal standard 17:1 FFA). Extracted ion chromatograms for SIR masses were used to quantify analytes: 19:2 FFA (m/z = 293.2) product of MGL enzyme assay and 17:1 FFA (m/z = 267.2) as internal standard. Signal to noise ratio was >10 for all quantitated results.

Quantitation of FAE Degradative Enzyme Activity Products

Data was acquired using equipment described above (see section "UPLC-MS/MS Detection of Analytes") and using the elution protocol described above (see section "Quantitation of MAG Degradative Enzyme Activity Assay Products"). Cone voltage for palmitic acid ($[^2H_4]$-PA) = 54. Lipids were quantified using a dilution series detecting deprotonated molecular ions in SIR mode (variable amounts of product $[^2H_4]$-PA versus fixed amount of internal standard 17:1 FFA). Extracted ion chromatograms for SIR masses were used to quantify $[^2H_4]$-PA (m/z = 259.3) product of FAAH enzyme assay.

Quantitation of MAGs and FAEs

Data was acquired using equipment described above (see section "UPLC-MS/MS Detection of Analytes") and using the elution protocol described above (see section "Quantitation of MAG Biosynthetic Enzyme Activity Assay Products"). Cone voltage and collision energy for each analyte are as follows, respectively: AEA = 30 v, 14 v; $[^2H_4]$-AEA = 26 v, 16v; OEA = 28 v, 16 v; $[^2H_4]$-OEA = 48 v, 14 v; DHEA = 30 v, 50 v; 2-AG (20:4) = 30 v, 12 v; $[^2H_5]$-2-AG = 25 v, 44v; 2-DG (22:6) = 34 v, 14 v; 2-PG (16:0) = 18 v, 10 v; 2-OG (18:1) = 42 v, 10 v; 2-LG (18:2) = 30 v, 10 v. MS/MS detection was in positive ion mode and capillary voltage set at 0.1 kV. Extracted ion chromatograms were used to quantify AEA (m/z = 348.3 > 62.0), $[^2H_4]$-AEA (m/z = 352.3 > 66.1), OEA (m/z = 326.4 > 62.1), $[^2H_4]$-OEA (m/z = 330.4 > 66.0), DHEA (m/z = 372.3 > 91.0), 2-AG (m/z = 379.3 > 287.3), $[^2H_5]$-2-AG (m/z = 384.3 > 93.4), 2-DG (m/z = 403.3 > 11.1), 2-PG (m/z = 331.3 > 239.3), 2-OG (m/z = 357.4 > 265.2), and 2-LG (m/z = 355.3 >

263.3). Quantitation occurred using a stable isotope dilution method to detect protonated adducts of the ions [M + H] + in MRM mode. Acyl migration is known to occur in many MAG species following silica-gel purification, therefore the sum of 1-AG and 2-AG, 1-PG and 2-PG, 1-OG and 2-OG, and 1-DG and 2-DG are reported (Stella et al., 1997). The established lower limit of quantitation (LLOQ: signal to noise ratio >10) for 2-AG, 2-DG, 2-PG, 2-OG, and 2-LG was 0.5 pmol. The LLOQ for AEA, OEA, and DHEA was 0.008 pmol.

Statistical Analysis

Data was analyzed using GraphPad Prism7 software. Analyte specific standard curves were generated using linear regression models. All protein curves were generated using Michaelis-Menten regression models. Inhibition curves were generated using non-linear regression showing log[inhibitor] vs. normalized response. Lastly, multiple unpaired t-tests were performed on jejunum mucosa MAGs and FAEs and lung MAGs and FAEs with significance indicated by a $p < 0.05$. All values are expressed as mean ± SEM.

Results

Enzyme Assay Standard Curves

Quantitation of products of all reactions were made by standard isotope dilution methods that include plotting the ratio between analyte of interest versus fixed amounts of assay-

specific internal standards. Each standard curve had high coefficient of determination (r^2 > 0.95) indicating the actual values are close to the generated linear regression (Figure 3.2). Additionally, all analyte specific values from the enzyme assays were within the limits of the generated standard curves. These standard curves were used to determine the amount of product generated during the enzyme activity assays. Representative chromatograms including retention times and predicted SIR and MRM masses are included in Figure 3.3.

Protein Concentration Optimization for Assaying Enzyme Activity in Jejunum Epithelium

Optimal protein concentrations for assays were determined for DGL activity (Figure 3.4A), MGL activity (Figure 3.4B), and FAE hydrolyzing activity (Figure 3.4C) in mouse jejunum mucosal tissue. All protein curves had a high coefficient of determination ($r^2 \geq 0.93$). Increasing levels of isolated protein from jejunum mucosa (1.56–50 mg) for the DGL activity assay (Figure 3.4A) led to associated increases in product recovery (0.000029 ± 0.000025–0.06 ± 0.002 nmol/min 19:2 MAG). MGL activity in the jejunum mucosa (Figure 3.4B) also indicated that as isolated protein (1.56–50 mg) increased, the amount of product recovered also increased (0.042 ± 0.005–1.396 ± 0.074 nmol/min 19:2 FFA). Lastly, FAE hydrolyzing activity in the mouse jejunum (Figure 3.4C) displayed a similar trend with increasing protein (0.78–50 mg) resulting in increased product recovery (0.004 ± 0.00013–0.099 ± 0.006 nmol/min [$^2H_4$]-PA).

Protein Concentration Optimization for Quantitating Enzyme Activity in Lung

Diacylglycerol lipase activity (Figure 3.4D), MGL/ABHD6 activity (Figure 3.4E), and FAE hydrolyzing activity (Figure 3.4F) were analyzed with increasing concentrations of protein from mouse lung tissue. All protein curves had a high coefficient of determination ($r^2 \geq 0.93$). Increasing levels of isolated protein from mouse lung (1.56–50 mg) for the DGL activity assay (Figure 3.4D) led to associated increases in product recovery (0.001 ± 0.00013–0.034 ± 0.002 nmol/min 19:2 MAG). Mouse lung MAG degradation showed increases in product recovery (0.001 ± 0.000022–0.605 ± 0.02 nmol/min 19:2 FFA) as isolated protein (0.39–50 mg) increased (Figure 3.4E). FAE hydrolyzing activity in mouse lung (Figure 3.4F) also indicated that as protein increased (3.12–50 mg), product recovery also increased (0.003 ± 0.000097–0.022 ± 0.003 nmol/min [$^2H_4$]-PA).

Validation of Enzyme Activity in Jejunum Epithelium

Known inhibitors of associated enzymes were used to validate specificity of each assay. All inhibition curves displayed a high coefficient of determination ($r^2 \geq 0.87$). Activity of DGL in protein isolates from mouse jejunum epithelium (50 mg) was inhibited in a concentration-dependent manner (108.85 ± 6.19–20.39 ± 6.65%; IC_{50} = 133.6 nM) when incubated with the DGL inhibitor, THL (3–1,000 nM) (Figure 3.5A). This IC_{50} for THL was higher than reported (60 nM) for human recombinant DGL (Bisogno et al., 2006). Activity of MGL in protein isolates from mouse jejunum epithelium (10 mg) was inhibited in a concentration-dependent manner (87.42 ± 9.82–

9.68 ± 3.59%; IC_{50} = 47.62 nM) when incubated with the MGL inhibitor, JZL 184 (3–1,000 nM) (Figure 3.5B). This IC_{50} for JZL 184 was higher than reported (8 nM) for mouse brain tissue (Long et al., 2009). Activity of FAAH in protein isolates from mouse jejunum epithelium (50 mg) was inhibited in a concentration-dependent manner (94.95 ± 7.89– 7.37 ± 0.001%; IC_{50} = 40.76 nM) when incubated with the FAAH inhibitor, URB597 (3–1,000 nM) (Figure 3.5C). This IC_{50} for URB597 was higher than reported (5 nM) for rat brain membranes (5 nM) (Piomelli et al., 2006). Collectively, differences in IC_{50} values for compounds in comparison to other reports suggest possible differential effects due to assay-specific conditions and tissues analyzed.

Validation of Enzyme Activity in Lung

Mouse lung protein isolates (50 mg) displayed a predictable reduction in DAG metabolism when incubated with THL (3–1,000 nM; 90.26 ± 9.07–10.19 ± 0.29%; IC_{50} = 74.64 nM) (Figure 3.6A). This IC_{50} for THL was similar to reported values (60 nM) for human recombinant DGL (Bisogno et al., 2006). Inhibition of MAG metabolism in lung protein isolates (25 mg) with JZL 184 (3–10,000 nM) was incomplete in reducing product recovery (94.99 ± 15.91–49.03 ± 2.32%; IC_{50} = 4,394 nM) (Figure 3.6B). This IC_{50} for JZL 184 was higher than reported (8 nM) for mouse brain tissue (Long et al., 2009). Similarly, incubation of lung protein isolates (25 mg) with ABHD6 inhibitor, WWL 70 (3–10,000 nM), was incomplete in reducing product recovery (87.89 ± 13.69–33.07 ± 1.72%; IC_{50} = 779.9 nM) (Figure 3.6C). This IC_{50} for WWL 70 was also higher than reported (70 nM) for a fibroblast cell line (Li et al., 2007), which again may suggest possible differential effects for compounds due to assay-specific conditions and tissues

analyzed. A predictable reduction in MAG metabolism in mouse lung tissue occurred when samples were pre-incubated with 10 mM WWL 70 and JZL 184 (3–10,000 nM; 94.25 ± 6.64–22.32 ± 2.73%; IC_{50} = 514.7 nM) (Figure 3.6D). To further analyze activity of both MGL and ABHD6 in mouse lung tissue, we incubated protein isolates with 10 times the IC_{50} of JZL 184 (43,940 nM) and WWL 70 (7,799 nM) when incubated alone, which significantly reduced MAG metabolism (14.62 ± 3.46%); however, a small amount of residual MAG metabolism persisted under these conditions (Figure 3.6E). Nearly all FAE metabolism in mouse lung protein isolates (10 mg) was inhibited (90.11 ± 8.58–4.15 ± 0.46%; IC_{50} = 22.95 nM) by incubation with URB597 (3–1,000 nM) (Figure 3.6F). This IC_{50} for URB597 was only moderately higher than reported values (5 nM) in rat brain membranes (Piomelli et al., 2006).

Effects of THL Oral Gavage on Levels of MAGs and FAEs in Intestinal Epithelium, Lung, and Circulation

Levels of common MAGs were quantified by UPLC-MS/MS in the jejunum mucosa from vehicle-treated mice that were food deprived for 24 h (Figure 3.7A: 2-AG = 45.81 ± 7.02 nmol/g; 2-DG = 7.53 ± 1.40 nmol/g; 2-PG = 13.52 ± 2.60 nmol/g; 2-OG = 100.71 ± 28.93 nmol/g; 2-LG = 194.08 ± 40.11 nmol/g). Levels of all MAGs were reduced after oral administration of the DGL inhibitor, THL (1 mg), 1 h prior to tissue harvest (2-AG = 8.04 ± 1.52 nmol/g; 2-DG = 0.85 ± 0.13 nmol/g; 2-PG = 4.91 0.51 nmol/g; 2-OG = 5.56 ± 1.10 nmol/g; 2-LG = 24.61 ± 7.48 nmol/g). Vehicle-treated mice displayed no significant changes in levels of MAGs in lung (Figure 3.7B: 2-AG = 4.47 ±

0.44 nmol/g; 2-DG = 1.17 ± 0.07 nmol/g; 2-PG = 3.15 ± 0.26 nmol/g; 2-OG = 1.81 ± 0.13 nmol/g; 2-LG = 0.51 ± 0.10 nmol/g) when compared to mice treated with THL (2-AG = 3.73 ± 0.37 nmol/g; 2-DG = 1.02 ± 0.07 nmol/g; 2-PG = 2.51 ± 0.15 nmol/g; 2-OG = 2.25 ± 0.37 nmol/g; 2-LG = 1.13 ± 0.35 nmol/g). No significant changes in plasma MAGs were observed when comparing THL-treated mice (Figure 3.7C: 2-AG = 29.34 ± 2.18 pmol/mL; 2-DG = 32.82 ± 1.67 pmol/mL; 2-PG 51.99 ± 9.87 pmol/mL; 2-OG = 1.53 ± 0.22 pmol/mL; 2-LG = 105.12 ± 11.41 pmol/mL) with vehicle-treated mice (2-AG = 31.59 ± 3.93 pmol/mL; 2-DG = 44.25 ± 11.63 pmol/mL; 2-PG = 46.63 ± 4.97 pmol/mL; 2-OG = 2.71 ± 0.68 pmol/mL; 2-LG = 156.32 ± 27.64 pmol/mL).

To assess if THL affected FAE metabolism, levels of commons FAEs were quantified in jejunum mucosa, lungs, and in circulation. Vehicle-treated mice displayed no changes in levels of FAEs in the jejunum mucosa (Figure 3.7D: AEA = 2.85 ± 0.29 pmol/g; OEA = 52.23 ± 6.73 pmol/g; DHEA = 14.53 ± 1.25 pmol/g) when compared to mice that received THL (AEA = 2.41 ± 0.24 pmol/g; OEA = 46.83 ± 9.00 pmol/g; DHEA = 18.97 ± 5.08 pmol/g). Vehicle-treated mice also exhibited no changes in levels of FAEs in lung tissue (AEA = 3.14 ± 0.14 pmol/g; OEA = 92.06 ± 4.99 pmol/g; DHEA = 14.25 ± 2.18 pmol/g) when compared to mice treated with THL (Figure 3.7E: AEA = 2.85 ± 0.08 pmol/g; OEA = 83.75 ± 3.44 pmol/g; DHEA = 16.13 ± 1.19 pmol/g). Plasma concentrations of FAEs were also unaffected when THL-treated mice (Figure 3.7F: AEA = 3.11 ± 0.50 pmol/mL; OEA = 36.12 ± 2.36 pmol/mL; DHEA = 5.62 ± 0.43 pmol/mL) were compared to vehicle-treated mice (AEA = 3.76 ± 0.07 pmol/mL; OEA = 41.19 ± 3.84 pmol/mL; DHEA = 6.41 ± 0.76 pmol/mL). Together, these results suggest that DGL

is a primary biosynthetic enzyme in mouse intestinal epithelium. Moreover, these methods can be utilized to manipulate production of MAGs specifically in the intestinal epithelium without affecting activity of DGL in extra-intestinal organs.

Discussion

We describe in this report UPLC-MS/MS-based methods for determining activity of enzymes that control eCB metabolism in distinct mouse mucosal tissues, which can be applied to other tissues of interest. These methods are optimized for quantitating the rate of (i) MAG biosynthesis in intestinal epithelium and lung tissue via DGL, (ii) MAG degradation in intestinal epithelium and lung tissue via MGL, (iii) MAG degradation via ABHD6 in lung tissue, and (iv) FAE degradation in intestinal epithelium and lung tissue via FAAH. Notably, we provide novel methods that do not require radioactive substrates to assess activity of FAAH in mouse mucosal tissues as described elsewhere (Dainese et al., 2020; Fu et al., 2007), and expand and optimize to lung tissue application of our previously-reported UPLC-MS/MS-based assays of DGL and MGL activity in intestinal epithelium (Argueta et al., 2019; Batugedara, Argueta, et al., 2018). Furthermore, the UPLC-MS/MS methods described here are ideal for detecting discrete changes in the activity of enzymes that metabolize eCBs and related lipids given that these enzymatic reactions involve hydrolysis of substrates leading to detectable changes in substrate mass. Moreover, we report significant MAG degradation in mouse lungs via ABHD6, which accounts for up to 66% of metabolism of MAGs in lung tissue when applying the

methods provided here. Lastly, we describe an in vivo model for intestinal-specific inhibition of MAG production in mice, with results that suggest DGL is a primary biosynthetic enzyme for MAGs in mouse intestinal epithelium. These methods can be applied to studying the activity of eCB system-related enzymes under physiological conditions and changes in their activity associated with pathophysiological conditions (e.g., diet-induced obesity).

Several biochemical and molecular assays are common for analyzing eCB system activity including qPCR-based analysis of expression of genes for specific components of the system (e.g., eCB biosynthetic and degradative enzymes) (Argueta et al., 2019; Avalos et al., 2020). Importantly, however, quantitating levels of gene expression does not provide a full – and at times accurate – depiction of the state of eCB system activity. For example, we reported that mice rendered obese by exposure to a "western-style" diet high in fats and sugars, when compared to lean control mice fed a low-fat/sugar diet, display elevated levels of 2-AG and other MAGs in the small-intestinal epithelium, and this heightened eCB activity at local CB1Rs promotes overeating associated with diet-induced obesity (Argueta et al., 2019). We then analyzed expression of genes for a host of eCB system components, including DGL and MGL, in order to assess if changes in expression of these key biosynthetic and degradative MAG enzymes, respectively, are responsible for elevated MAG levels. We found that expression of genes for the dominant isoform of DGL in the mouse intestinal epithelium, DGLβ, was decreased in obese mice versus lean controls. We then performed an *ex vivo* analysis of activity of DGL using our UPLC-MS/MS-based functional assay described here and found that activity of DGL in

tissue from the intestinal epithelium was *increased* in obese mice versus lean controls. This result suggests that despite decreases in expression of genes for DGL, activity of DGL was increased, which provides evidence that elevated levels of 2-AG and other MAGs in the intestinal epithelium of obese mice occur due to increases in their biosynthesis. Therefore, solely analyzing expression of genes for eCB system components inherently does not provide an accurate assessment of activity of the system under physiological and pathophysiological conditions. A combined approach is recommended in order to gain a more comprehensive understanding of eCB system activity.

We report that incubation of protein isolates from the lungs of healthy male mice with an ABHD6 inhibitor (WWL 70) led to a concentration-dependent blockade of MAG degradation by up to 66% of activity, which suggests that ABHD6 is a major enzyme involved in the degradation of MAGs in the murine lung. ABHD6 is well characterized in the mouse brain where it contributes to ~5–10% of MAG degradation in brain homogenates and ~50% of MAG degradation in neuronal cultures (Marrs et al., 2010; Savinainen et al., 2012); however, MGL is thought to be the dominant MAG degradative enzyme throughout the periphery. Evidence indicates macrophages produce significant 2-AG in the presence of LPS and WWL 70, which suggests a substantial role for ABHD6 activity in these cells (Bottemanne et al., 2019). Thus, it is plausible that resident lung macrophages may be responsible for ABHD6-mediated MAG metabolism. In addition, inhibition of MGL and ABHD6 in lung tissue decreased total MAG degradation in mouse lung homogenates; however, full inhibition was not achieved. Thus, alternate enzymatic

pathways in the mouse lung may contribute in part to degradation of MAGs including ABHD12, which has similar catalytic capabilities as ABHD6 (Fiskerstrand et al., 2010; Savinainen et al., 2012). Indeed, other studies suggest that mutations in ABHD12 may contribute to neurodegenerative diseases due to alterations in eCB metabolism (Fiskerstrand et al., 2010). It is also plausible that higher concentrations of WWL 70 or JZL 184 may be necessary for full in vitro inhibition of MAG metabolism in mouse lung tissue. Moreover, macrophages express the FAE metabolizing enzyme, NAAA, which in addition to FAAH, may contribute to FAE hydrolysis in lung (Tsuboi et al., 2007). Nonetheless, we report a near full inhibition of mouse lung FAE hydrolysis with URB597; however, our methods and conditions described above for assaying activity of FAAH differed from those reported for assaying activity of NAAA and may contribute to differential effects for inhibitors under assay conditions that favor FAAH over NAAA activity (e.g., differing centrifugation speeds) (Scalvini et al., 2020; Solorzano et al., 2009). It is also notable that the UPLC/MS/MS assays we describe here utilize tissue homogenates that, in contrast to assays using purified enzymes, contain a variety of enzymes in addition to DGL, MGL, and AHD6 that may contribute to hydrolysis of corresponding substrates. This possibility is reflected in the experiments using THL for inhibition of DAG hydrolysis (Figure 3.6A) and JZL 184 and WWL 70 for inhibition of MAG hydrolysis (Figure 3.6D), which identify two inflection points for inhibition of activity. Indeed, THL is not entirely selective for DGL (see (Hoover et al., 2008)) and at higher concentrations, may be affecting the activity of enzymes other than DGL.

The described methods in this work rely on highly sensitive UPLC-MS/MS technology which provides several advantages in assaying enzyme activity. The inclusion of internal standards and non-endogenous substrates in these assays increases the accuracy of the quantitative results when compared to other assays of enzyme activity, including fluorogenic assays. Indeed, the addition of fluorogenic residues on a substrate, including those previously reported for assaying FAAH activity (Ramarao et al., 2005), may alter its enzymatic conversion, decreasing assay sensitivity (Ohira et al., 2018; Su et al., 2006). Furthermore, isomerases are known to change molecular orientation of the substrate without changing its mass (Lambeth & Julian, 2019); however, changes in molecular orientation may lead to changes in solubility and, ultimately, changes in UPLC-MS/MS retention time. Therefore, the coupling of MS to the chromatographic step of liquid chromatography provides a sensitive method for determining enzyme activity with advantages over other methods described.

We previously reported that a 24-hour fast stimulates production of 2-AG in rat jejunal epithelium, and production of 2-AG under these conditions is blocked following oral gavage with the DGL inhibitor, THL, which suggests that DGL is a primary biosynthetic enzyme for 2-AG in this tissue in rats (DiPatrizio et al., 2015). We now provide evidence that THL blocks production of 2-AG along with several other MAG species in mouse intestinal epithelium, which suggests that DGL is a key enzyme in the biosynthesis of MAGs in the small-intestinal epithelium of rodents. Furthermore, these results suggest that THL does not broadly affect production of eCBs in the intestinal epithelium because levels of anandamide and other FAEs were not affected in this tissue.

Moreover, THL had no effect on levels of MAGs in the lung or in circulation, which suggests that THL suspended in PEG was not likely absorbed into circulation and can be utilized via these methods to block production of MAGs selectively in the rodent intestinal epithelium.

Collectively, these functional assays are useful for analyzing tissue-specific activity of eCB biosynthetic and degradative enzymes under physiological and pathophysiological conditions that may be associated with dysregulated eCB metabolism. Furthermore, these methods can be adapted and used as a guide for analyzing activity of eCB biosynthetic and degradative enzymes in other tissues of interest.

References

Alexander, S. P., & Kendall, D. A. (2007). The complications of promiscuity: endocannabinoid action and metabolism. *Br J Pharmacol*, *152*(5), 602-623. https://doi.org/10.1038/sj.bjp.0707456

Anthony, R. M., Rutitzky, L. I., Urban, J. F., Stadecker, M. J., & Gause, W. C. (2007). Protective immune mechanisms in helminth infection. *Nat Rev Immunol*, *7*(12), 975-987. https://doi.org/10.1038/nri2199

Argueta, D. A., & DiPatrizio, N. V. (2017). Peripheral endocannabinoid signaling controls hyperphagia in western diet-induced obesity. *Physiol Behav*, *171*, 32-39. https://doi.org/10.1016/j.physbeh.2016.12.044

Argueta, D. A., Perez, P. A., Makriyannis, A., & DiPatrizio, N. V. (2019). Cannabinoid CB. *Front Physiol*, *10*, 704. https://doi.org/10.3389/fphys.2019.00704

Avalos, B., Argueta, D. A., Perez, P. A., Wiley, M., Wood, C., & DiPatrizio, N. V. (2020). Cannabinoid CB. *Nutrients*, *12*(9). https://doi.org/10.3390/nu12092874

Batugedara, H. M., Argueta, D., Jang, J. C., Lu, D., Macchietto, M., Kaur, J., Ge, S., Dillman, A. R., DiPatrizio, N. V., & Nair, M. G. (2018). Host and helminth-derived endocannabinoids are generated during infection with effects on host immunity. *Infect Immun*. https://doi.org/10.1128/iai.00441-18

Batugedara, H. M., Li, J., Chen, G., Lu, D., Patel, J. J., Jang, J. C., Radecki, K. C., Burr, A. C., Lo, D. D., Dillman, A. R., & Nair, M. G. (2018). Hematopoietic cell-derived RELMα regulates hookworm immunity through effects on macrophages. *J Leukoc Biol*, *104*(4), 855-869. https://doi.org/10.1002/jlb.4a0917-369rr

Bisogno, T., Cascio, M. G., Saha, B., Mahadevan, A., Urbani, P., Minassi, A., Appendino, G., Saturnino, C., Martin, B., Razdan, R., & Di Marzo, V. (2006). Development of the first potent and specific inhibitors of endocannabinoid biosynthesis. *Biochim Biophys Acta*, *1761*(2), 205-212. https://doi.org/10.1016/j.bbalip.2005.12.009

Blankman, J. L., Simon, G. M., & Cravatt, B. F. (2007). A comprehensive profile of brain enzymes that hydrolyze the endocannabinoid 2-arachidonoylglycerol. *Chem Biol*, *14*(12), 1347-1356. https://doi.org/10.1016/j.chembiol.2007.11.006

Bottemanne, P., Paquot, A., Ameraoui, H., Alhouayek, M., & Muccioli, G. G. (2019). The alpha/beta-hydrolase domain 6 inhibitor WWL70 decreases endotoxin-induced lung inflammation in mice, potential contribution of 2-

arachidonoylglycerol, and lysoglycerophospholipids. *FASEB J*, *33*(6), 7635-7646. https://doi.org/10.1096/fj.201802259R

Bouchery, T., Filbey, K., Shepherd, A., Chandler, J., Patel, D., Schmidt, A., Camberis, M., Peignier, A., Smith, A. A. T., Johnston, K., Painter, G., Pearson, M., Giacomin, P., Loukas, A., Bottazzi, M. E., Hotez, P., & LeGros, G. (2018). A novel blood-feeding detoxification pathway in Nippostrongylus brasiliensis L3 reveals a potential checkpoint for arresting hookworm development. *PLoS Pathog*, *14*(3), e1006931. https://doi.org/10.1371/journal.ppat.1006931

Cadas, H., di Tomaso, E., & Piomelli, D. (1997). Occurrence and biosynthesis of endogenous cannabinoid precursor, N-arachidonoyl phosphatidylethanolamine, in rat brain. *J Neurosci*, *17*(4), 1226-1242. https://www.ncbi.nlm.nih.gov/pubmed/9006968

Cadas, H., Gaillet, S., Beltramo, M., Venance, L., & Piomelli, D. (1996). Biosynthesis of an endogenous cannabinoid precursor in neurons and its control by calcium and cAMP. *J Neurosci*, *16*(12), 3934-3942. https://www.ncbi.nlm.nih.gov/pubmed/8656287

Chen, C. M., Hwang, J., Chou, H. C., & Chen, C. (2020). Anti-Tn Monoclonal Antibody Attenuates Hyperoxia-Induced Lung Injury by Inhibiting Oxidative Stress and Inflammation in Neonatal Mice. *Front Pharmacol*, *11*, 568502. https://doi.org/10.3389/fphar.2020.568502

Chen, F., Liu, Z., Wu, W., Rozo, C., Bowdridge, S., Millman, A., Van Rooijen, N., Urban, J. F., Wynn, T. A., & Gause, W. C. (2012). An essential role for TH2-type responses in limiting acute tissue damage during experimental helminth infection. *Nat Med*, *18*(2), 260-266. https://doi.org/10.1038/nm.2628

Christensen, R., Kristensen, P. K., Bartels, E. M., Bliddal, H., & Astrup, A. (2007). Efficacy and safety of the weight-loss drug rimonabant: a meta-analysis of randomised trials. *Lancet*, *370*(9600), 1706-1713. https://doi.org/10.1016/S0140-6736(07)61721-8

Cinar, R., Gochuico, B. R., Iyer, M. R., Jourdan, T., Yokoyama, T., Park, J. K., Coffey, N. J., Pri-Chen, H., Szanda, G., Liu, Z., Mackie, K., Gahl, W. A., & Kunos, G. (2017). Cannabinoid CB1 receptor overactivity contributes to the pathogenesis of idiopathic pulmonary fibrosis. *JCI Insight*, *2*(8). https://doi.org/10.1172/jci.insight.92281

Cravatt, B. F., Giang, D. K., Mayfield, S. P., Boger, D. L., Lerner, R. A., & Gilula, N. B. (1996). Molecular characterization of an enzyme that degrades neuromodulatory fatty-acid amides. *Nature*, *384*(6604), 83-87. https://doi.org/10.1038/384083a0

Dainese, E., Oddi, S., Simonetti, M., Sabatucci, A., Angelucci, C. B., Ballone, A., Dufrusine, B., Fezza, F., De Fabritiis, G., & Maccarrone, M. (2020). The endocannabinoid hydrolase FAAH is an allosteric enzyme. *Sci Rep*, *10*(1), 2292. https://doi.org/10.1038/s41598-020-59120-1

de Rond, T., Gao, J., Zargar, A., de Raad, M., Cunha, J., Northen, T. R., & Keasling, J. D. (2019). A High-Throughput Mass Spectrometric Enzyme Activity Assay Enabling the Discovery of Cytochrome P450 Biocatalysts. *Angew Chem Int Ed Engl*, *58*(30), 10114-10119. https://doi.org/10.1002/anie.201901782

Devane, W. A., Hanus, L., Breuer, A., Pertwee, R. G., Stevenson, L. A., Griffin, G., Gibson, D., Mandelbaum, A., Etinger, A., & Mechoulam, R. (1992). Isolation and structure of a brain constituent that binds to the cannabinoid receptor. *Science*, *258*(5090), 1946-1949. https://doi.org/10.1126/science.1470919

Devane, W. A., Howlett, A. C., Johnson, M. R., Melvin, L. S., & Milne, G. M. (1987). Structural studies leading to the discovery of a physiologically relevant cannabinoid receptor-sidte in rat-brain. *Abstracts of Papers of the American Chemical Society*, *194*, 17-MEDI. <Go to ISI>://WOS:A1987J291202505

Di Marzo, V., Fontana, A., Cadas, H., Schinelli, S., Cimino, G., Schwartz, J. C., & Piomelli, D. (1994). Formation and inactivation of endogenous cannabinoid anandamide in central neurons. *Nature*, *372*(6507), 686-691. https://doi.org/10.1038/372686a0

DiPatrizio, N. V. (2016). Endocannabinoids in the Gut. *Cannabis Cannabinoid Res*, *1*(1), 67-77. https://doi.org/10.1089/can.2016.0001

DiPatrizio, N. V. (2021). Endocannabinoids and the Gut-Brain Control of Food Intake and Obesity. *Nutrients*, *13*(4). https://doi.org/10.3390/nu13041214

DiPatrizio, N. V., Igarashi, M., Narayanaswami, V., Murray, C., Gancayco, J., Russell, A., Jung, K. M., & Piomelli, D. (2015). Fasting stimulates 2-AG biosynthesis in the small intestine: role of cholinergic pathways. *Am J Physiol Regul Integr Comp Physiol*, *309*(8), R805-813. https://doi.org/10.1152/ajpregu.00239.2015

DiPatrizio, N. V., & Piomelli, D. (2012). The thrifty lipids: endocannabinoids and the neural control of energy conservation. *Trends Neurosci*, *35*(7), 403-411. https://doi.org/10.1016/j.tins.2012.04.006

Fiskerstrand, T., H'mida-Ben Brahim, D., Johansson, S., M'zahem, A., Haukanes, B. I., Drouot, N., Zimmermann, J., Cole, A. J., Vedeler, C., Bredrup, C., Assoum, M., Tazir, M., Klockgether, T., Hamri, A., Steen, V. M., Boman, H., Bindoff, L. A.,

Koenig, M., & Knappskog, P. M. (2010). Mutations in ABHD12 cause the neurodegenerative disease PHARC: An inborn error of endocannabinoid metabolism. *Am J Hum Genet*, *87*(3), 410-417. https://doi.org/10.1016/j.ajhg.2010.08.002

Fu, J., Astarita, G., Gaetani, S., Kim, J., Cravatt, B. F., Mackie, K., & Piomelli, D. (2007). Food intake regulates oleoylethanolamide formation and degradation in the proximal small intestine. *J Biol Chem*, *282*(2), 1518-1528. https://doi.org/10.1074/jbc.M607809200

Galiègue, S., Mary, S., Marchand, J., Dussossoy, D., Carrière, D., Carayon, P., Bouaboula, M., Shire, D., Le Fur, G., & Casellas, P. (1995). Expression of central and peripheral cannabinoid receptors in human immune tissues and leukocyte subpopulations. *Eur J Biochem*, *232*(1), 54-61. https://www.ncbi.nlm.nih.gov/pubmed/7556170

Ghafouri, N., Tiger, G., Razdan, R. K., Mahadevan, A., Pertwee, R. G., Martin, B. R., & Fowler, C. J. (2004). Inhibition of monoacylglycerol lipase and fatty acid amide hydrolase by analogues of 2-arachidonoylglycerol. *Br J Pharmacol*, *143*(6), 774-784. https://doi.org/10.1038/sj.bjp.0705948

Hawdon, J. M., & Hotez, P. J. (1996). Hookworm: developmental biology of the infectious process. *Curr Opin Genet Dev*, *6*(5), 618-623. https://www.ncbi.nlm.nih.gov/pubmed/8939719

Hirahara, K., Shinoda, K., Morimoto, Y., Kiuchi, M., Aoki, A., Kumagai, J., Kokubo, K., & Nakayama, T. (2019). Immune Cell-Epithelial/Mesenchymal Interaction Contributing to Allergic Airway Inflammation Associated Pathology. *Front Immunol*, *10*, 570. https://doi.org/10.3389/fimmu.2019.00570

Holgate, S. T. (2012). Innate and adaptive immune responses in asthma. *Nat Med*, *18*(5), 673-683. https://doi.org/10.1038/nm.2731

Hoover, H. S., Blankman, J. L., Niessen, S., & Cravatt, B. F. (2008). Selectivity of inhibitors of endocannabinoid biosynthesis evaluated by activity-based protein profiling. *Bioorg Med Chem Lett*, *18*(22), 5838-5841. https://doi.org/10.1016/j.bmcl.2008.06.091

Hotez, P. J. (2008). Neglected infections of poverty in the United States of America. *PLoS Negl Trop Dis*, *2*(6), e256. https://doi.org/10.1371/journal.pntd.0000256

Hussain, Z., Uyama, T., Tsuboi, K., & Ueda, N. (2017). Mammalian enzymes responsible for the biosynthesis of N-acylethanolamines. *Biochim Biophys Acta Mol Cell Biol Lipids*, *1862*(12), 1546-1561. https://doi.org/10.1016/j.bbalip.2017.08.006

Jang, J. C., Chen, G., Wang, S. H., Barnes, M. A., Chung, J. I., Camberis, M., Le Gros, G., Cooper, P. J., Steel, C., Nutman, T. B., Lazar, M. A., & Nair, M. G. (2015). Macrophage-derived human resistin is induced in multiple helminth infections and promotes inflammatory monocytes and increased parasite burden. *PLoS Pathog*, *11*(1), e1004579. https://doi.org/10.1371/journal.ppat.1004579

Kaminski, N. E., Abood, M. E., Kessler, F. K., Martin, B. R., & Schatz, A. R. (1992). Identification of a functionally relevant cannabinoid receptor on mouse spleen-cells that is involved in cannabinoid-mediated immune modulation. *Molecular Pharmacology*, *42*(5), 736-742. <Go to ISI>://WOS:A1992JY34200002

Kaplan, B. L., Lawver, J. E., Karmaus, P. W., Ngaotepprutaram, T., Birmingham, N. P., Harkema, J. R., & Kaminski, N. E. (2010). The effects of targeted deletion of cannabinoid receptors CB1 and CB2 on intranasal sensitization and challenge with adjuvant-free ovalbumin. *Toxicol Pathol*, *38*(3), 382-392. https://doi.org/10.1177/0192623310362706

Knott, M. L., Matthaei, K. I., Foster, P. S., & Dent, L. A. (2009). The roles of eotaxin and the STAT6 signalling pathway in eosinophil recruitment and host resistance to the nematodes Nippostrongylus brasiliensis and Heligmosomoides bakeri. *Mol Immunol*, *46*(13), 2714-2722. https://doi.org/10.1016/j.molimm.2009.05.016

Lambeth, T. R., & Julian, R. R. (2019). Differentiation of peptide isomers and epimers by radical-directed dissociation. *Methods Enzymol*, *626*, 67-87. https://doi.org/10.1016/bs.mie.2019.06.020

Larose, M. C., Turcotte, C., Chouinard, F., Ferland, C., Martin, C., Provost, V., Laviolette, M., & Flamand, N. (2014). Mechanisms of human eosinophil migration induced by the combination of IL-5 and the endocannabinoid 2-arachidonoyl-glycerol. *J Allergy Clin Immunol*, *133*(5), 1480-1482, 1482.e1481-1483. https://doi.org/10.1016/j.jaci.2013.12.1081

Li, W., Blankman, J. L., & Cravatt, B. F. (2007). A functional proteomic strategy to discover inhibitors for uncharacterized hydrolases. *J Am Chem Soc*, *129*(31), 9594-9595. https://doi.org/10.1021/ja073650c

Long, J. Z., Li, W., Booker, L., Burston, J. J., Kinsey, S. G., Schlosburg, J. E., Pavón, F. J., Serrano, A. M., Selley, D. E., Parsons, L. H., Lichtman, A. H., & Cravatt, B. F. (2009). Selective blockade of 2-arachidonoylglycerol hydrolysis produces cannabinoid behavioral effects. *Nat Chem Biol*, *5*(1), 37-44. https://doi.org/10.1038/nchembio.129

Marrs, W. R., Blankman, J. L., Horne, E. A., Thomazeau, A., Lin, Y. H., Coy, J., Bodor, A. L., Muccioli, G. G., Hu, S. S., Woodruff, G., Fung, S., Lafourcade, M., Alexander, J. P., Long, J. Z., Li, W., Xu, C., Möller, T., Mackie, K., Manzoni, O. J., Cravatt, B. F., & Stella, N. (2010). The serine hydrolase ABHD6 controls the accumulation and efficacy of 2-AG at cannabinoid receptors. *Nat Neurosci*, *13*(8), 951-957. https://doi.org/10.1038/nn.2601

Marsland, B. J., Kurrer, M., Reissmann, R., Harris, N. L., & Kopf, M. (2008). Nippostrongylus brasiliensis infection leads to the development of emphysema associated with the induction of alternatively activated macrophages. *Eur J Immunol*, *38*(2), 479-488. https://doi.org/10.1002/eji.200737827

Mechoulam, R., Benshabat, S., Hanus, L., Ligumsky, M., Kaminski, N. E., Schatz, A. R., Gopher, A., Almog, S., Martin, B. R., Compton, D. R., Pertwee, R. G., Griffin, G., Bayewitch, M., Barg, J., & Vogel, Z. (1995). Identification of an endogenous 2-monoglyceride, present in canine gut, that binds to cannabinoid receptors. *Biochemical Pharmacology*, *50*(1), 83-90. https://doi.org/10.1016/0006-2952(95)00109-d

Meng, F., & Alayash, A. I. (2017). Determination of extinction coefficients of human hemoglobin in various redox states. *Anal Biochem*, *521*, 11-19. https://doi.org/10.1016/j.ab.2017.01.002

Nagarkatti, P., Pandey, R., Rieder, S. A., Hegde, V. L., & Nagarkatti, M. (2009). Cannabinoids as novel anti-inflammatory drugs. *Future Med Chem*, *1*(7), 1333-1349. https://doi.org/10.4155/fmc.09.93

Ohira, M., Okuyama, T., & Mashima, R. (2018). Quantification of 11 enzyme activities of lysosomal storage disorders using liquid chromatography-tandem mass spectrometry. *Mol Genet Metab Rep*, *17*, 9-15. https://doi.org/10.1016/j.ymgmr.2018.08.005

Pandey, R., Mousawy, K., Nagarkatti, M., & Nagarkatti, P. (2009). Endocannabinoids and immune regulation. *Pharmacological Research*, *60*(2), 85-92. https://doi.org/10.1016/j.phrs.2009.03.019

Pertwee, R. G. (2015). Endocannabinoids and Their Pharmacological Actions. *Handb Exp Pharmacol*, *231*, 1-37. https://doi.org/10.1007/978-3-319-20825-1_1

Pine, G. M., Batugedara, H. M., & Nair, M. G. (2018). Here, there and everywhere: Resistin-like molecules in infection, inflammation, and metabolic disorders. *Cytokine*, *110*, 442-451. https://doi.org/10.1016/j.cyto.2018.05.014

Piomelli, D. (2003). The molecular logic of endocannabinoid signalling. *Nat Rev Neurosci*, *4*(11), 873-884. https://doi.org/10.1038/nrn1247

Piomelli, D., Scalvini, L., Fotio, Y., Lodola, A., Spadoni, G., Tarzia, G., & Mor, M. (2020). N-Acylethanolamine Acid Amidase (NAAA): Structure, Function, and Inhibition. *J Med Chem*, *63*(14), 7475-7490. https://doi.org/10.1021/acs.jmedchem.0c00191

Piomelli, D., Tarzia, G., Duranti, A., Tontini, A., Mor, M., Compton, T. R., Dasse, O., Monaghan, E. P., Parrott, J. A., & Putman, D. (2006). Pharmacological profile of the selective FAAH inhibitor KDS-4103 (URB597). *CNS Drug Rev*, *12*(1), 21-38. https://doi.org/10.1111/j.1527-3458.2006.00021.x

Powell, W. S., & Rokach, J. (2013). The eosinophil chemoattractant 5-oxo-ETE and the OXE receptor. *Prog Lipid Res*, *52*(4), 651-665. https://doi.org/10.1016/j.plipres.2013.09.001

Ramarao, M. K., Murphy, E. A., Shen, M. W., Wang, Y., Bushell, K. N., Huang, N., Pan, N., Williams, C., & Clark, J. D. (2005). A fluorescence-based assay for fatty acid amide hydrolase compatible with high-throughput screening. *Anal Biochem*, *343*(1), 143-151. https://doi.org/10.1016/j.ab.2005.04.032

Reece, J. J., Siracusa, M. C., & Scott, A. L. (2006). Innate immune responses to lung-stage helminth infection induce alternatively activated alveolar macrophages. *Infect Immun*, *74*(9), 4970-4981. https://doi.org/10.1128/iai.00687-06

Roulette, C. J., Kazanji, M., Breurec, S., & Hagen, E. H. (2016). High prevalence of cannabis use among Aka foragers of the Congo Basin and its possible relationship to helminthiasis. *Am J Hum Biol*, *28*(1), 5-15. https://doi.org/10.1002/ajhb.22740

Roxana, I., Kiyomi, F., Kazuhiko, H., Iwasakib, Y., & Tsuneo, Y. (2001). Two-step enzymatic synthesis of docosahexaenoic acid-rich symmetrically structured triacylglycerols via 2-monoacylglycerols. In (pp. 743-748). Journal of American Oil Chemist Society.

Savinainen, J. R., Saario, S. M., & Laitinen, J. T. (2012). The serine hydrolases MAGL, ABHD6 and ABHD12 as guardians of 2-arachidonoylglycerol signalling through cannabinoid receptors. *Acta Physiol (Oxf)*, *204*(2), 267-276. https://doi.org/10.1111/j.1748-1716.2011.02280.x

Scalvini, L., Ghidini, A., Lodola, A., Callegari, D., Rivara, S., Piomelli, D., & Mor, M. (2020). N-Acylethanolamine Acid Amidase (NAAA): Mechanism of Palmitoylethanolamide Hydrolysis Revealed by Mechanistic Simulations. *ACS Catalysis*, *10*(20), 11797-11813.

Solorzano, C., Zhu, C., Battista, N., Astarita, G., Lodola, A., Rivara, S., Mor, M., Russo, R., Maccarrone, M., Antonietti, F., Duranti, A., Tontini, A., Cuzzocrea, S., Tarzia, G., & Piomelli, D. (2009). Selective N-acylethanolamine-hydrolyzing acid amidase inhibition reveals a key role for endogenous palmitoylethanolamide in inflammation. *Proc Natl Acad Sci U S A, 106*(49), 20966-20971. https://doi.org/10.1073/pnas.0907417106

Stella, N., Schweitzer, P., & Piomelli, D. (1997). A second endogenous cannabinoid that modulates long-term potentiation. *Nature, 388*(6644), 773-778. https://doi.org/10.1038/42015

Stevens, W. W., Kim, T. S., Pujanauski, L. M., Hao, X., & Braciale, T. J. (2007). Detection and quantitation of eosinophils in the murine respiratory tract by flow cytometry. *J Immunol Methods, 327*(1-2), 63-74. https://doi.org/10.1016/j.jim.2007.07.011

Su, J., Rajapaksha, T. W., Peter, M. E., & Mrksich, M. (2006). Assays of endogenous caspase activities: a comparison of mass spectrometry and fluorescence formats. *Anal Chem, 78*(14), 4945-4951. https://doi.org/10.1021/ac051974i

Sun, H., Zhang, H., Ang, E. L., & Zhao, H. (2018). Biocatalysis for the synthesis of pharmaceuticals and pharmaceutical intermediates. *Bioorg Med Chem, 26*(7), 1275-1284. https://doi.org/10.1016/j.bmc.2017.06.043

Sutherland, T. E., Rückerl, D., Logan, N., Duncan, S., Wynn, T. A., & Allen, J. E. (2018). Ym1 induces RELMα and rescues IL-4Rα deficiency in lung repair during nematode infection. *PLoS Pathog, 14*(11), e1007423. https://doi.org/10.1371/journal.ppat.1007423

Tchantchou, F., & Zhang, Y. M. (2013). Selective Inhibition of Alpha/Beta-Hydrolase Domain 6 Attenuates Neurodegeneration, Alleviates Blood Brain Barrier Breakdown, and Improves Functional Recovery in a Mouse Model of Traumatic Brain Injury. *Journal of Neurotrauma, 30*(7), 565-579. https://doi.org/10.1089/neu.2012.2647

Tsuboi, K., Uyama, T., Okamoto, Y., & Ueda, N. (2018). Endocannabinoids and related N-acylethanolamines: biological activities and metabolism. *Inflamm Regen, 38*, 28. https://doi.org/10.1186/s41232-018-0086-5

Tsuboi, K., Zhao, L. Y., Okamoto, Y., Araki, N., Ueno, M., Sakamoto, H., & Ueda, N. (2007). Predominant expression of lysosomal N-acylethanolamine-hydrolyzing acid amidase in macrophages revealed by immunochemical studies. *Biochim Biophys Acta, 1771*(5), 623-632. https://doi.org/10.1016/j.bbalip.2007.03.005

Weatherhead, J. E., Hotez, P. J., & Mejia, R. (2017). The Global State of Helminth Control and Elimination in Children. *Pediatr Clin North Am*, *64*(4), 867-877. https://doi.org/10.1016/j.pcl.2017.03.005

Wei, B. Q., Mikkelsen, T. S., McKinney, M. K., Lander, E. S., & Cravatt, B. F. (2006). A second fatty acid amide hydrolase with variable distribution among placental mammals. *J Biol Chem*, *281*(48), 36569-36578. https://doi.org/10.1074/jbc.M606646200

Figures and Legends

Figure 3.1

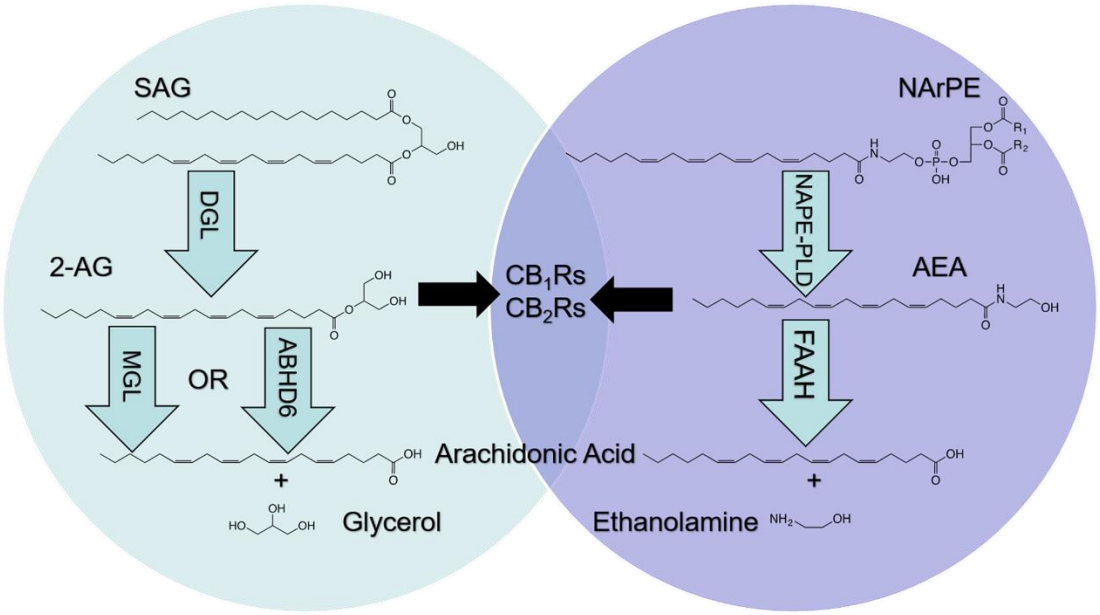

Figure 3.1: Metabolism of endocannabinoids (eCBs). The eCBs, 2-arachidonoyl-*sn*-glycerol (2-AG) and arachidonoyl ethanolamide (AEA), activate cannabinoid receptor subtype-1 (CB1Rs) and subtype-2 (CB2Rs) located in cells throughout the body; however, metabolic pathways are not shared. 2-AG is produced following hydrolysis of the 2-AG precursor, 1, stearoyl,2-arachidonoyl-sn-glycerol (SAG), by diacyl glycerol lipase (DGL). 2-AG is degraded by monoacylglycerol lipase (MGL) and alpha/beta hydrolase domain-6 (ABHD6) into arachidonic acid (AA) and glycerol (left). AEA is produced following hydrolysis of the AEA precursor, N-arachidonoylphosphatidylethanolamide (NArPE), by N-acylphosphatidylethanolamide phospholipase D (NAPE-PLD). AEA is degraded by fatty acid amide hydrolase (FAAH) into AA and ethanolamine (right).

Figure 3.2

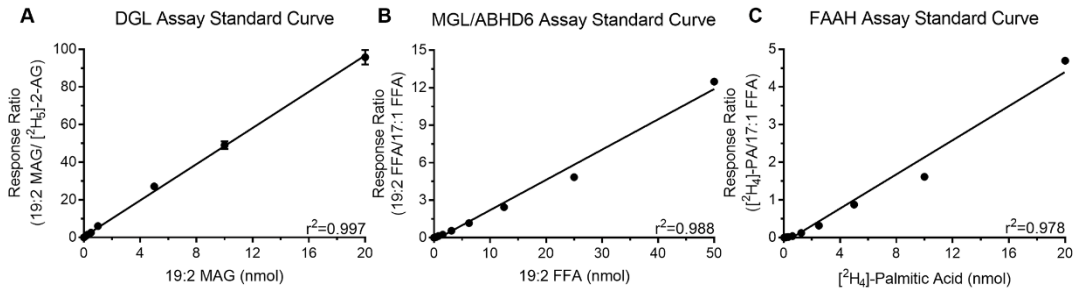

Figure 3.2: Standard curves for quantitation of the products generated during the DGL (A), MGL/ABHD6 (B), and FAAH (C) activity assays.

Figure 3.3

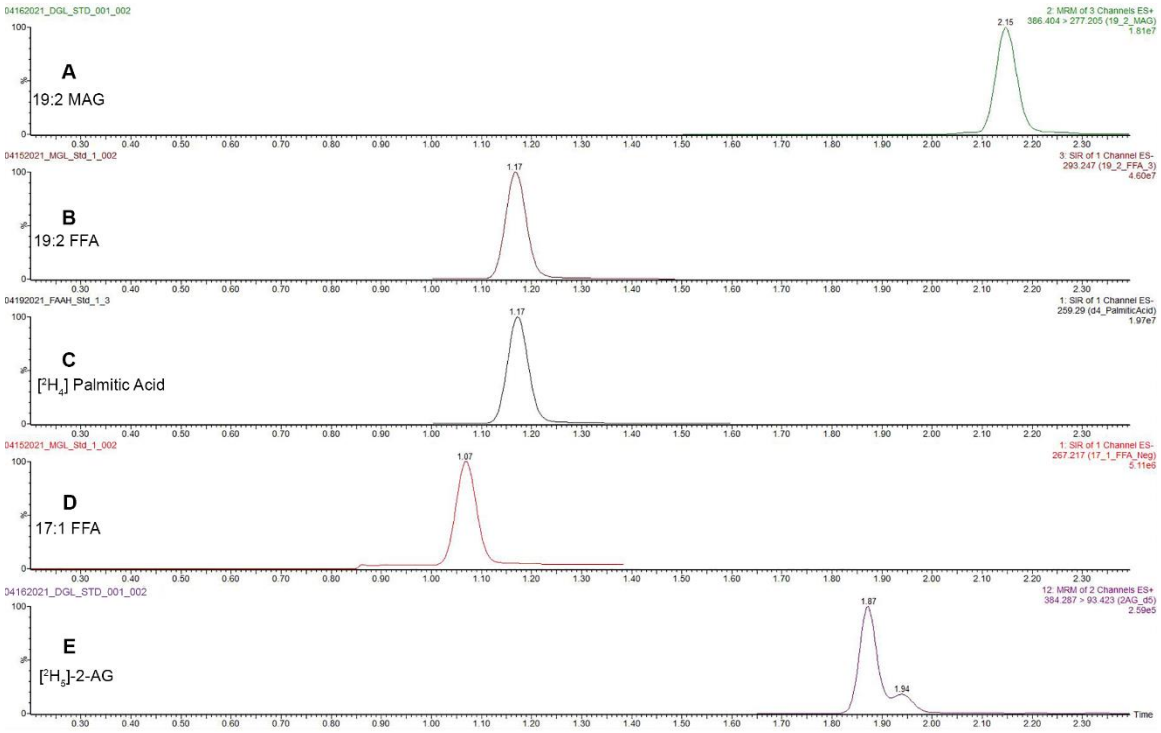

Figure 3.3: Representative chromatograms including retention times and predicted masses of products from the reactions of the DGL (A), MGL/ABHD6 (B), and FAAH assays (C) and for the internal standards for the DGL (D) and MGL/ABHD6/FAAH assays (E).

Figure 3.4

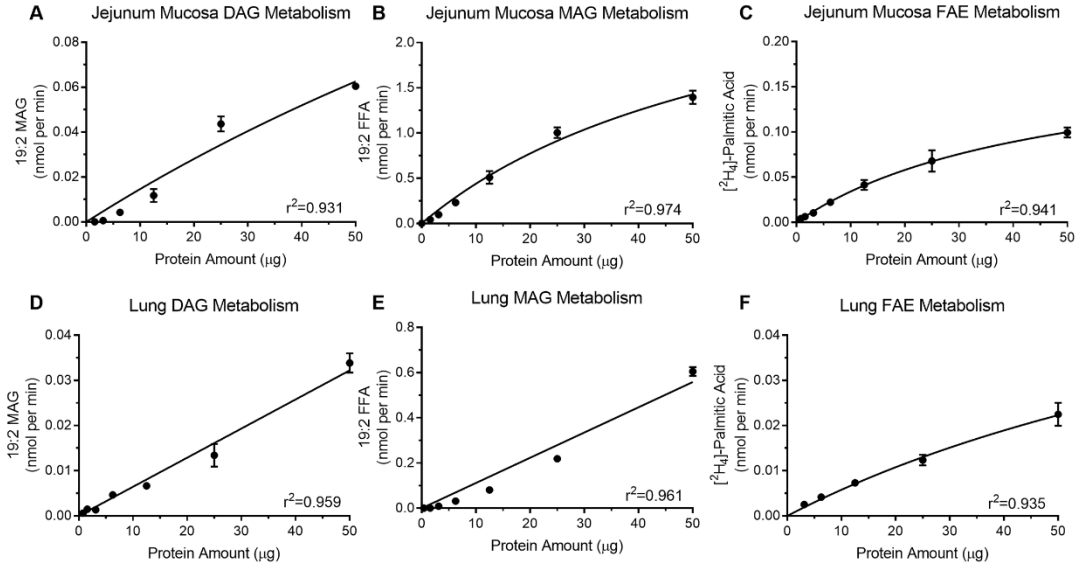

Figure 3.4: Isolated protein from mouse jejunum mucosa display increases in product recovery as protein amount increases for DGL activity (A), MGL activity (B), and FAAH (C). Mouse lung protein isolates exhibit increases in product recovery as the amount of protein increased for DGL (D), MGL (E), and FAAH (F).

Figure 3.5

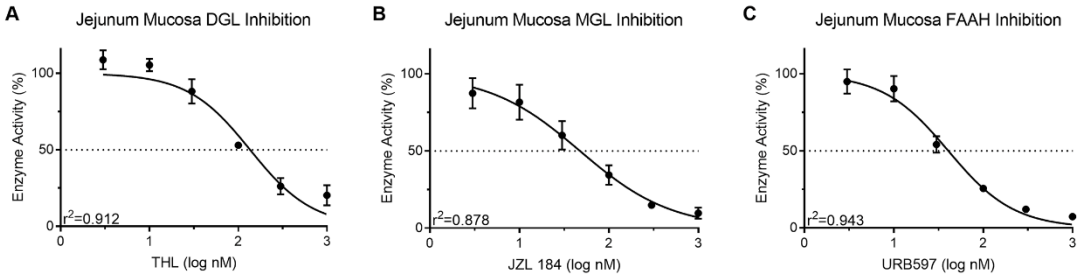

Figure 3.5: Activity of the MAG biosynthetic enzyme, DGL, in mouse small-intestinal epithelium was dose-dependently inhibited by the DGL inhibitor, THL (A) IC_{50} = 136.3 nM. Activity of the MAG degradative enzyme, MGL, in small-intestinal epithelium was dose-dependently inhibited by the MGL inhibitor, JZL 184 (B) IC_{50} = 47.62 nM. Activity of the FAE degradative enzyme, FAAH, in small-intestinal epithelium was inhibited by the FAAH inhibitor, URB597 (C) IC_{50} = 40.76 nM.

Figure 3.6

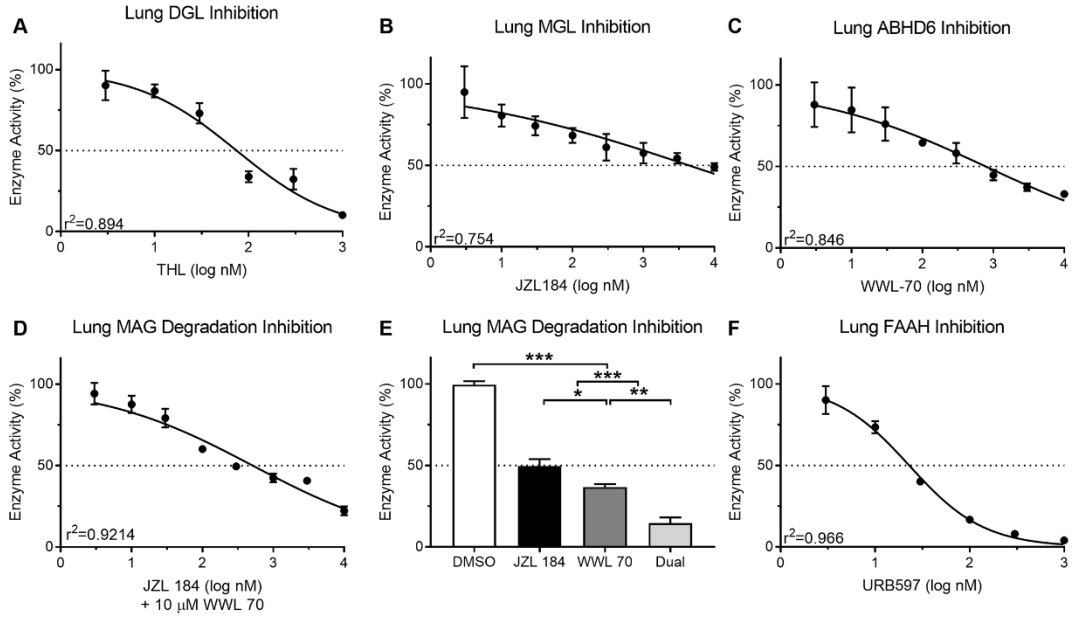

Figure 3.6: Activity of the MAG biosynthetic enzyme, DGL, in mouse lung protein isolates was dose-dependently inhibited by the DGL inhibitor, THL (A) IC_{50} = 74.64 nM. In contrast to small-intestinal epithelium, activity of the MAG degradative enzyme, MGL, in mouse lung was not effectively reduced past 50% with concentrations up to nearly 10 mM of the MGL inhibitor, JZL 184 (B) IC_{50} = 4,394 nM. Activity of the MAG degradative enzyme, ABHD6, in mouse lung was inhibited by the ABHD6 inhibitor, WWL 70 (C) IC_{50} = 779.9 nM. Dose-dependent inhibition of MAG metabolism in mouse lung tissue was achieved when all samples were also incubated with 10 mM WWL 70 (D) IC_{50} = 510.14 nM. When mouse lung was incubated together at 10x the respective IC_{50} for each MAG degradation inhibitor (JZL 184 = 43,940 nM; WWL 70 = 7,799 nM), MAG degradative enzyme activity was reduced to 14.62% (E). Activity of the FAE degradative enzyme, FAAH, in mouse lung protein isolates was inhibited by the FAAH inhibitor, URB597 (F) IC_{50} = 22.95 nM.

Figure 3.7

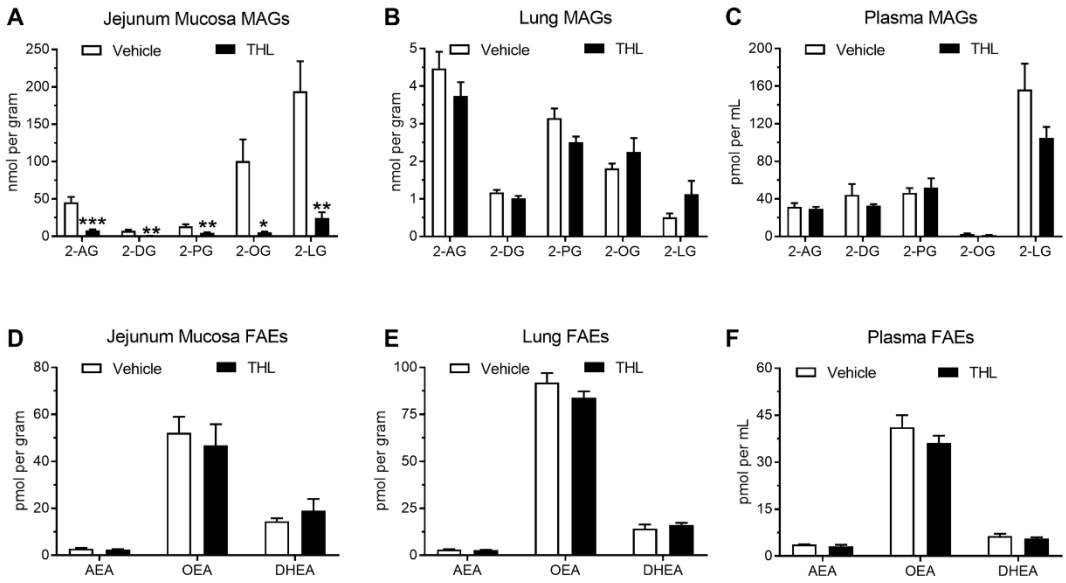

Figure 3.7: Oral gavage of the DGL inhibitor, THL, inhibited production of MAGs in the upper small-intestinal epithelium (A), but not in lung (B) or in circulation (C). THL had no effect on levels of FAEs in upper small-intestinal epithelium (D), lung (E), and circulation (F). *-indicates p-value < 0.05, **-indicates p-value < 0.01, ***-indicates p-value < 0.001, n = 6–8.

Chapter 4 – CB1 Receptors in the Intestinal Epithelium are Protective Against Gut Barrier Dysfunction in Diet Induced Obesity

Abstract

More than 70% of Americans are considered overweight or obese which leads to the development of several chronic comorbidities. One ailment associated with obesity is Inflammatory Bowel Disease (IBD) which has an idiopathic etiology and more than 3 million Americans diagnosed. The expansion of IBD development is observed exclusively in well-developed regions of the world where a western-style diet high in both fat and carbohydrates, derived from sucrose, has been adopted. Western-diet induced obesity leads to disruptions in the endocannabinoid (eCB) system throughout the intestinal tract and has been shown to contribute to gut-barrier function. Gut-barrier function is essential to providing protection from potentially pathogenic organisms ingested in a meal and its dysfunction directly contributes to IBD pathogenesis. Here, we tested the hypothesis that intestinal epithelial cannabinoid receptor subtype-1 (CB_1R) signaling provides protection from diet-induced gut-barrier dysfunction. We found that WD-fed mice display significantly reduced levels of the eCB, 2-arachidonoyl-*sn*-glycerol (2-AG), and several other monoacylglycerol (MAG) species when compared to SD-fed mice; an effect due to a down regulation in DGL activity. Furthermore, WD-fed mice lacking intestinal epithelial CB_1R display significantly worsened paracellular permeability compared to Flox control litter mates. NanoString analysis on colon mucosa samples from these mice indicate that $iCB_1R^{-/-}$ mice have a down regulation of tight

junction protein RNA with an upregulation in inflammatory associated RNA. Chronic THC treatment for 14 days ameliorated the diet-induced disruption in gut-barrier function. Furthermore, the dysregulation of tight junction protein and inflammatory associated RNA was rescued in the THC treated mice indicating a significant role for CB_1R and the eCB system in diet-induced gut-barrier disruption. Future experiments will include analysis of the mechanism in this response. Furthermore, chronic THC administration to $iCB_1R^{-/-}$ after 60 days on WD will be performed to identify if intestinal epithelial CB_1R signaling is required for the THC-induced rescue of gut-barrier function.

Introduction

It is estimated that more than 70% of US adults are considered to be overweight or obese which disrupts several systems throughout the human body leading to comorbidities (Ogden et al., 2012). Inflammatory bowel disease (IBD) is heavily associated with obesity with more than 3.5 million individuals diagnosed across the US and UK (Ng et al., 2017). Development of IBD is associated with an over-active immune response which compromises the barrier function of the intestinal tissue with idiopathic etiology (Bouma & Strober, 2003; Vancamelbeke & Vermeire, 2017). The gut-barrier is essential for protecting the organism from pathogens ingested via the alimentary canal and consists of 3 layers: 1) the mucous barrier consistent of IgA antibodies and mucins, 2) single cell layer of epithelial cells lining the entire small and large intestine, and 3) transmembrane tight junction proteins which provide protection from organisms and ions

that can pass between epithelial cells (Vancamelbeke & Vermeire, 2017). IBD diagnosis rates have increased exclusively in well-developed regions of the world where a western-style diet has been adopted which is high in both fat and sugar, derived from sucrose (Actis et al., 2019; Martinez-Medina et al., 2014).

Western diet-induced obesity has been shown to severely dysregulate the lipid signaling endocannabinoid (eCB) system as well (Argueta & DiPatrizio, 2017; DiPatrizio, 2021). This eCB system consists of the endogenously produced ligands 2-arachidonoyl-*sn*-glycerol (2-AG) and anandamide (AEA), the cannabinoid receptors [cannabinoid receptor subtype-1 (CB_1R), -2 (CB_2R), and possibly others], and the enzymatic machinery necessary to produce and degrade these lipids (Devane et al., 1992; Devane et al., 1987; DiPatrizio, 2021; Kaminski et al., 1992; Mechoulam et al., 1995; Pertwee, 2015; Piomelli, 2003). ECBs are derived from the plasma membrane of the cell and are produced on demand through distinct metabolic pathways (DiPatrizio, 2021). Production of 2-AG, and several other monoacylglycerol (MAG) species, is catalyzed via diacylglycerol lipase (DGL) and is degraded, primarily, via monoacylglycerol lipase (MGL) (Alexander & Kendall, 2007; DiPatrizio, 2021). Anandamide is produced through a multi-step Ca^{2+}-dependent mechanism involving first N-acyltransferase (NAT) then N-acyl phosphatidylethanolamine-specific phospholipase D (NAPE-PLD) to produce AEA which can be further degraded via Fatty Acid Amide Hydrolase (FAAH) (Cadas et al., 1997; Cadas et al., 1996; Cravatt et al., 1996; Di Marzo et al., 1994; Wei et al., 2006).

The eCB system is expressed in cells throughout the human body including the intestinal tract and large intestine contributing to a variety of homeostatic functions

(Argueta et al., 2019; Lee et al., 2016; Wright et al., 2005). Activation of CB_1R has been shown to contribute to the development of obesity through both central and peripheral mechanisms (Argueta & DiPatrizio, 2017; Argueta et al., 2019; Higuchi et al., 2012). More specifically, activation of CB_1R on small intestinal enteroendocrine cells controls release of the satiety hormone cholecystokinin (CCK), indicating an essential role for CB_1R signaling on intestinal epithelial cell function (Argueta et al., 2019). CB_2R has been found to be most highly expressed in immune tissue where activation is associated with immunosuppression (Carayon et al., 1998; Galiègue et al., 1995; Turcotte et al., 2016). Due to the enhanced inflammatory response in IBD models, several studies have implicated the role for CB_2R signaling in directly modulating the immune response (Acharya et al., 2017; Harvey et al., 2013; Harvey et al., 2014). Studies implicating the role for CB_1R activation in controlling gut-barrier function provide conflicting results which appear to be dependent upon both the receptor localization (i.e. basolateral vs. apical) and the model by which barrier function is disrupted (Alhamoruni et al., 2010; Alhamoruni et al., 2012; Karwad et al., 2017). Thus, more research is necessary to identify the exact mechanism by which CB_1R signaling is contributing to gut-barrier function.

Several models exist to elucidate IBD development, including ones that employ harsh chemicals (i.e. dextran sodium sulfate, DSS) which cause epithelial cell apoptosis along the intestinal tract stimulating a strong inflammatory response at the site of damage (Eichele & Kharbanda, 2017). Diet-induced obesity provides a less severe model for inducing gut-barrier dysfunction while maintaining the integrity of the tissue. Previous

studies have identified that DIO stimulates an increase in paracellular permeability in the large intestine through a down regulation of tight-junction protein expression (ZO-1, Occludin) and an increase in inflammatory makers (IL-6, TNFα, T-cell infiltrate) in the tissue (Lam et al., 2012; Lee et al., 2017). This provides an ideal model for identifying discrete changes in gut-barrier function without compromising the architecture of the intestinal tract.

Here, we employ a high-fat, high-sucrose western diet (WD) to stimulate DIO in male WT mice and in mice lacking intestinal epithelial CB_1R ($iCB_1R^{-/-}$) signaling to study the role for intestinal epithelial CB_1R signaling in diet-induced gut-barrier dysfunction.

Materials and Methods

Mice and Diets

Male C57BL/6N (Taconic, Oxnard, CA, USA), conditional intestinal epithelium-specific CB_1R-deficient ($iCB_1R^{-/-}$) (Argueta et al., 2019; Avalos et al., 2020), or Flox control mice were given *ad libitum* access to water and either a standard laboratory rodent diet (SD; Teklad 202x, Envigo, Huntingdon, UK; 16% kcal from fat, 24% kcal from protein, 60% kcal from carbohydrate as primarily starch) or a Western Diet (WD; Research Diets D12079B, New Brunswick, NJ, USA; 40% kcal from fat, 17% kcal from protein, 43% kcal from carbohydrates as mostly sucrose). All protocols for animal use and euthanasia were approved by the University of California Riverside Institutional

Animal Care and Use Committee (protocol A-20200022) and were in accordance with National Institutes of Health guidelines, the Animal Welfare Act, and Public Health Service Policy on Humane Care and Use of Laboratory Animals. A schematic displaying the design of the experiments is provided in Figure 4.1A.

Chemical Preparation and Administration

Flox control and $iCB_1R^{-/-}$ mice received daily intraperitoneal (IP) injections of tamoxifen (Sigma-Aldrich, St. Louis, MO, USA) for five consecutive days as previously described (Avalos et al., 2020). Mice in the two-week rescue experiments received daily IP injections of either vehicle (90% saline, 5% ethanol, 5% tween-80) or Δ^9-Tetrahydrocannabinol (National Institute on Drug Abuse Drug Supply Program) for 14 consecutive days. Fluorescein isothiocyanate (FITC) conjugated to dextran (4 kDa; Sigma-Aldrich, St. Louis, MO, USA) was administered via oral gavage in the *in vivo* gut-barrier permeability experiments.

***in vivo* Gut-barrier Permeability Assay and Tissue Harvest**

To prevent coprophagia, animals were maintained on elevated wire-bottom cages for a 72-hour acclimation period and throughout the FITC-Dextran experiment. Food was removed from the cages 4 hours prior to gavage with FITC-Dextran and was withheld throughout the experiment. Water was removed after oral gavage with FITC-Dextran to control for metabolism and rate of urination and was returned to the cages immediately after serum was collected (four hours later). At the time of gavage, mice received 0.6 mg/g of 4 kDa FITC-Dextran (100 mg/mL in pure H_2O). Evidence indicates that nearly

all FITC-Dextran will have diffused into the large intestine four hours following oral gavage (Woting & Blaut, 2018); therefore, retro-orbital bleeds were performed four hours following administration to collect serum for quantitation of circulating FITC-Dextran as a marker for large intestinal paracellular permeability. At the time of harvest, the epididymal fat pad was removed, rinsed in chilled 1x PBS, dried, and weighed prior to being snap frozen in liquid N_2. Large intestines were removed, rinsed in chilled 1x PBS, and fecal matter was removed prior to the recording of the weight and length of the tissue. The large intestine was opened longitudinally and gently washed. Glass slides were used to scrape the intestinal epithelium layer, which was then placed on dry ice, snap frozen in liquid N_2, and stored at -80^{O}C until further analysis was performed.

Tissue Lipid Extraction

Lipid extractions and analysis were performed as previously described (Argueta et al., 2019; Batugedara, Argueta, et al., 2018). Briefly, frozen large intestine mucosa scrapes were weighed and placed into 1.0 mL of chilled MeOH containing the internal standards [$^{2}H_5$]-2-AG (500 pmol; Cayman Chemical, Ann Arbor, MI, United States), [$^{2}H_4$]-AEA (1 pmol; Cayman Chemical, Ann Arbor, MI, United States), and [$^{2}H_4$]-OEA (10 pmol; Cayman Chemical, Ann Arbor, MI, United States).). Lipids were extracted using chloroform (2.0 mL) prior to being washed with 1.0 mL 0.2-micron ultra-purified water. Following centrifugation (1,500 x g, 15 min, 4^{O}C), the lower organic phase was collected and dried under N_2 steam (99.998% pure). A second chloroform wash (1.0 mL) was then performed followed by another centrifugation (1,500 x g, 15 min, 4^{O}C) and collection of the lower phase. Samples were reconstituted in 2.0 mL of chloroform and purified via

open-bed silica gel column chromatography. Columns were washed with a 9:1 chloroform:methanol mixture to elute MAGs and FAEs for collection. Collected eluates were dried under N_2 steam (99.998% pure) and resuspended in 0.2 mL of methanol:chloroform (1:1) prior to analysis via UPLC-MS/MS.

UPLC-MS/MS Analysis of FAEs, MAGs, and Enzyme Assay Products

Quantitation of FAEs and MAGs

Data was acquired using an Acquity I-Class UPLC with direct line connection to a Xevo TQ-S Micro Mass Spectrometer (Waters Corporation, Milford, MA, United States) with electrospray ionization (ESI) sample delivery. Lipids were separated using an Acquity UPLC BEH C_{18} column (2.1 x 50 mm i.d., 1.7 mm, Waters) and inline Acquity guard column (UPLC BEH C_{18} VanGuard PreColumn; 2.1 x 5 mm i.d.; 1.7 mm, Waters), and eluted by an analyte specific gradient of water and methanol (both containing 0.25% acetic acid, 5mM ammonium acetate). Samples were kept at 10^{O}C in the sample manager and the column was maintained at 40^{O}C. Argon (99.998%) was used as collision gas. Analytes were eluted at a flow rate of 0.4 mL/min and gradient: 80% methanol 0.0–0.5 min, 80–100% methanol 0.5–2.5 min, 100% methanol 2.5–3.0 min, 100–80% methanol 3.0–3.1 min, and 80% methanol 3.1–4.5 min. MS/MS detection was in positive ion mode and capillary voltage set at 0.1 kV. Extracted ion chromatograms were used to quantify AEA (m/z = 348.3 > 62.0), [$^2H_4$]-AEA (m/z = 352.3 > 66.1), OEA (m/z = 326.4 > 62.1), [$^2H_4$]-OEA (m/z = 330.4 > 66.0), DHEA (m/z = 372.3 > 91.0), 2-AG (m/z = 379.3 > 287.3), [$^2H_5$]-2-AG (m/z = 384.3 > 93.4), 2-DG (m/z = 403.3 > 11.1),

2-OG (m/z = 357.4 > 265.2), and 2-LG (m/z = 355.3 > 263.3). Quantitation occurred using a stable isotope dilution method to detect protonated adducts of the ions [M + H] + in multiple reactions monitoring (MRM) mode. Acyl migration is known to occur in many MAG species following silica-gel purification, therefore the sum of 1-AG and 2-AG, 1-OG and 2-OG, and 1-DG and 2-DG are reported (Stella et al., 1997).

Quantitation of DGL Assay Product

Data was acquired using the equipment and the elution protocol described above ("Quantitation of FAEs and MAGs"). MS/MS detection was in positive ion mode with capillary voltage maintained at 1.10 kV. Cone voltages and collision energies for respective analytes: 19:2 MAG = 18 v, 10 v; [$^2H_5$]-2-AG = 25 v, 44 v. Lipids were quantified using a stable isotope serial dilution method detecting H^+ or Na^+ adducts of the molecular ions [M + H/Na] + in multiple reactions monitoring (MRM) mode (variable amounts of product dinonadecadienoin (19:2 DAG, Nu-Chek Prep, Waterville, MN, USA) versus fixed amount of internal standard [$^2H_5$]-2-AG). Acyl migration from sn-2 to sn-1 positions in monoacylglycerols is known to occur (Roxana et al., 2001; Stella et al., 1997); thus the sum of these isoforms ([$^2H_5$]-1-AG and [$^2H_5$]-2-AG) is presented. Extracted ion chromatograms for MRM transitions were used to quantify analytes: 19:2 MAG (m/z = 386.4 > 277.2) product of DGL assay and [$^2H_5$]-2-AG (m/z = 384.3 > 93.4) as internal standard.

Quantitation of MGL Activity Assay Product

Data acquired using equipment described above ("Quantitation of FAEs and MAGs"). Samples were eluted by a gradient of water and methanol (containing 0.25% acetic acid, 5 mM ammonium acetate) at a flow rate of 0.4 mL/min and gradient: 90% methanol 0.0–0.1 min, 90–100% methanol 0.1–2.0 min, 100% methanol 2.0–2.1 min, 100–90% methanol 2.1–2.2 min, and 90% methanol 2.2–2.5 min. MS detection was in negative ion mode with capillary voltage maintained at 3.00 kV. Cone voltages for nonadecadienoic acid (19:2 FFA; Nu-Chek Prep, Waterville, MN, USA) = 48 v and heptadecanoic acid (17:1 FFA; Nu-Chek Prep, Waterville, MN, USA) = 64 v. Lipids were quantified using a dilution series detecting deprotonated molecular ions in selected ion reading (SIR) mode (variable amounts of product 19:2 FFA versus fixed amount of internal standard 17:1 FFA). Extracted ion chromatograms for SIR masses were used to quantify analytes: 19:2 FFA (m/z = 293.2) product of MGL enzyme assay and 17:1 FFA (m/z = 267.2) as internal standard.

DGL and MGL Activity Assays

Protein Isolation

Assays performed to determine DGL and MGL activity were performed as previously described (Argueta et al., 2019; Batugedara, Argueta, et al., 2018). Briefly, samples homogenized in 2 mL of chilled 50 mM Tris–HCl, 320 mM sucrose buffer (pH = 7.5) were centrifuged at 800 x g for 15 min at 4^{O}C. The supernatant was collected in a 2.0 mL centrifuge tube and sonicated twice for 10 s prior to two sequential freeze thaw

cycles. Centrifuged (800 x g, 15 min, 4^{O}C) supernatants were then quantified via BCA assay and normalized between all samples.

DGL Activity Assay

Normalized large intestine protein samples (100 mL) were incubated at 37^{O}C for 30 min with 20 nmol/reaction of 19:2 DAG in buffer (50 mM Tris-HCl, 0.2% Triton x-100, pH=7.0). The reaction was stopped by the addition of 1.0 mL of chilled methanol containing 25 pmol of the internal standard [$^{2}H_{5}$]-2-AG. Lipids were extracted as described above ("Tissue Lipid Extraction") and quantified as described above ("UPLC-MS/MS Analysis of FAEs, MAGs, and Enzyme Assay Products").

MGL Activity Assay

Normalized large intestine protein samples (100 mL) were incubated at 37^{O}C for 10 min with 50 nmol/reaction of 19:2 MAG in buffer (50 mM Tris-HCl, 0.25% Fatty-Acid Free BSA, pH=8.0). The reaction was stopped by the addition of 1.0 mL of chilled methanol containing 5 nmol/reaction of the internal standard 17:1 FFA. Lipids were extracted as described above ("Tissue Lipid Extraction") and quantified as described above ("UPLC-MS/MS Analysis of FAEs, MAGs, and Enzyme Assay Products").

Large Intestine Imaging

At the time of harvest the large intestine was removed and flushed with 4% Paraformaldehyde (PFA) and then stored in a 4% PFA solution over-night. The large intestine was then transferred to a 30% sucrose solution for 48 hours, blocked in OCT,

and sliced at 5 µm thick sections for staining. Hematoxylin and eosin staining and imaging under a DM5500B microscope (Leica) was performed as previously described (Wiley et al., 2021).

RNA Analysis

RNA Isolation and Quantitative Real-time PCR (qPCR)

Total RNA was isolated from large intestine mucosal scrapes using a RNeasy kit (Qiagen, Valencia, CA, USA) and first-strand cDNA was generated using M-MLV reverse transcriptase (Invitrogen, Carlsbad, CA, USA). PrimePCR Assays (Biorad, Irvine, CA, USA) were used to perform quantitative RT-PCR including primers for CB_1R (Cnr1), Tight junction protein-1 (Tjp-1), Occludin (Ocln), and Claudin-1 (Cldn-1) gene transcripts under preconfigured SYBR Green assays (Biorad, Irvine, CA, USA). Identification of differential expression between $iCB_1R^{-/-}$ and Flox control mice was performed using the delta-delta ($2^{-\Delta\Delta Cq}$) method with Hprt as the housekeeping gene.

NanoString nCounter Gene Expression Assays and Analysis

nCounter gene expression assays (NanoString Technologies) were performed using a custom NanoString Panel which probed for 100 genes. Briefly, panel codeset probes were hybridized with 500ng of total RNA per large intestine mucosa sample over 18 hr at 65°C according to NanoString protocol. Molecular grade water was used to dilute hybridized RNA which was then loaded into nCounter SPRINT cartridge (NanoString, Seattle, WA, USA), and quantified. NanoString Spring Profiler technology was utilized to count RNA-conjugated probes.

nSolver and Advanced Analysis

Results from the panel were normalized in nSolver following best practices, and analyzed using nSolver and Advanced Analysis software according to previously published protocols (Bergersen et al., 2021; Danaher et al., 2017). nSolver-generated heat maps were created using normalized data and agglomerative clustering, a bottom-up form of hierarchical clustering (NanoString User Manual C0019-08). For Advanced Analysis, normalized data was used (NanoString User Manual 10030-03). Differential expression (DE) analysis was performed to identify specific targets that exhibit significantly increased or decreased expression compared to control group indicated in the figure. Summary pathway score plot colors are based on calculated scores and are represented as down regulation (yellow) to upregulation (blue).

Statistical Analysis

Data was analyzed using GraphPad Prism7 software using unpaired Student's t-tests (two-tailed) and regular or repeated measures two-way analysis of variances with Newman-Keuls or Sidak's multiple comparisons post hoc test, respectively, when appropriate. Differentially expressed genes (DEGs) were defined by a p-value < 0.05 when a Welch's t-test was performed (RRID:SCR_002798). Gene enrichment and functional annotation analyses of DEGs was performed using open source functional enrichment tool DAVID. All data sets expressed as mean ± standard error (SEM) and significance was determined as $p < 0.05$.

Results

Diet Induced Obesity Disrupts the eCB system of the Large Intestine Mucosa

Male WT mice maintained on a WD for 60d gain significantly more weight when compared to their SD-fed litter mates (Figure 4.1B, C). Analysis of the large intestine mucosa of these mice revealed dysregulation of lipid levels in response to diet (Figure 4.1D). DIO mice displayed significantly lower levels of several MAG species (2-AG: 18,000 ± 4,474 pmol/g; 2-DG: 1,829 ± 467 pmol/g; 2-LG: 40,730 ± 11,360 pmol/g) as well as OEA (156.7 ± 9.329 pmol/g) when compared to SD-fed mice (2-AG: 24,080 ± 2,031 pmol/g; 2-DG: 5,646 ± 1,616 pmol/g; 2-LG: 181,800 ± 42,380 pmol/g; OEA: 343.4 ± 57.93 pmol/g). No changes were observed in WD-fed mice in 2-OG (74,170 ± 17,340 pmol/g), AEA (10.14 ± 1.879 pmol/g), and DHEA (35.65 ± 2.8 pmol/g) when compared to SD-fed mice (2-OG: 97,680 ± 17,210 pmol/g; AEA: 10.04 ± 1.892 pmol/g; DHEA: 34.76 ± 3.677 pmol/g). These changes in lipid content in the large intestine were coupled to alterations in lipid metabolism (Figure 4.1E) with an increase in DGL activity in DIO mice (1.253 ± 0.1883 nmol/mg/min) when compared to SD-fed mice (1.938 ± 0.2459 nmol/mg/min), which was not coupled to any changes in MGL activity (Figure 4.1F: SD: 24.09 ± 1.048 nmol/mg/min; WD: 23.65 ± 1.789 nmol/mg/min).

Mice Lacking Intestinal Epithelial CB_1R Signaling Display no Baseline Changes in Gut-Barrier Protein mRNA Expression and are not Diet Induced Obese Resistant

Baseline expression (10 days following the final tamoxifen administration) of Cnr1 in the colon mucosa of $iCB_1R^{-/-}$ mice was significantly reduced (0.364 ± 0.031 RE)

when compared to Flox control mice (1.000 ± 0.269 RE) with no changes in the tight junction protein mRNA transcripts in the Flox control mice (Tjp-1: 1.000 ± 0.295 RE; Ocln: 1.000 ± 0.254 RE; Cldn-1: 1.000 ± 0.416 RE) when compared with the $iCB_1R^{-/-}$ mice (Tjp-1: 0.893 ± 0.369 RE; Ocln: 0.757 ± 0.127 RE; Cldn-1: 1.283 ± 0.259 RE) (Figure 4.2A). Furthermore, $iCB_1R^{-/-}$ mice gained the same amount of weight and at the same rate as Flox controls when placed on either a SD or a WD for 60 days (Figure 4.2B).

Intestinal Epithelial CB_1R Signaling is Required to Conserve Gut-Barrier Permeability in Diet Induced Obesity

Baseline gut-barrier permeability was tested across genotypes (Figure 4.2C) prior to being placed on any diet which revealed no changes in serum FITC-Dextran when comparing Flox control mice (0.7255 ± 0.1379 µg/mL) with $iCB_1R^{-/-}$ mice (0.5804 ± 0.1146 µg/mL). No changes were observed in serum FITC-dextran as a marker for large intestine permeability after two weeks on either a SD (Flox: 0.657 ± 0.075 µg/mL; $iCB_1R^{-/-}$: 0.487 ± 0.040 µg/mL) or WD (Flox: 1.059 ± 0.170 µg/mL; $iCB_1R^{-/-}$: 0.982 ± 0.133 µg/mL) regardless of genotype (Figure 4.2D). After DIO was achieved, large intestine paracellular permeability was compromised (Figure 4.2E) across diet within the Flox control mice (SD: 0.559 ± 0.047 µg/mL; WD: 1.281 ± 0.206 µg/mL) and across diet within the $iCB_1R^{-/-}$ mice (SD: 0.583 ± 0.103; WD: 2.454 ± 0.276 µg/mL). Furthermore, DIO mice lacking $iCB_1R^{-/-}$ displayed a significant increase in serum FITC-Dextran as a marker for large intestine permeability when compared to DIO Flox control mice (p-value < 0.001).

Diet Induced Obesity Stimulates Changes in Gut-Barrier Function *Without* Altering Whole Tissue Morphology

Mice placed on a WD display significant increases in epididymal fat pad weight (Flox: 2.035 ± 0.211 g; $iCB_1R^{-/-}$: 2.441 ± 0.139 g) when compared to SD fed mice (Flox: 0.616 ± 0.091 g; $iCB_1R^{-/-}$: 0.636 ± 0.122 g) regardless of genotype (Figure 4.3A). Significant reductions in colon length was observed in WD-fed mice (Flox: 6.867 ± 0.138 cm; $iCB_1R^{-/-}$: 6.75 ± 0.079 cm) when compared to SD-fed mice (Flox: 7.625 ± 0.157 cm; $iCB_1R^{-/-}$: 7.321 ± 0.158 cm) irrespective of genotype (Figure 4.3B). However, no changes in WD colon weight (Flox: 165.833 ± 9.959 mg; $iCB_1R^{-/-}$: 172.500 ± 7.600 mg) or WD colon weight:length ratio (Flox: 22.816 ± 2.277 mg/cm; $iCB_1R^{-/-}$: 25.540 ± 1.188 mg/cm) were observed when compared to SD colon weight (Flox: 189.091 ± 5.470 mg; $iCB_1R^{-/-}$: 168.182 ± 120.856 mg) or SD colon weight:length ratio (Flox: 23.015 ± 2.028 mg/cm; $iCB_1R^{-/-}$: 23.188 ± 1.875 mg/cm) respectively, regardless of genotype (Figure 4.3C, D). Representative images taken at 4x display no obvious qualitative changes in tissue morphology across diet and/or genotype (Figure 4.3E-H).

Obese Mice Lacking Intestinal Epithelial CB_1R Signaling Have an Increased Inflammatory Response in the Colon

A representative heatmap of all 19 differentially expressed genes (DEGs) across diet or genotype (Figure 4.4A). DAVID analysis was performed to determine how many DEGs are implicated in specific pathways while simultaneously determining how strongly correlated the DEGs and pathways are using a false discovery rate threshold of: -

LOG(FDR)>2. This analysis discovered several pathways effected in the large intestine mucosa by these DEGs in molecular functions (Figure 4.4B), cellular components (Figure 4.4C), and biological processes (Figure 4.4C). Cldn19 was the only gene that was found to be significantly altered in the large intestine across genotype only after 60d on a SD (Figure 4.4E). Flox control mice displayed a significant reduction in large intestine mucosa Cldn8 (p-value = 0.05), Cldn12, and Cldn19 expression after 60d on a WD when compared to SD-fed litter mates (Figure 4.4F). Several more DEGs were discovered in response to WD in mice lacking intestinal epithelial CB_1R signaling (Figure 4.4G). The greatest number of DEGs were discovered when Flox control WD-fed mice were compared to $iCB_1R^{-/-}$ WD-fed mice (Figure 4.4H) with an increase in RNA associated with the inflammatory response (Figure 4.4I), and a decrease in tight-junction protein associated RNA (Figure 4.4J).

Chronic THC Administration Rescues Diet-Induced Gut-Barrier Dysfunction

Flox control mice placed on a WD for 60d gain significantly more weight than SD-fed litter mates and two weeks of THC/vehicle administration did not alter the difference in weight (Figure 4.5A). Flox control DIO mice display significant increases in serum FITC-Dextran as a marker for *in vivo* large intestine permeability (2.12 ± 0.3938 µg/mL) when compared to SD-fed litter mates (0.9423 ± 0.068 µg/mL) (Figure 4.5B). Following two weeks of vehicle injections, the DIO mice displayed a persistent increase in serum FITC-Dextran (2.077 ± 0.561 µg/mL) when compared to the SD-fed vehicle treated mice (0.637 ± 0.111 µg/mL), however, after two weeks of THC treatment, serum

FITC-Dextran levels were returned to baseline (1.141 ± 0.285 μg/mL) when compared to THC treated SD-fed mice (0.698 ± 0.124 μg/mL) (Figure 4.5C).

Chronic THC Administration Rescues Diet-Induced Disruptions in Large Intestine Mucosa RNA Expression

A representative heatmap of all 14 DEGs found in the large intestine mucosa across diet or treatment in the Flox control only experiment (Figure 4.6A). Eight DEGs were discovered when SD-fed vehicle treated mice were compared to WD-fed vehicle treated mice (Figure 4.6B). Of the 100 genes that were probed in the custom NanoString panel, zero DEGs were discovered when SD-fed THC treated mice were compared to WD-fed THC treated mice (Figure 4.6C). DIO mice given THC displayed several DEGs when compared to vehicle treated DIO mice (Figure 4.6D).

Discussion

In the work described here, we report a vital role for the eCB system in diet-induced gut-barrier dysfunction. We also report that THC may have therapeutic potential in rescuing paracellular permeability in the large intestine. These data provide evidence that: (i) DIO dysregulates the eCB system through a down regulation in DGL activity leading to reductions in 2-AG levels in the large intestine mucosa, (ii) intestinal epithelial CB_1R signaling is protective in WD-induced gut-barrier dysfunction through both tight-junction and inflammatory mechanisms, and (iii) over-activation of the eCB system via THC rescues diet-induced gut-barrier dysfunction and gene dysregulation in the large

intestine mucosa. Notably, mice lacking intestinal epithelial CB_1R signaling display little to no significant changes in gut-barrier function or RNA expression in the large intestine unless challenged with a WD. Furthermore, DIO mice displayed significant alterations in large intestine paracellular permeability and RNA expression in the colon mucosa, however, no significant changes in tissue architecture were observed (Figure 4.3). Lastly, THC administration not only rescued paracellular permeability, but also returned expression of all inflammatory and gut-barrier associated RNA levels to baseline (Figure 4.5, 4.6).

Diet-induced obesity stimulates distinct changes in eCB content throughout the organism with elevated levels found in the jejunum mucosa and in circulation (Argueta & DiPatrizio, 2017; Argueta et al., 2019), however, lipid content in the large intestine mucosa has not been well characterized in either lean or DIO-conditions. Lean mice given *ad libitum* access to SD display levels of 2-AG at ~50 nmol/g in the jejunum mucosa which are chronically elevated in DIO mice, regardless of the post-prandial state (Argueta & DiPatrizio, 2017; Argueta et al., 2019). Conversely, in the large intestine mucosa, SD-fed mice display levels of 2-AG at ~25 nmol/g which are significantly reduced in response to DIO (Figure 4.1D). Furthermore, this reduction in 2-AG was coupled to a decrease in several MAG species measured in the colon mucosa due to a reduction in DGL activity. Previous research identified increases in mRNA levels of DGL in response to WD in the small intestine, despite increased levels of the eCB 2-AG (Argueta et al., 2019). Further experimentation revealed that enzymatic activity of DGL was increased in the WD-fed mice with no changes in MGL activity, leading to an

increase in 2-AG content in the tissue (Argueta et al., 2019). Expression levels of these enzymes in the large intestine under DIO and lean conditions need to be elucidated in future experiments, however the change in DGL activity observed in Figure 4.1E suggests distinct changes in the rate of enzyme catalysis are responsible for the observed changes in eCB content.

Previous research has identified distinct changes in gut-barrier function *in vitro* when levels of eCBs are increased apically vs. basolaterally, suggesting an important role for eCBs in the mucosa of the large intestine specifically (Karwad et al., 2017). To further elucidate the role for eCBs in the colon mucosa, we placed mice lacking intestinal epithelial CB_1R on a SD or WD for 60d and tested *in vivo* gut-barrier permeability. We first confirmed that the $iCB_1R^{-/-}$ mice had reduced qPCR expression of the gene encoding CB_1R (Cnr1) in the colon mucosa with no change in baseline mRNA levels of the three gut-barrier associated genes probed. Furthermore, $iCB_1R^{-/-}$ mice also displayed no changes in baseline serum FITC-Dextran, indicating no initial shift in gut-barrier function *in vivo*. Once DIO had been achieved in the WD-fed mice, both Flox control and $iCB_1R^{-/-}$ mice displayed significant increases in serum FITC-Dextran when compared to SD-fed litter mates. This effect was exacerbated in mice lacking intestinal epithelial CB_1R, suggesting a more severely compromised gut-barrier in these mice. Despite marked changes in gut-barrier permeability in these mice, significant changes in tissue morphology that often accompany other models of gut-barrier dysfunction (DSS, TNBS) were not observed (Antoniou et al., 2016; Eichele & Kharbanda, 2017).

This method of moderate gut-barrier disruption provided an opportunity to probe the RNA levels of several inflammatory and gut-barrier related genes to determine what pathways may be involved in initiating disruptions in large intestine paracellular permeability. A custom NanoString panel of 100 genes covering several inflammatory processes, tight-junction formation/maintenance pathways, and eCB-related genes was used to probe for changes in gene expression in the large intestine mucosa across diet or genotype. Several DEGs were found and plugged into the open source functional enrichment tool, DAVID, which identified biological pathways implicated by these DEGs and calculated how many genes and how strongly associated those genes were with each pathway. The Molecular Functions that are potentially altered include changes in receptor activity, importantly in multiple chemokine and cytokine receptor pathways which may be skewing the inflammatory response. The cellular components implicated by the discovered DEGs included those involved in anchoring, forming, and maintaining the cell membrane and cell-cell junction. Biological Processes that were identified included several inflammatory processes and a few other processes involved in immune cell adhesion and transmigration into tissue. Taken together, the pathways implicated may be altering tight-junction formation, inflammatory cell transmigration, and immune cell signaling which are all key role players in maintaining gut-barrier function (Vancamelbeke & Vermeire, 2017).

Previous research has identified a role for several genes in diet-induced gut-barrier disruption implicated in both the tight-junction (ZO-1 and Occludin) and the inflammatory response (IL-6, TNFα, and number of T-cells in the large intestine) (Lam et

al., 2012; Lee et al., 2017). After 60d on a WD, Flox control mice displayed no changes in the inflammatory-associated genes probed, but a decrease in three claudin-family RNA transcripts were observed. However, when intestinal epithelial CB_1R signaling was removed, several more DEGs were discovered, including a host of inflammatory-associated genes. Upregulation of many of these genes may result in increases in inflammatory cell numbers found in the tissue (ICAM1, HLA-DQA1), with an increased state of activation and signaling (CXCR5/CXCL13, CXCR3, IL1A). Lastly, the greatest number of DEGs were discovered when samples were compared across genotype within WD. This indicated that $iCB_1R^{-/-}$ mice had an increased inflammatory profile with evidence of increased immune cell infiltrate (HLA-DRA, HLA-DQA1, ICAM1, CD247), and a decrease in tight-junction associated RNA expression (TJP2, TJP3, CLDN7). The state of this tissue may have permitted more pathogen-associated molecules to pass between epithelial cells, thereby stimulating immune cell transmigration and activation into the large intestine. Distinct differences in DEGs found in the data presented here and previously reported data may be due to the use of WD vs. high-fat diet (Lam et al., 2012; Lee et al., 2017). Diet has been identified as a key contributor to the microbiota populations that will thrive in the gut which can directly manipulate the inflammatory state of the gut (Cani, 2016; Cani et al., 2016; Pujo et al., 2021). Future studies should consider what families of bacteria thrive in the colon in response to WD vs. HFD to further elucidate the role for the microbiome in diet-induced gut-barrier dysfunction.

To determine if WD-induced gut-barrier dysfunction and gene dysregulation can be rescued, chronic over-activation of the eCB system via THC was performed in Flox

control mice over two weeks after DIO had been achieved. After 60d on the diet serum FITC-Dextran indicated that diet-induced gut-barrier dysfunction had been achieved. After two weeks of THC/Vehicle injections, *in vivo* paracellular permeability was measured which indicated that over-activation of the eCB system via THC rescued diet-induced gut-barrier dysfunction. NanoString analysis was performed using the same custom panel described for Figure 4.4, and several more DEGs were discovered across diet or treatment. After an additional two weeks on the WD, many more DEGs were discovered across diet including an increase in inflammatory associated RNA (IL1B, IL27, IL5RA) and a decrease in CLDN3 and CLDN12. Although the role for CLDN12 is not well understood, CLDN3 has been shown to be a critical barrier-forming protein, therefore its down regulation may be contributing to a compromised gut-barrier (Milatz et al., 2010). Strikingly, no DEGs were discovered across any of the 100 genes probed for when colon mucosa samples from THC treated SD-fed mice were compared to THC treated WD-fed mice, suggesting that THC rescued gene expression/dysregulation caused by WD in the colon mucosa. Furthermore, the inflammatory profile of the WD-fed THC treated mice was significantly reduced when compared with the WD-fed vehicle treated mice. This effect was coupled to an increase in CLDN15 expression which is a key regulator of paracellular water and Na^+ transport (Rosenthal et al., 2020). These data indicate that THC may be acting as more than an anti-inflammatory agent and may be contributing to the epithelial expression of master regulators of the tight-junction complex. Future experimentation will test this hypothesis directly via chronic THC/vehicle injections in DIO $iCB_1R^{-/-}$ mice to determine if gene expression and *in vivo*

gut-barrier function can be rescued with over-activation of the eCB system everywhere in the organism *except* the intestinal epithelial cells.

References

Acharya, N., Penukonda, S., Shcheglova, T., Hagymasi, A. T., Basu, S., & Srivastava, P. K. (2017). Endocannabinoid system acts as a regulator of immune homeostasis in the gut. *Proc Natl Acad Sci U S A*, *114*(19), 5005-5010. https://doi.org/10.1073/pnas.1612177114

Actis, G. C., Pellicano, R., Fagoonee, S., & Ribaldone, D. G. (2019). History of Inflammatory Bowel Diseases. *J Clin Med*, *8*(11). https://doi.org/10.3390/jcm8111970

Alexander, S. P., & Kendall, D. A. (2007). The complications of promiscuity: endocannabinoid action and metabolism. *Br J Pharmacol*, *152*(5), 602-623. https://doi.org/10.1038/sj.bjp.0707456

Alhamoruni, A., Lee, A. C., Wright, K. L., Larvin, M., & O'Sullivan, S. E. (2010). Pharmacological effects of cannabinoids on the Caco-2 cell culture model of intestinal permeability. *J Pharmacol Exp Ther*, *335*(1), 92-102. https://doi.org/10.1124/jpet.110.168237

Alhamoruni, A., Wright, K. L., Larvin, M., & O'Sullivan, S. E. (2012). Cannabinoids mediate opposing effects on inflammation-induced intestinal permeability. *British Journal of Pharmacology*, *165*(8), 2598-2610. https://doi.org/10.1111/j.1476-5381.2011.01589.x

Alhouayek, M., & Muccioli, G. G. (2014). COX-2-derived endocannabinoid metabolites as novel inflammatory mediators. *Trends in Pharmacological Sciences*, *35*(6), 284-292. https://doi.org/10.1016/j.tips.2014.03.001

Anthony, R. M., Rutitzky, L. I., Urban, J. F., Stadecker, M. J., & Gause, W. C. (2007). Protective immune mechanisms in helminth infection. *Nat Rev Immunol*, *7*(12), 975-987. https://doi.org/10.1038/nri2199

Antoniou, E., Margonis, G. A., Angelou, A., Pikouli, A., Argiri, P., Karavokyros, I., Papalois, A., & Pikoulis, E. (2016). The TNBS-induced colitis animal model: An overview. *Ann Med Surg (Lond)*, *11*, 9-15. https://doi.org/10.1016/j.amsu.2016.07.019

Argueta, D. A., & DiPatrizio, N. V. (2017). Peripheral endocannabinoid signaling controls hyperphagia in western diet-induced obesity. *Physiol Behav*, *171*, 32-39. https://doi.org/10.1016/j.physbeh.2016.12.044

Argueta, D. A., Perez, P. A., Makriyannis, A., & DiPatrizio, N. V. (2019). Cannabinoid CB1 receptors inhibit gut-brain satiation signaling in diet-induced obesity. *Front Physiol*, *10*, 704. https://doi.org/10.3389/fphys.2019.00704

Avalos, B., Argueta, D. A., Perez, P. A., Wiley, M., Wood, C., & DiPatrizio, N. V. (2020). Cannabinoid CB1 receptors in the intestinal epithelium are required for acute western-diet preferences in mice. *Nutrients*, *12*(9). https://doi.org/10.3390/nu12092874

Batugedara, H. M., Argueta, D., Jang, J. C., Lu, D., Macchietto, M., Kaur, J., Ge, S., Dillman, A. R., DiPatrizio, N. V., & Nair, M. G. (2018). Host and helminth-derived endocannabinoids are generated during infection with effects on host immunity. *Infect Immun*. https://doi.org/10.1128/iai.00441-18

Batugedara, H. M., Li, J., Chen, G., Lu, D., Patel, J. J., Jang, J. C., Radecki, K. C., Burr, A. C., Lo, D. D., Dillman, A. R., & Nair, M. G. (2018). Hematopoietic cell-derived RELMα regulates hookworm immunity through effects on macrophages. *J Leukoc Biol*, *104*(4), 855-869. https://doi.org/10.1002/jlb.4a0917-369rr

Bergersen, K. V., Barnes, A., Worth, D., David, C., & Wilson, E. H. (2021). Targeted Transcriptomic Analysis of C57BL/6 and BALB/c Mice During Progressive Chronic Toxoplasma gondii Infection Reveals Changes in Host and Parasite Gene Expression Relating to Neuropathology and Resolution. *Front Cell Infect Microbiol*, *11*, 645778. https://doi.org/10.3389/fcimb.2021.645778

Bisogno, T., Cascio, M. G., Saha, B., Mahadevan, A., Urbani, P., Minassi, A., Appendino, G., Saturnino, C., Martin, B., Razdan, R., & Di Marzo, V. (2006). Development of the first potent and specific inhibitors of endocannabinoid biosynthesis. *Biochim Biophys Acta*, *1761*(2), 205-212. https://doi.org/10.1016/j.bbalip.2005.12.009

Blankman, J. L., Simon, G. M., & Cravatt, B. F. (2007). A comprehensive profile of brain enzymes that hydrolyze the endocannabinoid 2-arachidonoylglycerol. *Chem Biol*, *14*(12), 1347-1356. https://doi.org/10.1016/j.chembiol.2007.11.006

Bottemanne, P., Paquot, A., Ameraoui, H., Alhouayek, M., & Muccioli, G. G. (2019). The alpha/beta-hydrolase domain 6 inhibitor WWL70 decreases endotoxin-induced lung inflammation in mice, potential contribution of 2-arachidonoylglycerol, and lysoglycerophospholipids. *FASEB J*, *33*(6), 7635-7646. https://doi.org/10.1096/fj.201802259R

Bouchery, T., Filbey, K., Shepherd, A., Chandler, J., Patel, D., Schmidt, A., Camberis, M., Peignier, A., Smith, A. A. T., Johnston, K., Painter, G., Pearson, M., Giacomin, P., Loukas, A., Bottazzi, M. E., Hotez, P., & LeGros, G. (2018). A

novel blood-feeding detoxification pathway in Nippostrongylus brasiliensis L3 reveals a potential checkpoint for arresting hookworm development. *PLoS Pathog*, *14*(3), e1006931. https://doi.org/10.1371/journal.ppat.1006931

Bouma, G., & Strober, W. (2003). The immunological and genetic basis of inflammatory bowel disease. *Nat Rev Immunol*, *3*(7), 521-533. https://doi.org/10.1038/nri1132

Cadas, H., di Tomaso, E., & Piomelli, D. (1997). Occurrence and biosynthesis of endogenous cannabinoid precursor, N-arachidonoyl phosphatidylethanolamine, in rat brain. *J Neurosci*, *17*(4), 1226-1242. https://www.ncbi.nlm.nih.gov/pubmed/9006968

Cadas, H., Gaillet, S., Beltramo, M., Venance, L., & Piomelli, D. (1996). Biosynthesis of an endogenous cannabinoid precursor in neurons and its control by calcium and cAMP. *J Neurosci*, *16*(12), 3934-3942. https://www.ncbi.nlm.nih.gov/pubmed/8656287

Cani, P. D. (2016). Interactions between gut microbes and host cells control gut barrier and metabolism. *Int J Obes Suppl*, *6*(Suppl 1), S28-S31. https://doi.org/10.1038/ijosup.2016.6

Cani, P. D., Plovier, H., Van Hul, M., Geurts, L., Delzenne, N. M., Druart, C., & Everard, A. (2016). Endocannabinoids - at the crossroads between the gut microbiota and host metabolism. *Nature Reviews Endocrinology*, *12*(3), 133-143. https://doi.org/10.1038/nrendo.2015.211

Carayon, P., Marchand, J., Dussossoy, D., Derocq, J. M., Jbilo, O., Bord, A., Bouaboula, M., Galiegue, S., Mondiere, P., Penarier, G., Le Fur, G., Defrance, T., & Casellas, P. (1998). Modulation and functional involvement of CB2 peripheral cannabinoid receptors during B-cell differentiation. *Blood*, *92*(10), 3605-3615. <Go to ISI>://WOS:000076962500015

Cardinal, P., Bellocchio, L., Clark, S., Cannich, A., Klugmann, M., Lutz, B., Marsicano, G., & Cota, D. (2012). Hypothalamic CB1 Cannabinoid Receptors Regulate Energy Balance in Mice. *Endocrinology*, *153*(9), 4136-4143. https://doi.org/10.1210/en.2012-1405

Chen, C. M., Hwang, J., Chou, H. C., & Chen, C. (2020). Anti-Tn Monoclonal Antibody Attenuates Hyperoxia-Induced Lung Injury by Inhibiting Oxidative Stress and Inflammation in Neonatal Mice. *Front Pharmacol*, *11*, 568502. https://doi.org/10.3389/fphar.2020.568502

Chen, F., Liu, Z., Wu, W., Rozo, C., Bowdridge, S., Millman, A., Van Rooijen, N., Urban, J. F., Wynn, T. A., & Gause, W. C. (2012). An essential role for TH2-type

responses in limiting acute tissue damage during experimental helminth infection. *Nat Med*, *18*(2), 260-266. https://doi.org/10.1038/nm.2628

Chiurchiu, V., Battistini, L., & Maccarrone, M. (2015). Endocannabinoid signalling in innate and adaptive immunity. *Immunology*, *144*(3), 352-364. https://doi.org/10.1111/imm.12441

Christensen, R., Kristensen, P. K., Bartels, E. M., Bliddal, H., & Astrup, A. (2007). Efficacy and safety of the weight-loss drug rimonabant: a meta-analysis of randomised trials. *Lancet*, *370*(9600), 1706-1713. https://doi.org/10.1016/S0140-6736(07)61721-8

Cinar, R., Gochuico, B. R., Iyer, M. R., Jourdan, T., Yokoyama, T., Park, J. K., Coffey, N. J., Pri-Chen, H., Szanda, G., Liu, Z., Mackie, K., Gahl, W. A., & Kunos, G. (2017). Cannabinoid CB1 receptor overactivity contributes to the pathogenesis of idiopathic pulmonary fibrosis. *JCI Insight*, *2*(8). https://doi.org/10.1172/jci.insight.92281

Cravatt, B. F., Giang, D. K., Mayfield, S. P., Boger, D. L., Lerner, R. A., & Gilula, N. B. (1996). Molecular characterization of an enzyme that degrades neuromodulatory fatty-acid amides. *Nature*, *384*(6604), 83-87. https://doi.org/10.1038/384083a0

Dainese, E., Oddi, S., Simonetti, M., Sabatucci, A., Angelucci, C. B., Ballone, A., Dufrusine, B., Fezza, F., De Fabritiis, G., & Maccarrone, M. (2020). The endocannabinoid hydrolase FAAH is an allosteric enzyme. *Sci Rep*, *10*(1), 2292. https://doi.org/10.1038/s41598-020-59120-1

Danaher, P., Warren, S., Dennis, L., D'Amico, L., White, A., Disis, M. L., Geller, M. A., Odunsi, K., Beechem, J., & Fling, S. P. (2017). Gene expression markers of Tumor Infiltrating Leukocytes. *J Immunother Cancer*, *5*, 18. https://doi.org/10.1186/s40425-017-0215-8

de Rond, T., Gao, J., Zargar, A., de Raad, M., Cunha, J., Northen, T. R., & Keasling, J. D. (2019). A High-Throughput Mass Spectrometric Enzyme Activity Assay Enabling the Discovery of Cytochrome P450 Biocatalysts. *Angew Chem Int Ed Engl*, *58*(30), 10114-10119. https://doi.org/10.1002/anie.201901782

Devane, W. A., Hanus, L., Breuer, A., Pertwee, R. G., Stevenson, L. A., Griffin, G., Gibson, D., Mandelbaum, A., Etinger, A., & Mechoulam, R. (1992). Isolation and structure of a brain constituent that binds to the cannabinoid receptor. *Science*, *258*(5090), 1946-1949. https://doi.org/10.1126/science.1470919

Devane, W. A., Howlett, A. C., Johnson, M. R., Melvin, L. S., & Milne, G. M. (1987). Structural studies leading to the discovery of a physiologically relevant

cannabinoid receptor-site in rat-brain. *Abstracts of Papers of the American Chemical Society*, *194*, 17-MEDI. <Go to ISI>://WOS:A1987J291202505

Di Marzo, V., Fontana, A., Cadas, H., Schinelli, S., Cimino, G., Schwartz, J. C., & Piomelli, D. (1994). Formation and inactivation of endogenous cannabinoid anandamide in central neurons. *Nature*, *372*(6507), 686-691. https://doi.org/10.1038/372686a0

Di Marzo, V., Goparaju, S. K., Wang, L., Liu, J., Batkai, S., Jarai, Z., Fezza, F., Miura, G. I., Palmiter, R. D., Sugiura, T., & Kunos, G. (2001). Leptin-regulated endocannabinoids are involved in maintaining food intake. *Nature*, *410*(6830), 822-825. https://doi.org/10.1038/35071088

DiPatrizio, N. V. (2016). Endocannabinoids in the Gut. *Cannabis Cannabinoid Res*, *1*(1), 67-77. https://doi.org/10.1089/can.2016.0001

DiPatrizio, N. V. (2021). Endocannabinoids and the Gut-Brain Control of Food Intake and Obesity. *Nutrients*, *13*(4). https://doi.org/10.3390/nu13041214

DiPatrizio, N. V., Igarashi, M., Narayanaswami, V., Murray, C., Gancayco, J., Russell, A., Jung, K. M., & Piomelli, D. (2015). Fasting stimulates 2-AG biosynthesis in the small intestine: role of cholinergic pathways. *Am J Physiol Regul Integr Comp Physiol*, *309*(8), R805-813. https://doi.org/10.1152/ajpregu.00239.2015

DiPatrizio, N. V., & Piomelli, D. (2012). The thrifty lipids: endocannabinoids and the neural control of energy conservation. *Trends Neurosci*, *35*(7), 403-411. https://doi.org/10.1016/j.tins.2012.04.006

Eichele, D. D., & Kharbanda, K. K. (2017). Dextran sodium sulfate colitis murine model: An indispensable tool for advancing our understanding of inflammatory bowel diseases pathogenesis. *World J Gastroenterol*, *23*(33), 6016-6029. https://doi.org/10.3748/wjg.v23.i33.6016

Fiskerstrand, T., H'mida-Ben Brahim, D., Johansson, S., M'zahem, A., Haukanes, B. I., Drouot, N., Zimmermann, J., Cole, A. J., Vedeler, C., Bredrup, C., Assoum, M., Tazir, M., Klockgether, T., Hamri, A., Steen, V. M., Boman, H., Bindoff, L. A., Koenig, M., & Knappskog, P. M. (2010). Mutations in ABHD12 cause the neurodegenerative disease PHARC: An inborn error of endocannabinoid metabolism. *Am J Hum Genet*, *87*(3), 410-417. https://doi.org/10.1016/j.ajhg.2010.08.002

Fu, J., Astarita, G., Gaetani, S., Kim, J., Cravatt, B. F., Mackie, K., & Piomelli, D. (2007). Food intake regulates oleoylethanolamide formation and degradation in

the proximal small intestine. *J Biol Chem*, *282*(2), 1518-1528. https://doi.org/10.1074/jbc.M607809200

Galiègue, S., Mary, S., Marchand, J., Dussossoy, D., Carrière, D., Carayon, P., Bouaboula, M., Shire, D., Le Fur, G., & Casellas, P. (1995). Expression of central and peripheral cannabinoid receptors in human immune tissues and leukocyte subpopulations. *Eur J Biochem*, *232*(1), 54-61. https://www.ncbi.nlm.nih.gov/pubmed/7556170

Ghafouri, N., Tiger, G., Razdan, R. K., Mahadevan, A., Pertwee, R. G., Martin, B. R., & Fowler, C. J. (2004). Inhibition of monoacylglycerol lipase and fatty acid amide hydrolase by analogues of 2-arachidonoylglycerol. *Br J Pharmacol*, *143*(6), 774-784. https://doi.org/10.1038/sj.bjp.0705948

Haley, A. J. (1961). Biology of the rat-nematode *Nippostrongylus brasiliensis*. Systematics, hosts, and geographic distribution. *Journal of Parasitology*, *47*(5), 727-731. https://doi.org/10.2307/3275460

Hammond, R. A., & Levine, R. (2010). The economic impact of obesity in the United States. *Diabetes Metab Syndr Obes*, *3*, 285-295. https://doi.org/10.2147/dmsott.S7384

Harris, N. L., & Loke, P. (2017). Recent Advances in Type-2-Cell-Mediated Immunity: Insights from Helminth Infection. *Immunity*, *47*(6), 1024-1036. https://doi.org/10.1016/j.immuni.2017.11.015

Harvey, B. S., Nicotra, L. L., Vu, M., & Smid, S. D. (2013). Cannabinoid CB2 receptor activation attenuates cytokine-evoked mucosal damage in a human colonic explant model without changing epithelial permeability. *Cytokine*, *63*(2), 209-217. https://doi.org/10.1016/j.cyto.2013.04.032

Harvey, B. S., Sia, T. C., Wattchow, D. A., & Smid, S. D. (2014). Interleukin 17A evoked mucosal damage is attenuated by cannabidiol and anandamide in a human colonic explant model. *Cytokine*, *65*(2), 236-244. https://doi.org/10.1016/j.cyto.2013.10.006

Hawdon, J. M., & Hotez, P. J. (1996). Hookworm: developmental biology of the infectious process. *Curr Opin Genet Dev*, *6*(5), 618-623. https://www.ncbi.nlm.nih.gov/pubmed/8939719

Heier, C., Taschler, U., Rengachari, S., Oberer, M., Wolinski, H., Natter, K., Kohlwein, S. D., Leber, R., & Zimmermann, R. (2010). Identification of Yju3p as functional orthologue of mammalian monoglyceride lipase in the yeast

Saccharomycescerevisiae. *Biochim Biophys Acta*, *1801*(9), 1063-1071. https://doi.org/10.1016/j.bbalip.2010.06.001

Higuchi, S., Irie, K., Yamaguchi, R., Katsuki, M., Araki, M., Ohji, M., Hayakawa, K., Mishima, S., Akitake, Y., Matsuyama, K., Mishima, K., Iwasaki, K., & Fujiwara, M. (2012). Hypothalamic 2-arachidonoylglycerol regulates multistage process of high-fat diet preferences. *PLoS One*, *7*(6), e38609. https://doi.org/10.1371/journal.pone.0038609

Hirahara, K., Shinoda, K., Morimoto, Y., Kiuchi, M., Aoki, A., Kumagai, J., Kokubo, K., & Nakayama, T. (2019). Immune Cell-Epithelial/Mesenchymal Interaction Contributing to Allergic Airway Inflammation Associated Pathology. *Front Immunol*, *10*, 570. https://doi.org/10.3389/fimmu.2019.00570

Holden-Dye, L., & Walker, R. J. (2014). Anthelmintic drugs and nematicides: studies in Caenorhabditis elegans. *WormBook*, 1-29. https://doi.org/10.1895/wormbook.1.143.2

Holgate, S. T. (2012). Innate and adaptive immune responses in asthma. *Nat Med*, *18*(5), 673-683. https://doi.org/10.1038/nm.2731

Hoover, H. S., Blankman, J. L., Niessen, S., & Cravatt, B. F. (2008). Selectivity of inhibitors of endocannabinoid biosynthesis evaluated by activity-based protein profiling. *Bioorg Med Chem Lett*, *18*(22), 5838-5841. https://doi.org/10.1016/j.bmcl.2008.06.091

Hotez, P. J. (2008). Neglected infections of poverty in the United States of America. *PLoS Negl Trop Dis*, *2*(6), e256. https://doi.org/10.1371/journal.pntd.0000256

Hotez, P. J., Brindley, P. J., Bethony, J. M., King, C. H., Pearce, E. J., & Jacobson, J. (2008). Helminth infections: the great neglected tropical diseases. *J Clin Invest*, *118*(4), 1311-1321. https://doi.org/10.1172/jci34261

Hussain, Z., Uyama, T., Tsuboi, K., & Ueda, N. (2017). Mammalian enzymes responsible for the biosynthesis of N-acylethanolamines. *Biochim Biophys Acta Mol Cell Biol Lipids*, *1862*(12), 1546-1561. https://doi.org/10.1016/j.bbalip.2017.08.006

Jang, J. C., Chen, G., Wang, S. H., Barnes, M. A., Chung, J. I., Camberis, M., Le Gros, G., Cooper, P. J., Steel, C., Nutman, T. B., Lazar, M. A., & Nair, M. G. (2015). Macrophage-derived human resistin is induced in multiple helminth infections and promotes inflammatory monocytes and increased parasite burden. *PLoS Pathog*, *11*(1), e1004579. https://doi.org/10.1371/journal.ppat.1004579

Kaminski, N. E., Abood, M. E., Kessler, F. K., Martin, B. R., & Schatz, A. R. (1992). Identification of a functionally relevant cannabinoid receptor on mouse spleen-cells that is involved in cannabinoid-mediated immune modulation. *Molecular Pharmacology*, *42*(5), 736-742. <Go to ISI>://WOS:A1992JY34200002

Kaplan, B. L., Lawver, J. E., Karmaus, P. W., Ngaotepprutaram, T., Birmingham, N. P., Harkema, J. R., & Kaminski, N. E. (2010). The effects of targeted deletion of cannabinoid receptors CB1 and CB2 on intranasal sensitization and challenge with adjuvant-free ovalbumin. *Toxicol Pathol*, *38*(3), 382-392. https://doi.org/10.1177/0192623310362706

Karwad, M. A., Couch, D. G., Theophilidou, E., Sarmad, S., Barrett, D. A., Larvin, M., Wright, K. L., Lund, J. N., & O'Sullivan, S. E. (2017). The role of CB1 in intestinal permeability and inflammation. *Faseb Journal*, *31*(8), 3267-3277. https://doi.org/10.1096/fj.201601346R

Knott, M. L., Matthaei, K. I., Foster, P. S., & Dent, L. A. (2009). The roles of eotaxin and the STAT6 signalling pathway in eosinophil recruitment and host resistance to the nematodes Nippostrongylus brasiliensis and Heligmosomoides bakeri. *Mol Immunol*, *46*(13), 2714-2722. https://doi.org/10.1016/j.molimm.2009.05.016

Kozak, K. R., Rowlinson, S. W., & Marnett, L. J. (2000). Oxygenation of the endocannabinoid, 2-arachidonylglycerol, to glyceryl prostaglandins by cyclooxygenase-2. *Journal of Biological Chemistry*, *275*(43), 33744-33749. https://doi.org/10.1074/jbc.M007088200

Krause, G., Winkler, L., Mueller, S. L., Haseloff, R. F., Piontek, J., & Blasig, I. E. (2008). Structure and function of claudins. *Biochim Biophys Acta*, *1778*(3), 631-645. https://doi.org/10.1016/j.bbamem.2007.10.018

Kudalkar, S. N., Kingsley, P. J., & Marnett, L. J. (2016). Assay of Endocannabinoid Oxidation by Cyclooxygenase-2. *Endocannabinoid Signaling: Methods and Protocols*, *1412*, 205-215. https://doi.org/10.1007/978-1-4939-3539-0_21

Lam, Y. Y., Ha, C. W., Campbell, C. R., Mitchell, A. J., Dinudom, A., Oscarsson, J., Cook, D. I., Hunt, N. H., Caterson, I. D., Holmes, A. J., & Storlien, L. H. (2012). Increased gut permeability and microbiota change associate with mesenteric fat inflammation and metabolic dysfunction in diet-induced obese mice. *PLoS One*, *7*(3), e34233. https://doi.org/10.1371/journal.pone.0034233

Lambeth, T. R., & Julian, R. R. (2019). Differentiation of peptide isomers and epimers by radical-directed dissociation. *Methods Enzymol*, *626*, 67-87. https://doi.org/10.1016/bs.mie.2019.06.020

Larose, M. C., Turcotte, C., Chouinard, F., Ferland, C., Martin, C., Provost, V., Laviolette, M., & Flamand, N. (2014). Mechanisms of human eosinophil migration induced by the combination of IL-5 and the endocannabinoid 2-arachidonoyl-glycerol. *J Allergy Clin Immunol*, *133*(5), 1480-1482, 1482.e1481-1483. https://doi.org/10.1016/j.jaci.2013.12.1081

Lee, J. C., Lee, H. Y., Kim, T. K., Kim, M. S., Park, Y. M., Kim, J., Park, K., Kweon, M. N., Kim, S. H., Bae, J. W., Hur, K. Y., & Lee, M. S. (2017). Obesogenic diet-induced gut barrier dysfunction and pathobiont expansion aggravate experimental colitis. *PLoS One*, *12*(11), e0187515. https://doi.org/10.1371/journal.pone.0187515

Lee, Y., Jo, J., Chung, H. Y., Pothoulakis, C., & Im, E. (2016). Endocannabinoids in the gastrointestinal tract. *Am J Physiol Gastrointest Liver Physiol*, *311*(4), G655-G666. https://doi.org/10.1152/ajpgi.00294.2015

Li, W., Blankman, J. L., & Cravatt, B. F. (2007). A functional proteomic strategy to discover inhibitors for uncharacterized hydrolases. *J Am Chem Soc*, *129*(31), 9594-9595. https://doi.org/10.1021/ja073650c

Long, J. Z., Li, W., Booker, L., Burston, J. J., Kinsey, S. G., Schlosburg, J. E., Pavón, F. J., Serrano, A. M., Selley, D. E., Parsons, L. H., Lichtman, A. H., & Cravatt, B. F. (2009). Selective blockade of 2-arachidonoylglycerol hydrolysis produces cannabinoid behavioral effects. *Nat Chem Biol*, *5*(1), 37-44. https://doi.org/10.1038/nchembio.129

Lynn, M. K., Morrissey, J. A., & Conserve, D. F. (2021). Soil-Transmitted Helminths in the USA: a Review of Five Common Parasites and Future Directions for Avenues of Enhanced Epidemiologic Inquiry. *Curr Trop Med Rep*, 1-11. https://doi.org/10.1007/s40475-020-00221-2

Marrs, W. R., Blankman, J. L., Horne, E. A., Thomazeau, A., Lin, Y. H., Coy, J., Bodor, A. L., Muccioli, G. G., Hu, S. S., Woodruff, G., Fung, S., Lafourcade, M., Alexander, J. P., Long, J. Z., Li, W., Xu, C., Möller, T., Mackie, K., Manzoni, O. J., Cravatt, B. F., & Stella, N. (2010). The serine hydrolase ABHD6 controls the accumulation and efficacy of 2-AG at cannabinoid receptors. *Nat Neurosci*, *13*(8), 951-957. https://doi.org/10.1038/nn.2601

Marsland, B. J., Kurrer, M., Reissmann, R., Harris, N. L., & Kopf, M. (2008). Nippostrongylus brasiliensis infection leads to the development of emphysema associated with the induction of alternatively activated macrophages. *Eur J Immunol*, *38*(2), 479-488. https://doi.org/10.1002/eji.200737827

Martinez-Medina, M., Denizot, J., Dreux, N., Robin, F., Billard, E., Bonnet, R., Darfeuille-Michaud, A., & Barnich, N. (2014). Western diet induces dysbiosis with increased E coli in CEABAC10 mice, alters host barrier function favouring AIEC colonisation. *Gut*, *63*(1), 116-124. https://doi.org/10.1136/gutjnl-2012-304119

Massa, F., Marsicano, G., Hermann, H., Cannich, A., Monory, K., Cravatt, B. F., Ferri, G. L., Sibaev, A., Storr, M., & Lutz, B. (2004). The endogenous cannabinoid system protects against colonic inflammation. *J Clin Invest*, *113*(8), 1202-1209. https://doi.org/10.1172/jci19465

Mechoulam, R., Benshabat, S., Hanus, L., Ligumsky, M., Kaminski, N. E., Schatz, A. R., Gopher, A., Almog, S., Martin, B. R., Compton, D. R., Pertwee, R. G., Griffin, G., Bayewitch, M., Barg, J., & Vogel, Z. (1995). Identification of an endogenous 2-monoglyceride, present in canine gut, that binds to cannabinoid receptors. *Biochemical Pharmacology*, *50*(1), 83-90. https://doi.org/10.1016/0006-2952(95)00109-d

Meng, F., & Alayash, A. I. (2017). Determination of extinction coefficients of human hemoglobin in various redox states. *Anal Biochem*, *521*, 11-19. https://doi.org/10.1016/j.ab.2017.01.002

Milatz, S., Krug, S. M., Rosenthal, R., Gunzel, D., Muller, D., Schulzke, J. D., Amasheh, S., & Fromm, M. (2010). Claudin-3 acts as a sealing component of the tight junction for ions of either charge and uncharged solutes. *Biochim Biophys Acta*, *1798*(11), 2048-2057. https://doi.org/10.1016/j.bbamem.2010.07.014

Nagarkatti, P., Pandey, R., Rieder, S. A., Hegde, V. L., & Nagarkatti, M. (2009). Cannabinoids as novel anti-inflammatory drugs. *Future Med Chem*, *1*(7), 1333-1349. https://doi.org/10.4155/fmc.09.93

Ng, S. C., Shi, H. Y., Hamidi, N., Underwood, F. E., Tang, W., Benchimol, E. I., Panaccione, R., Ghosh, S., Wu, J. C. Y., Chan, F. K. L., Sung, J. J. Y., & Kaplan, G. G. (2017). Worldwide incidence and prevalence of inflammatory bowel disease in the 21st century: a systematic review of population-based studies. *Lancet*, *390*(10114), 2769-2778. https://doi.org/10.1016/S0140-6736(17)32448-0

Nutman, T. B. (2015). Looking beyond the induction of Th2 responses to explain immunomodulation by helminths. *Parasite Immunol*, *37*(6), 304-313. https://doi.org/10.1111/pim.12194

Ogden, C. L., Carroll, M. D., Kit, B. K., & Flegal, K. M. (2012). Prevalence of obesity in the United States, 2009-2010. *NCHS Data Brief*(82), 1-8. https://www.ncbi.nlm.nih.gov/pubmed/22617494

Ohira, M., Okuyama, T., & Mashima, R. (2018). Quantification of 11 enzyme activities of lysosomal storage disorders using liquid chromatography-tandem mass spectrometry. *Mol Genet Metab Rep*, *17*, 9-15. https://doi.org/10.1016/j.ymgmr.2018.08.005

Pandey, R., Mousawy, K., Nagarkatti, M., & Nagarkatti, P. (2009). Endocannabinoids and immune regulation. *Pharmacological Research*, *60*(2), 85-92. https://doi.org/10.1016/j.phrs.2009.03.019

Pertwee, R. G. (2015). Endocannabinoids and Their Pharmacological Actions. *Handb Exp Pharmacol*, *231*, 1-37. https://doi.org/10.1007/978-3-319-20825-1_1

Pine, G. M., Batugedara, H. M., & Nair, M. G. (2018). Here, there and everywhere: Resistin-like molecules in infection, inflammation, and metabolic disorders. *Cytokine*, *110*, 442-451. https://doi.org/10.1016/j.cyto.2018.05.014

Piomelli, D. (2003). The molecular logic of endocannabinoid signalling. *Nat Rev Neurosci*, *4*(11), 873-884. https://doi.org/10.1038/nrn1247

Piomelli, D., Scalvini, L., Fotio, Y., Lodola, A., Spadoni, G., Tarzia, G., & Mor, M. (2020). N-Acylethanolamine Acid Amidase (NAAA): Structure, Function, and Inhibition. *J Med Chem*, *63*(14), 7475-7490. https://doi.org/10.1021/acs.jmedchem.0c00191

Piomelli, D., Tarzia, G., Duranti, A., Tontini, A., Mor, M., Compton, T. R., Dasse, O., Monaghan, E. P., Parrott, J. A., & Putman, D. (2006). Pharmacological profile of the selective FAAH inhibitor KDS-4103 (URB597). *CNS Drug Rev*, *12*(1), 21-38. https://doi.org/10.1111/j.1527-3458.2006.00021.x

Powell, W. S., & Rokach, J. (2013). The eosinophil chemoattractant 5-oxo-ETE and the OXE receptor. *Prog Lipid Res*, *52*(4), 651-665. https://doi.org/10.1016/j.plipres.2013.09.001

Pujo, J., Petitfils, C., Le Faouder, P., Eeckhaut, V., Payros, G., Maurel, S., Perez-Berezo, T., Van Hul, M., Barreau, F., Blanpied, C., Chavanas, S., Van Immerseel, F., Bertrand-Michel, J., Oswald, E., Knauf, C., Dietrich, G., Cani, P. D., & Cenac, N. (2021). Bacteria-derived long chain fatty acid exhibits anti-inflammatory properties in colitis. *Gut*, *70*(6), 1088-1097. https://doi.org/10.1136/gutjnl-2020-321173

Ramarao, M. K., Murphy, E. A., Shen, M. W., Wang, Y., Bushell, K. N., Huang, N., Pan, N., Williams, C., & Clark, J. D. (2005). A fluorescence-based assay for fatty acid amide hydrolase compatible with high-throughput screening. *Anal Biochem*, *343*(1), 143-151. https://doi.org/10.1016/j.ab.2005.04.032

Reece, J. J., Siracusa, M. C., & Scott, A. L. (2006). Innate immune responses to lung-stage helminth infection induce alternatively activated alveolar macrophages. *Infect Immun*, *74*(9), 4970-4981. https://doi.org/10.1128/iai.00687-06

Rosenthal, R., Gunzel, D., Piontek, J., Krug, S. M., Ayala-Torres, C., Hempel, C., Theune, D., & Fromm, M. (2020). Claudin-15 forms a water channel through the tight junction with distinct function compared to claudin-2. *Acta Physiol (Oxf)*, *228*(1), e13334. https://doi.org/10.1111/apha.13334

Roulette, C. J., Kazanji, M., Breurec, S., & Hagen, E. H. (2016). High prevalence of cannabis use among Aka foragers of the Congo Basin and its possible relationship to helminthiasis. *Am J Hum Biol*, *28*(1), 5-15. https://doi.org/10.1002/ajhb.22740

Roxana, I., Kiyomi, F., Kazuhiko, H., Iwasakib, Y., & Tsuneo, Y. (2001). Two-step enzymatic synthesis of docosahexaenoic acid-rich symmetrically structured triacylglycerols via 2-monoacylglycerols. In (pp. 743-748). Journal of American Oil Chemist Society.

Savinainen, J. R., Saario, S. M., & Laitinen, J. T. (2012). The serine hydrolases MAGL, ABHD6 and ABHD12 as guardians of 2-arachidonoylglycerol signalling through cannabinoid receptors. *Acta Physiol (Oxf)*, *204*(2), 267-276. https://doi.org/10.1111/j.1748-1716.2011.02280.x

Scalvini, L., Ghidini, A., Lodola, A., Callegari, D., Rivara, S., Piomelli, D., & Mor, M. (2020). N-Acylethanolamine Acid Amidase (NAAA): Mechanism of Palmitoylethanolamide Hydrolysis Revealed by Mechanistic Simulations. *ACS Catalysis*, *10*(20), 11797-11813.

Solorzano, C., Zhu, C., Battista, N., Astarita, G., Lodola, A., Rivara, S., Mor, M., Russo, R., Maccarrone, M., Antonietti, F., Duranti, A., Tontini, A., Cuzzocrea, S., Tarzia, G., & Piomelli, D. (2009). Selective N-acylethanolamine-hydrolyzing acid amidase inhibition reveals a key role for endogenous palmitoylethanolamide in inflammation. *Proc Natl Acad Sci U S A*, *106*(49), 20966-20971. https://doi.org/10.1073/pnas.0907417106

Stella, N., Schweitzer, P., & Piomelli, D. (1997). A second endogenous cannabinoid that modulates long-term potentiation. *Nature*, *388*(6644), 773-778. https://doi.org/10.1038/42015

Stevens, W. W., Kim, T. S., Pujanauski, L. M., Hao, X., & Braciale, T. J. (2007). Detection and quantitation of eosinophils in the murine respiratory tract by flow cytometry. *J Immunol Methods*, *327*(1-2), 63-74. https://doi.org/10.1016/j.jim.2007.07.011

Su, J., Rajapaksha, T. W., Peter, M. E., & Mrksich, M. (2006). Assays of endogenous caspase activities: a comparison of mass spectrometry and fluorescence formats. *Anal Chem*, *78*(14), 4945-4951. https://doi.org/10.1021/ac051974i

Sun, H., Zhang, H., Ang, E. L., & Zhao, H. (2018). Biocatalysis for the synthesis of pharmaceuticals and pharmaceutical intermediates. *Bioorg Med Chem*, *26*(7), 1275-1284. https://doi.org/10.1016/j.bmc.2017.06.043

Sutherland, T. E., Rückerl, D., Logan, N., Duncan, S., Wynn, T. A., & Allen, J. E. (2018). Ym1 induces RELMα and rescues IL-4Rα deficiency in lung repair during nematode infection. *PLoS Pathog*, *14*(11), e1007423. https://doi.org/10.1371/journal.ppat.1007423

Tchantchou, F., & Zhang, Y. M. (2013). Selective Inhibition of Alpha/Beta-Hydrolase Domain 6 Attenuates Neurodegeneration, Alleviates Blood Brain Barrier Breakdown, and Improves Functional Recovery in a Mouse Model of Traumatic Brain Injury. *Journal of Neurotrauma*, *30*(7), 565-579. https://doi.org/10.1089/neu.2012.2647

Tsuboi, K., Uyama, T., Okamoto, Y., & Ueda, N. (2018). Endocannabinoids and related N-acylethanolamines: biological activities and metabolism. *Inflamm Regen*, *38*, 28. https://doi.org/10.1186/s41232-018-0086-5

Tsuboi, K., Zhao, L. Y., Okamoto, Y., Araki, N., Ueno, M., Sakamoto, H., & Ueda, N. (2007). Predominant expression of lysosomal N-acylethanolamine-hydrolyzing acid amidase in macrophages revealed by immunochemical studies. *Biochim Biophys Acta*, *1771*(5), 623-632. https://doi.org/10.1016/j.bbalip.2007.03.005

Turcotte, C., Blanchet, M. R., Laviolette, M., & Flamand, N. (2016). The CB2 receptor and its role as a regulator of inflammation. *Cell Mol Life Sci*, *73*(23), 4449-4470. https://doi.org/10.1007/s00018-016-2300-4

Vancamelbeke, M., & Vermeire, S. (2017). The intestinal barrier: a fundamental role in health and disease. *Expert Rev Gastroenterol Hepatol*, *11*(9), 821-834. https://doi.org/10.1080/17474124.2017.1343143

Weatherhead, J. E., Hotez, P. J., & Mejia, R. (2017). The Global State of Helminth Control and Elimination in Children. *Pediatr Clin North Am*, *64*(4), 867-877. https://doi.org/10.1016/j.pcl.2017.03.005

Wei, B. Q., Mikkelsen, T. S., McKinney, M. K., Lander, E. S., & Cravatt, B. F. (2006). A second fatty acid amide hydrolase with variable distribution among placental mammals. *J Biol Chem*, *281*(48), 36569-36578. https://doi.org/10.1074/jbc.M606646200

Wiley, M. B., Bobardt, S. D., Nordgren, T. M., Nair, M. G., & DiPatrizio, N. V. (2021). Cannabinoid Receptor Subtype-1 Regulates Allergic Airway Eosinophilia During Lung Helminth Infection. *Cannabis Cannabinoid Res*. https://doi.org/10.1089/can.2020.0167

Woting, A., & Blaut, M. (2018). Small Intestinal Permeability and Gut-Transit Time Determined with Low and High Molecular Weight Fluorescein Isothiocyanate-Dextrans in C3H Mice. *Nutrients*, *10*(6). https://doi.org/10.3390/nu10060685

Wright, K., Rooney, N., Feeney, M., Tate, J., Robertson, D., Welham, M., & Ward, S. (2005). Differential expression of cannabinoid receptors in the human colon: cannabinoids promote epithelial wound healing. *Gastroenterology*, *129*(2), 437-453. https://doi.org/10.1016/j.gastro.2005.05.026

Figure and Legends

Figure 4.1

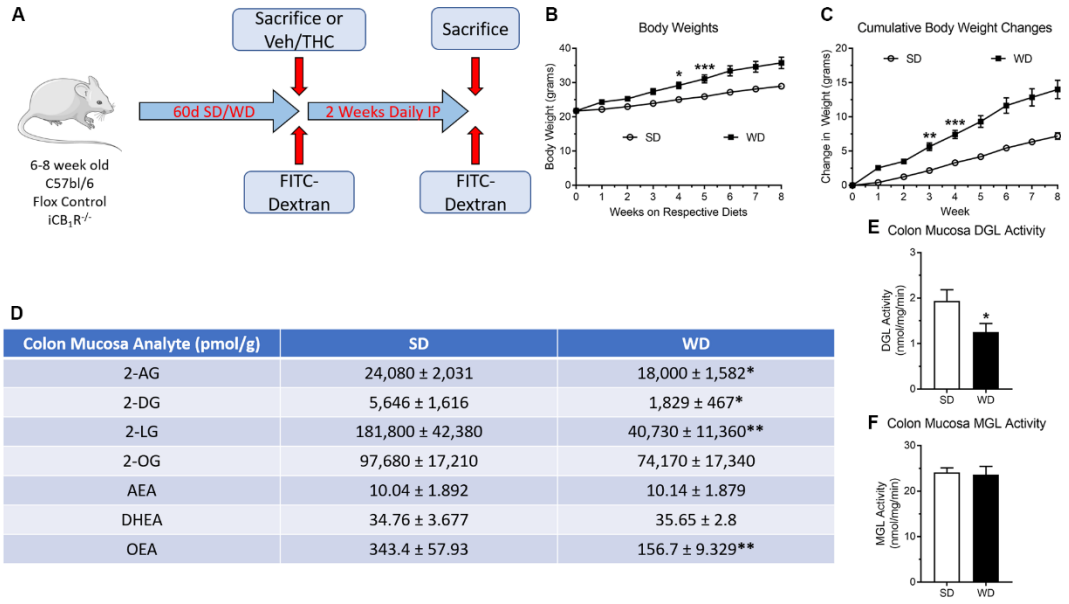

D

Colon Mucosa Analyte (pmol/g)	SD	WD
2-AG	24,080 ± 2,031	18,000 ± 1,582*
2-DG	5,646 ± 1,616	1,829 ± 467*
2-LG	181,800 ± 42,380	40,730 ± 11,360**
2-OG	97,680 ± 17,210	74,170 ± 17,340
AEA	10.04 ± 1.892	10.14 ± 1.879
DHEA	34.76 ± 3.677	35.65 ± 2.8
OEA	343.4 ± 57.93	156.7 ± 9.329**

Figure 4.1: Schematic displaying the design of the experiments performed (**A**). WD-fed mice gain significantly more weight when compared to SD-fed litter mates (**B** and **C**). Mice fed a WD for 60d have significantly decreased levels of 2-AG, 2-DG, 2-LG, and OEA when compared to SD-fed litter mates (**D**). The decrease in MAGs in DIO mice was coupled to a decrease in DGL activity with no changes in MGL activity when compared to lean mice. *-indicates p-value<0.05, **-indicates p-value<0.01, ***-indicates p-value<0.001, n=6-8.

Figure 4.2

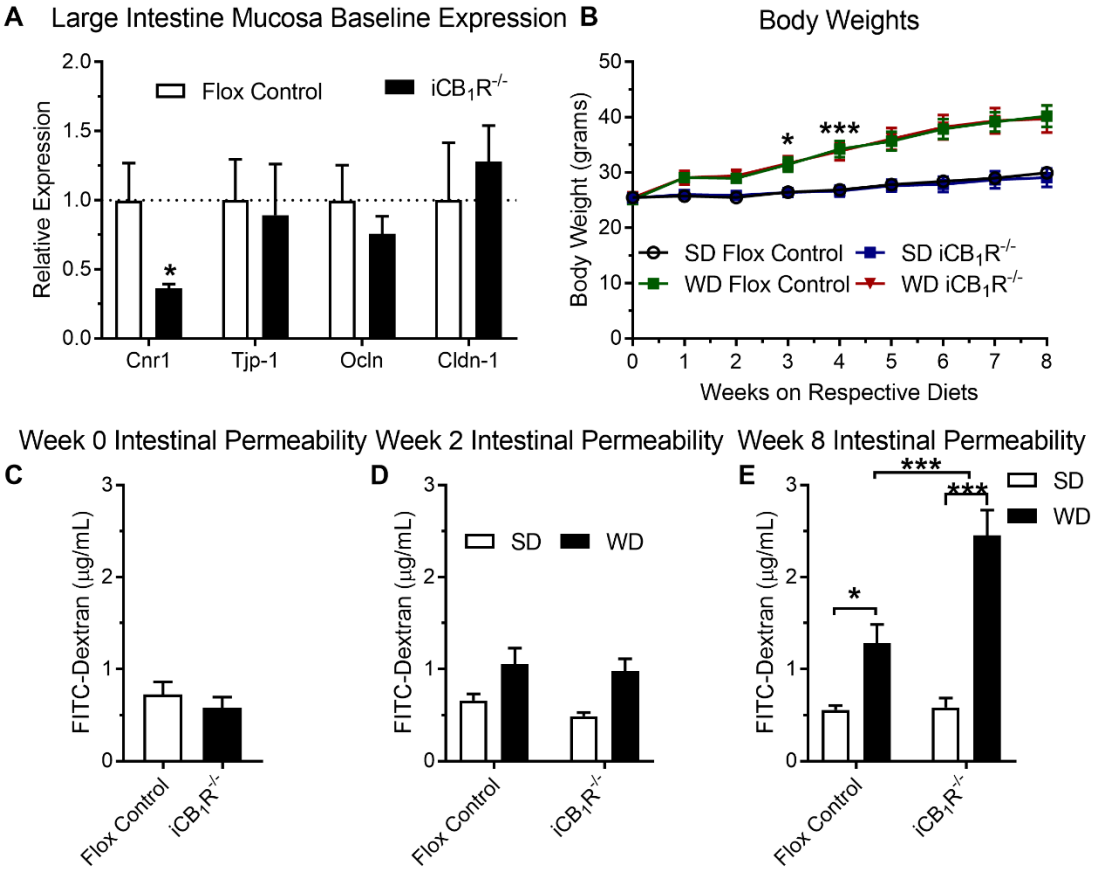

Figure 4.2: Large intestine mucosal scrapes from $iCB_1R^{-/-}$ mice displayed significantly reduced levels of Cnr1 mRNA when compared to Flox controls with no changes in any other genes probed (**A**). Mice lacking intestinal epithelial CB_1R and Flox control mice gain significantly more weight on a WD when compared to SD-fed litter mates (**B**). $iCB_1R^{-/-}$ mice display no changes in baseline paracellular permeability when compared to Flox controls (**C**). Two weeks on a WD did not induce significant changes in *in vivo* gut-barrier permeability in the large intestine in either genotype (**D**). Once DIO was achieved, Flox control mice displayed significant increases in large intestine paracellular permeability which was exacerbated in mice lacking intestinal epithelial CB_1R signaling (**E**). *-indicates p-value<0.05, ***-indicates p-value<0.001, n=4-8, 15.

Figure 4.3

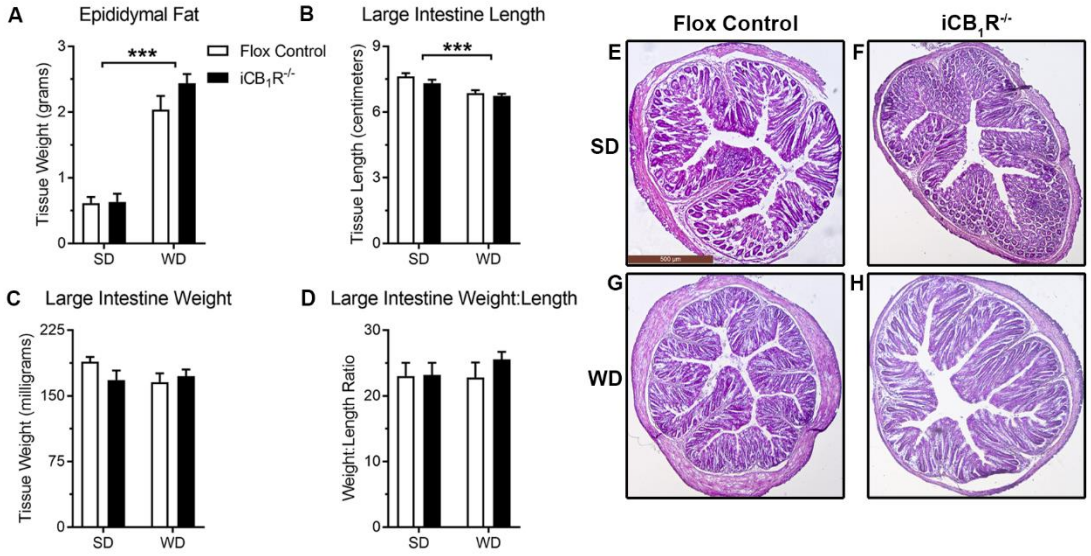

Figure 4.3: Mice fed a WD for 60d displayed significant increases in white adipose depot weight (**A**) and significant decreases in colon length (**B**) regardless of genotype. However, no changes in colon weight or weight:length ratio were observed across diet or genotype (**C** and **D**). No significant alterations were observed in tissue architecture in representative 4x images of 5 µm thick colon slices. ***-indicates p-value<0.001, n=11-15.

Figure 4.4

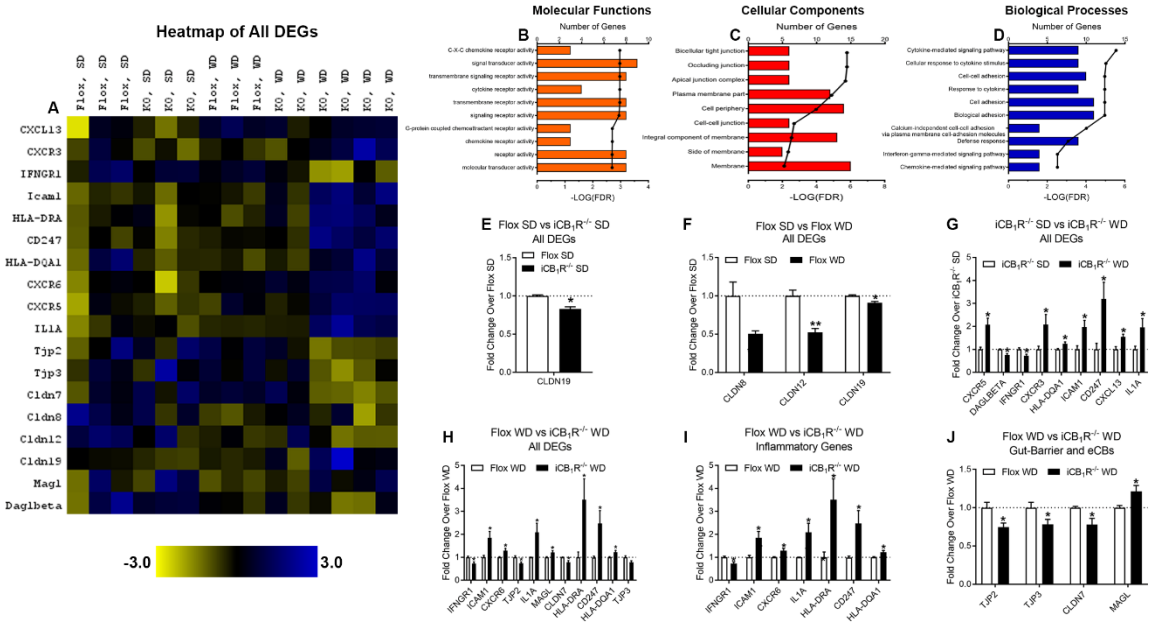

Figure 4.4: Representative heatmap of all differentially expressed genes (DEGs) in the large intestine mucosa across either diet or genotype (**A**). DAVID analysis of the DEGs revealed several pathways that may be implicated in diet-induced gut-barrier disruptions in molecular functions (**B**), cellular components (**C**), and biological processes (**D**). $iCB_1R^{-/-}$ mice displayed a down regulation in Cldn19 only after 60d on SD when compared to Flox control SD-fed litter mates (**E**). DIO caused dysregulation of three genes probed (**F**) and obese mice lacking intestinal epithelial CB_1R signaling had nine genes dysregulated (**G**). Several more DEGs were observed when WD-fed Flox controls were compared to WD-fed $iCB_1R^{-/-}$ mice (**H**) which included upregulation of several inflammatory genes (**I**) and a down regulation of a few gut-barrier related genes (**J**). *-indicates p-value<0.05, **-indicates p-value<0.01, n=3-6.

Figure 4.5

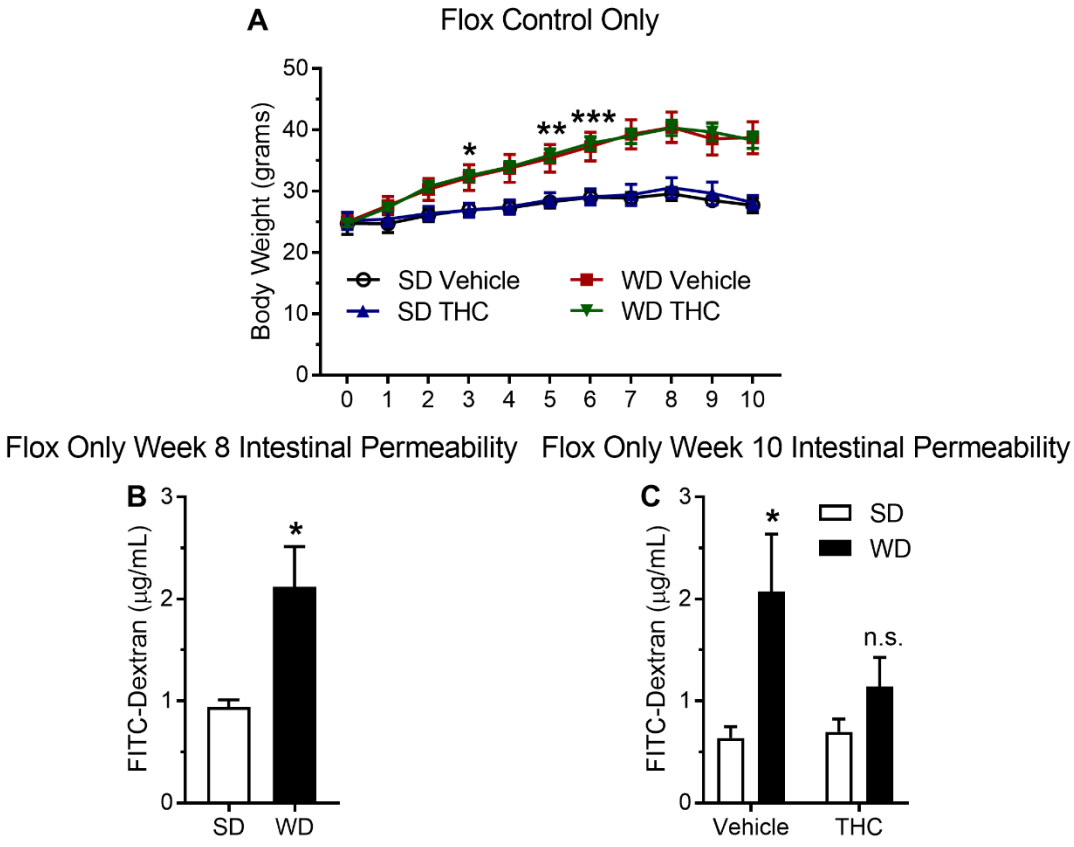

Figure 4.5: Two weeks of THC or vehicle injections did not significantly alter weights of WD- or SD-fed mice regardless of genotype (**A**). Flox control mice displayed significant increases in large intestine paracellular permeability after eight weeks on WD (**B**) which was rescued via chronic THC injections (**C**). *-indicates p-value<0.05, **-indicates p-value<0.01, ***-indicates p-value<0.001, n=6, 12-13

Figure 4.6

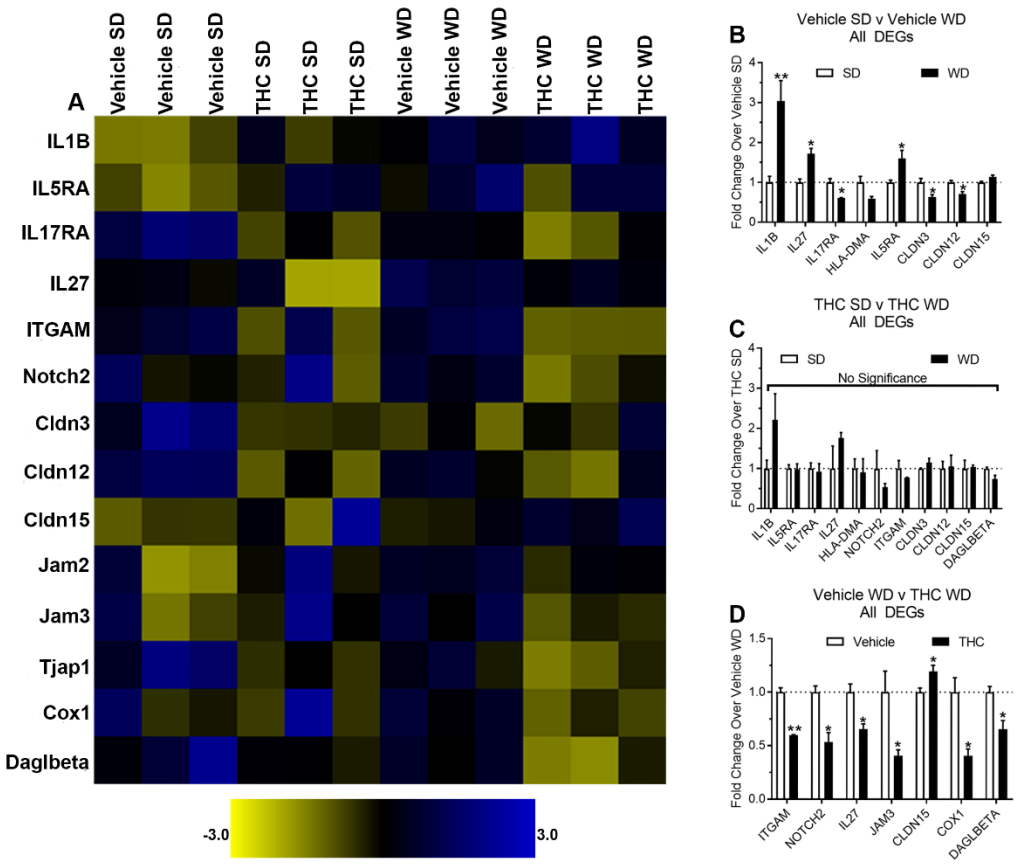

Figure 4.6: Representative heatmap of all differentially expressed genes (DEGs) in the large intestine mucosa across either diet or treatment (**A**). Several DEGs were observed when SD-fed vehicle treated mice were compared with WD-fed vehicle treated mice (**B**). of the 100 genes probed in the NanoString panel, zero DEGs were found when comparing SD-fed THC treated mice and WD-fed THC treated mice (**C**). THC treated WD-fed mice displayed a significant reduction in inflammatory genes and an increase in Cldn15 when compared to vehicle treated WD-fed mice (**D**). *-indicates p-value<0.05, **-indicates p-value<0.01, n=3.

Chapter 5 – Conclusions

The discovery that lipids, such as eCBs, can signal along receptors and induce cellular changes has led to a paradigm shift in molecular therapeutic development with a significant increase in attention to lipid metabolism. Although this eCB system is found throughout the human body, overwhelming evidence indicates a significant role for CB_2R signaling in immune cell functions and processes in the T-helper type 1 immune response (Harvey et al., 2013; Robinson et al., 2015; Turcotte et al., 2016). However, the roles for CB_1R or CB_2R signaling in the Th2 immune response and host-parasite interactions are not well understood. Previous studies found that eCB production is increased in response to *N. brasiliensis* infection in the tissue where the parasite is found (lungs, jejunum mucosa) (Batugedara et al., 2018). Furthermore, previous research indicates CB_1R signaling in *N. brasiliensis* infection is vital to host immune responses and health in the intestinal phase of infection (Batugedara et al., 2018). The work described here implicates a substantial role for CB_1R signaling in the lung phase of *N. brasiliensis* infection, where it provides protection from over-active and ineffective immune responses in the lungs (Wiley et al., 2021). Strikingly, CB_2R blockade had no effect on any of the measured outcomes, suggesting a stronger potential role for CB_1R signaling in parasitic infections and the Th2 response (M. B. Wiley et al., 2021). These data implicate the potential for targeting CB_1R activity in response to helminth infection to promote host health. This may prove to be extremely useful in regions of the world where healthcare is not readily accessible, but cannabis is regularly cultivated.

These studies explored the role for eCB signaling in host pathology and inflammatory responses to *N. brasiliensis* infection, however, it was also recently discovered that *N. brasiliensis* produces eCBs at quantifiable levels throughout its life-cycle (Batugedara et al., 2018). However, no enzymatic machinery capable of producing and degrading these eCBs has been discovered in any soil-transmitted helminth yet. Therefore, novel methods to quantitate the rate of eCB metabolism in both lung and jejunum mucosa tissue were developed to enhance available technology for characterization of the eCB system in any given tissue or organism (Wiley et al., 2021). This led to the discovery that ~55% of MAG metabolism in mouse lung tissue was mediated by the serine hydrolase ABHD6 (Wiley et al., 2021). These assays can potentially be further optimized in several mucosal tissues and disease models where dysregulation of lipid metabolism is suspected.

Due to the dysregulation of the eCB system observed in the small intestine in DIO, these enzyme assays were applied to the large intestine mucosa in DIO male mice to determine how eCB metabolism is altered in response to diet. Production of MAGs was found to be significantly reduced in the colon mucosa of DIO mice due to a down regulation in DGL activity with no changes in MGL activity. Previous research has found that dysregulation of the eCB system in the colon contributes to significant alterations in host metabolism and the functionality of the gut-barrier (Acharya et al., 2017; Cani, 2016; Cani et al., 2016). Furthermore, previous studies have found that diet-induced obesity can cause changes in paracellular permeability in the large intestine with a down regulation of tight-junction proteins and an upregulation of inflammatory

processes and infiltrate (Lam et al., 2012; Lee et al., 2017). The data provided here indicates that WD-induced obesity leads to significant changes in gut-barrier permeability in the colon which is exacerbated in mice lacking intestinal epithelial CB_1R signaling. Furthermore, $iCB_1R^{-/-}$ mice displayed significant alterations in RNA expression/regulation with a decrease in gut-barrier associated RNA and an increase in inflammatory processes. Chronic THC treatment rescued these changes in response to WD in Flox control mice, suggesting a significant role for CB_1R signaling in initiating severe gut-barrier dysfunction. Future research will identify the mechanism by which CB_1R may be controlling these outcomes and if intestinal epithelial CB_1R activation is sufficient to rescue gut-barrier dysfunction in more severe models of IBD (i.e. DSS).

These studies implicate a substantial role for the eCB system in several disease models in mucosal tissues. Taken together, this work provides evidence that: (i) CB_1R signaling may have a significant role in regulating the Th2 immune response and eosinophil migration/activation, (ii) UPLC-MS/MS technology can be utilized to identify discrete changes in mucosal FAAH activity, and that characterization of the entire eCB system must be performed in tissues of interest in disease models to identify the source of dysregulation in lipid metabolism/signaling, and (iii) intestinal epithelial CB_1R signaling provides protection from diet-induced gut-barrier dysfunction. Furthermore, chronic THC treatment rescues paracellular permeability and expression of several inflammatory and tight-junction protein associated RNA in the large intestine mucosa. Ultimately, this body of work suggests that the eCB system provides a unique target for therapeutic

development in several disease models in which lipid signaling and/or metabolism may be significantly dysregulated.

References

Acharya, N., Penukonda, S., Shcheglova, T., Hagymasi, A. T., Basu, S., & Srivastava, P. K. (2017). Endocannabinoid system acts as a regulator of immune homeostasis in the gut. *Proc Natl Acad Sci U S A*, *114*(19), 5005-5010. https://doi.org/10.1073/pnas.1612177114

Batugedara, H. M., Argueta, D., Jang, J. C., Lu, D., Macchietto, M., Kaur, J., Ge, S., Dillman, A. R., DiPatrizio, N. V., & Nair, M. G. (2018). Host and helminth-derived endocannabinoids are generated during infection with effects on host immunity. *Infect Immun*. https://doi.org/10.1128/iai.00441-18

Cani, P. D. (2016). Interactions between gut microbes and host cells control gut barrier and metabolism. *Int J Obes Suppl*, *6*(Suppl 1), S28-S31. https://doi.org/10.1038/ijosup.2016.6

Cani, P. D., Plovier, H., Van Hul, M., Geurts, L., Delzenne, N. M., Druart, C., & Everard, A. (2016). Endocannabinoids - at the crossroads between the gut microbiota and host metabolism. *Nature Reviews Endocrinology*, *12*(3), 133-143. https://doi.org/10.1038/nrendo.2015.211

Harvey, B. S., Nicotra, L. L., Vu, M., & Smid, S. D. (2013). Cannabinoid CB2 receptor activation attenuates cytokine-evoked mucosal damage in a human colonic explant model without changing epithelial permeability. *Cytokine*, *63*(2), 209-217. https://doi.org/10.1016/j.cyto.2013.04.032

Lam, Y. Y., Ha, C. W., Campbell, C. R., Mitchell, A. J., Dinudom, A., Oscarsson, J., Cook, D. I., Hunt, N. H., Caterson, I. D., Holmes, A. J., & Storlien, L. H. (2012). Increased gut permeability and microbiota change associate with mesenteric fat inflammation and metabolic dysfunction in diet-induced obese mice. *PLoS One*, *7*(3), e34233. https://doi.org/10.1371/journal.pone.0034233

Lee, J. C., Lee, H. Y., Kim, T. K., Kim, M. S., Park, Y. M., Kim, J., Park, K., Kweon, M. N., Kim, S. H., Bae, J. W., Hur, K. Y., & Lee, M. S. (2017). Obesogenic diet-induced gut barrier dysfunction and pathobiont expansion aggravate experimental colitis. *PLoS One*, *12*(11), e0187515. https://doi.org/10.1371/journal.pone.0187515

Robinson, R. H., Meissler, J. J., Fan, X., Yu, D., Adler, M. W., & Eisenstein, T. K. (2015). A CB2-Selective Cannabinoid Suppresses T-Cell Activities and Increases Tregs and IL-10. *J Neuroimmune Pharmacol*, *10*(2), 318-332. https://doi.org/10.1007/s11481-015-9611-3

Turcotte, C., Blanchet, M. R., Laviolette, M., & Flamand, N. (2016). The CB2 receptor and its role as a regulator of inflammation. *Cell Mol Life Sci*, *73*(23), 4449-4470. https://doi.org/10.1007/s00018-016-2300-4

Wiley, M. B., Bobardt, S. D., Nordgren, T. M., Nair, M. G., & DiPatrizio, N. V. (2021). Cannabinoid Receptor Subtype-1 Regulates Allergic Airway Eosinophilia During Lung Helminth Infection. *Cannabis Cannabinoid Res*. https://doi.org/10.1089/can.2020.0167

Wiley, M. B., Perez, P. A., Argueta, D. A., Avalos, B., Wood, C. P., & DiPatrizio, N. V. (2021). UPLC-MS/MS Method for Analysis of Endocannabinoid and Related Lipid Metabolism in Mouse Mucosal Tissue [Methods]. *Frontiers in Physiology*, *12*(1084). https://doi.org/10.3389/fphys.2021.699712